NASA CR-72832

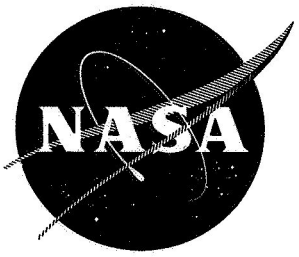

STRUCTURAL STABILITY AND MECHANICAL BEHAVIOR OF THERMOMECHANICALLY PROCESSED DISPERSION STRENGTHENED NICKEL ALLOYS

by

B. A. Wilcox, A. H. Clauer, and W. B. Hutchinson

BATTELLE MEMORIAL INSTITUTE

prepared for

NATIONAL AERONAUTICS AND SPACE ADMINISTRATION

Technical Management
NASA Lewis Research Center
Contract NAS 3-11167
Cleveland, Ohio
F. H. Harf
C. W. Andrews
T. K. Glasgow

Requests for copies of this report should be referred to

National Aeronautics and Space Administration
Scientific and Technical Information Facility
P.O. Box 33
College Park, Md. 20740

NASA CR-72832

FINAL REPORT

on

STRUCTURAL STABILITY AND MECHANICAL BEHAVIOR OF THERMOMECHANICALLY PROCESSED DISPERSION STRENGTHENED NICKEL ALLOYS

by

B. A. Wilcox*, A. H. Clauer*, and W. B. Hutchinson**

Prepared for

NATIONAL AERONAUTICS AND SPACE ADMINISTRATION

March 18, 1971

CONTRACT NAS3-11167

Technical Management
NASA Lewis Research Center
Cleveland, Ohio
F. H. Harf
C. W. Andrews
T. K. Glasgow

---

* Metal Science Group, Battelle's Columbus Laboratories.

** Department of Physical Metallurgy and Science of Materials, University of Birmingham.

BATTELLE MEMORIAL INSTITUTE
Columbus Laboratories
505 King Avenue
Columbus, Ohio 43201

TABLE OF CONTENTS

	Page
ABSTRACT	ix
SUMMARY	1
INTRODUCTION	3
MATERIALS AND PROCEDURES	4
Materials	4
Procedures	9
Thermomechanical Processing	9
Metallography	10
Tensile and Creep Testing	10
Texture Measurements	11
RESULTS AND DISCUSSION	13
Ni and Ni-2ThO_2	13
Microstructure	13
Tensile Deformation	28
Creep and Creep Rupture	59
Texture	69
Ni-20Cr, Ni-20Cr-2ThO_2, Ni-20Cr-10W, and Ni-20Cr-10W-2ThO_2	82
Microstructure	82
Tensile Deformation	94
Creep and Creep Rupture	109
Texture	116
GENERAL DISCUSSION	118
Microstructure and Mechanical Properties	118
The Possible Role of Texture	126

TABLE OF CONTENTS
(Continued)

	Page
CONCLUSIONS	128
ACKNOWLEDGEMENTS	130
REFERENCES	131
APPENDIX A	
PLOTS OF NORMALIZED INTENSITY VERSUS ANGLE OF INCLINATION FOR THE {111} AND {200} REFLECTIONS	A-1
APPENDIX B	
NEW TECHNOLOGY	B-1
APPENDIX C	
DISTRIBUTION LIST FOR SUMMARY REPORT	C-1

LIST OF TABLES

		Page
Table 1.	Composition of Experimental Alloys (Weight Percent).	5
Table 2.	ThO_2 Particle Sizes and Spacings in Experimental Alloys. . . .	8
Table 3.	Grain Size or Cell Size of Ni and Ni-2ThO_2 as a Function of Drawing by Procedures A and B.	20
Table 4.	Average Ratio of Void Length, X, to Particle Diameter, $2r_v$, in Ni-2ThO_2 Drawn by Procedure A (No Intermediate Anneals). . .	27
Table 5.	Tensile Properties of Ni at 25 and 1093°C After Drawing by Procedure A (No Intermediate Anneals).	29
Table 5a.	Same as Table 5, SI Units.	30
Table 6.	Tensile Properties of Ni at 25 and 1093°C After Drawing by Procedure B (Intermediate Anneals, 1 hour, 1200°C, H_2 atm, after each 50-percent Reduction by Drawing). All specimens were Tested in Annealed Condition.	31
Table 6a.	Same as Table 6, SI Units.	32
Table 7.	Tensile Properties of Ni-2ThO_2 at 25 and 1093°C After Drawing by Procedure A (No Intermediate Anneals)	33
Table 7a.	Same as Table 7, SI Units.	34
Table 8.	Tensile Properties of Ni-2ThO_2 at 25 and 1093°C After Drawing by Procedure B (Intermediate Anneals, 1 hour, 1200°C, H_2, atm., after each 50-percent Reduction by Drawing). All specimens were Tested in Annealed Condition.	35
Table 8a.	Same as Table 8, SI Units.	36
Table 9.	0.2% Yield Strength, 100 hour Rupture Stress, and Stress to Give a Minimum Creep Rate of 10^{-4} hr^{-1} of Ni-2ThO_2 at 1093°C as a Function of L/ℓ. L = Grain or Cell Length, ℓ = Grain or Cell Diameter	50
Table 9a.	Same as Table 9, SI Units.	51
Table 10.	Creep Properties of Ni-2ThO_2 at 1093°C as a Function of Drawing by Procedure B (Intermediate Anneals at 1200°C). Each Specimen was Tested in the Annealed Condition, unless Otherwise Specified.	62
Table 11.	Quantitative Measures of Texture Intensity in Ni and Ni-2ThO_2 as a Function of Drawing Strain.	72

LIST OF TABLES
(Continued)

Page

Table 12. Grain or Cell Size in Ni-20Cr and Ni-20Cr-2ThO_2 as a Function of Drawing by Procedures A and B. 91

Table 13. Tensile Properties of Ni-20Cr at 25 and 1093°C After Drawing and Swaging by Procedures A and B 97

Table 13a. Same as Table 13, SI Units. 98

Table 14. Tensile Properties of Ni-20Cr-2ThO_2 at 25 and 1093°C After Drawing and Swaging by Procedures A and B 99

Table 14a. Same as Table 14, SI Units. 100

Table 15. Tensile Properties of Ni-20Cr-10W and Ni-20Cr-10W-2ThO_2 at 25 and 1093°C After Swaging by Procedure B (Intermediate Anneals, 1200°C, 1 hour, H_2 After Each 25% Reduction). 101

Table 15a. Same as Table 15, SI Units. 102

Table 16. Creep Properties of Ni-20Cr-2ThO_2 at 1093°C as a Function of Drawing and Swaging by Procedure B (Intermediate Anneals at 1200°C). Each Specimen was Tested in the Annealed Condition 110

Table 17. Creep Properties of Ni-20Cr-10W-2ThO_2 at 1093°C. All Specimens Tested in Annealed Condition (1 hour, 1200°C, H_2 atm.) 111

Table 18. Quantitative Measures of Texture Intensity in Ni-20Cr, Ni-20Cr-2ThO_2, Ni-20Cr-10W and Ni-20Cr-10W-2ThO_2 After Drawing or Swaging by Procedures A and B. 117

Table 19. Summary of Grain Aspect Ratio Effects on Yield Strength, Creep Rate, and Rupture Life of Dispersion Strengthened Ni Alloys at 1093°C. All Alloys had 2 to 3 vol.% ThO_2 (or Y_2O_3). . . . 122

Table 19a. Same as Table 19, SI Units. 123

LIST OF FIGURES

Page

Figure 1. Particle size distributions of experimental ThO_2-containing alloys, expressed as volume percent of the total ThO_2 content. 7

Figure 2. Microstructure of as-extruded Ni; (a) optical micrograph, (b) transmission electron micrograph. 14

Figure 3. Microstructure of as-extruded Ni-2ThO_2; (a) optical micrograph, (b) replica electron micrograph, (c) transmission electron micrograph 15

Figure 4. Microstructure of extruded-plus-annealed Ni; (a) optical micrograph, (b) transmission electron micrograph. 18

Figure 5. Microstructure of extruded-plus-annealed Ni-2ThO_2; (a) optical micrograph, (b) replica electron micrograph, (c) transmission electron micrograph. 19

Figure 6. Optical micrographs of Ni drawn by Procedure A (no intermediate anneals). 21

Figure 7. Transmission electron micrographs of Ni drawn by Procedure A (no intermediate anneals) 22

Figure 8. Transmission electron micrographs of Ni-2ThO_2 drawn by Procedure A (no intermediate anneals) 23

Figure 9. Optical micrograph of Ni-2ThO_2, drawn 92.5% by Procedure B. After the final anneal, about 30% of the cross-section had recrystallized. 24

Figure 10. Transmission electron micrographs of Ni-2ThO_2 drawn by Procedure B (intermediate anneals). 25

Figure 11. Transmission micrographs of Ni-2ThO_2 drawn by Procedure A, illustrating increasing growth of voids at ThO_2 particles with increasing drawing strain. 26

Figure 12. Growth of voids at ThO_2 particles during drawing of Ni-2ThO_2 by Procedure A. 27

Figure 13. Effect of drawing by Procedures A and B on tensile properties of Ni at 25°C. 37

Figure 14. Effect of drawing by Procedures A and B on tensile properties of Ni-2ThO_2 at 25°C. 38

Figure 15. Effect of drawing by Procedures A and B on tensile properties of Ni at 1093°C. 39

Figure 16. Effect of drawing by Procedures A and B on tensile properties of Ni-2ThO_2 at 1093°C 40

LIST OF FIGURES (Continued)

Page

Figure 17. Dependence of room temperature proportional limit of Ni and Ni-2ThO_2 on grain size and cell size produced by drawing Procedures A and B. The value of $\Delta \sigma_{P.L.}$ at $\ell^{-1/2} = 0$ is 18,500 psi (128 MN/m^2) 43

Figure 18. Dependence of room temperature yield strength (0.2% offset of Ni and Ni-2ThO_2 on grain size and cell size produced by drawing Procedures A and B. The value of $\Delta \sigma_{Y.S.}$ at $\ell^{-1/2} = 0$ is 21,000 psi (145 MN/m^2). 44

Figure 19. Dependence of 0.2% offset yield strength on grain or cell size for Ni-2ThO_2 tested at 1093°C 48

Figure 20. The effect of grain or cell aspect ratio, L/ℓ, in Ni-2ThO_2 on strength properties at 1093°C: (a) 0.2% offset yield strength, (b) 100-hour rupture strength, and (c) stress to give a minimum creep rate of 10^{-4} hr^{-1}. See Table 9 for a description of specimen conditions 52

Figure 21. Schematic plots showing how test temperature and strain rate may influence the relation between yield strength and grain aspect ratio, L/ℓ, in Ni-ThO_2 alloys 54

Figure 22. Room temperature and high temperature strength, and grain size of Ni-ThO_2 alloys as a function of reduction by drawing or swaging. Results of this work are compared with those of previous investigators, and in each case the starting material was extruded bar 57

Figure 23. Creep curves of Ni-2ThO_2 specimens drawn by Procedures A and B. 61

Figure 24. Effect of drawing by Procedure B (intermediate anneals) on minimum creep rate of Ni-2ThO_2 at 1093°C 63

Figure 25. Effect of drawing by Procedure B (intermediate anneals) on creep rupture life of Ni-2ThO_2 at 1093°C 64

Figure 26. Influence of drawing Ni-2ThO_2 by Procedure B (intermediate anneals) on stress to cause a minimum creep of 10^{-4} hr^{-1} and stress to cause rupture in 100 hr at 1093°C. 66

Figure 27. Effect of drawing by Procedure A (no intermediate anneals) on the fiber texture of Ni and Ni-2ThO_2. Texture concentrations are (a) within 10° of the rod axis, and (b) within 20° of the rod axis. 73

Figure 28. Effect of drawing by Procedure B (intermediate anneals) on the fiber texture of Ni and Ni-2ThO_2. Texture concentrations are (a) within 10° of the rod axis, and (b) within 20° of the rod axis 73

LIST OF FIGURES (Continued)

Page

Figure 29. Microstructure of as-extruded Ni-20Cr; (a) optical micrograph, (b) transmission electron micrograph 83

Figure 30. Microstructure of as-extruded Ni-20Cr-2ThO_2; (a) optical micrograph , (b) transmission electron micrograph. 84

Figure 31. Dislocation loops around particles (probably Cr_2O_3) in as-extruded Ni-20Cr. Photographs are from region of foil which was damaged in handling. 85

Figure 32. Optical micrographs of (a) extruded plus annealed Ni-20Cr, (b) extruded plus annealed Ni-20Cr-2ThO_2 87

Figure 33. Transmission electron micrographs of (a) Ni-20Cr drawn 24.4% by Procedure A, (b) Ni-20Cr-2ThO_2 drawn 23.7% by Procedure A. 88

Figure 34. Examples of optical microstructures of Ni-20Cr (a) drawn 24.4% by Procedure B, (b) swaged 49.1% by Procedure B. . . . 89

Figure 35. Microstructure of Ni-20Cr-2ThO_2 drawn 25.6% by Procedure B; (a) optical micrograph, (b) transmission electron micrograph 90

Figure 36. Microstructure of extruded plus annealed Ni-20Cr-10W; (a) optical micrograph, (b) transmission electron micrograph. Note particle (presumably Cr_2O_3) blocking non-coherent twin boundary 92

Figure 37. Microstructure of extruded plus annealed Ni-20Cr-10W-2ThO_2; (a) optical micrograph, (b) transmission electron micrograph 93

Figure 38. Optical micrographs of (a) Ni-20Cr-10W swaged 53.9% by Procedure B, (b) Ni-20Cr-10W-2ThO_2 swaged 53.9% by Procedure B. 95

Figure 39. Recrystallized microstructure of Ni-20Cr-2ThO_2 annealed 1 hour in H_2 at 1316°C; (a) optical micrograph, (b) transmission electron micrograph. 96

Figure 40. Effect of drawing and swaging by Procedures A and B on tensile properties of Ni-20Cr at 25°C. 104

Figure 41. Effect of drawing and swaging by Procedures A and B on tensile properties of Ni-20Cr-2ThO_2 at 25°C. 105

Figure 42. Effect of drawing and swaging by Procedures A and B on tensile properties of Ni-20Cr at 1093°C. 106

LIST OF FIGURES (Continued)

Page

Figure 43. Effect of drawing and swaging by Procedures A and B on tensile properties of Ni-20Cr-2ThO_2 at 1093°C 107

Figure 44. Dependence of room temperature yield strength (0.2% offset) of Ni-20Cr and Ni-20Cr-2ThO_2 on grain size and cell size. The value of $\Delta \sigma_{Y.S.}$ at $\ell^{-1/2} = 0$ is 42,000 psi (290MN/m^2) . 108

Figure 45. Effect of drawing or swaging by Procedure B on minimum creep rate of Ni-20Cr-2ThO_2 at 1093°C 112

Figure 46. Effect of drawing or swaging by Procedure B on creep rupture life of Ni-20Cr-2ThO_2 at 1093°C 113

Figure 47. Effect of swaging by Procedure B on the minimum creep rate of Ni-20Cr-10W-2ThO_2 at 1093°C. 114

Figure 48. Effect of swaging by Procedure B on the rupture life of Ni-20Cr-10W-2ThO_2 at 1093°C 115

Figure 49. Hall-Petch plots for Ni, Ni-2ThO_2, Ni-20Cr, and Ni-20Cr-2ThO_2 at room temperature. 119

Figure 50. The effect of grain or cell aspect ratio, L/ℓ, in dispersion strengthened Ni alloys on strength properties at 1093°C: (a) 0.2% offset yield strength, (b) 100-hour rupture strength, and (c) stress to give a minimum creep rate of 10^{-4} hr^{-1}. See Tables 19 and 9 for a description of specimen compositions and conditions 124

STRUCTURAL STABILITY AND MECHANICAL BEHAVIOR OF THERMOMECHANICALLY PROCESSED DISPERSION STRENGTHENED NICKEL ALLOYS

by

B. A. Wilcox, A. H. Clauer, and W. B. Hutchinson

ABSTRACT

Thermomechanical processing of dispersion-strengthened and dispersion-free Ni-base alloys influences the microstructure, crystallographic texture, and strength. The alloys studied were: (1) Ni, (2) Ni-2ThO_2, (3) Ni-20Cr, (4) Ni-20Cr-2ThO_2, (5) Ni-20Cr-10W, and (6) Ni-20Cr-10W-2ThO_2. Refining the substructure is a much more potent means of strengthening at room temperature than is dispersion hardening. The major microstructural feature which affects high temperature strength is the grain aspect ratio, i.e., grain length divided by grain width. The yield strength and creep strength at 1093^{o}C increased linearly with increasing grain aspect ratio. The role of deformation texture in recrystallization resistance and in development of microstructures during recrystallization is discussed.

STRUCTURAL STABILITY AND MECHANICAL BEHAVIOR OF THERMOMECHANICALLY PROCESSED DISPERSION STRENGTHENED NICKEL ALLOYS

by

B. A. Wilcox, A. H. Clauer, and W. B. Hutchinson

SUMMARY

Thermomechanical processing (TMP) by drawing and swaging have been used to work three dispersion strengthened Ni alloys and their dispersion-free counterparts: Ni-2ThO_2, Ni, Ni-20Cr-2ThO_2, Ni-20Cr, Ni-20Cr-10W-2ThO_2, and Ni-20Cr-10W. The purpose was to examine the important features of indirect strengthening[1,2] due to dispersed particles, and this was done by evaluating how TMP influenced microstructure, tensile deformation behavior at 25 and 1093°C, creep behavior at 1093°C, and crystallographic texture.

Room temperature strength was increased by TMP as a result of refining the grain size and substructure spacing (cell size), ℓ, in accord with the usual Hall-Petch relation. This substructure strengthening increment was five to six times greater than the strength increment, σ_p, due to particles alone. For a given alloy base, the Hall-Petch plots of thoriated and ThO_2-free materials converged at high values of $\ell^{-1/2}$. Thus, particle strengthening and substructure strengthening are not additive, since the value of σ_p depends on the value of ℓ. Similarly, the increment in strength due to solid solution additions of Cr is not directly additive to grain size strengthening, since this also depends on ℓ.

At high temperatures (1093°C) no good correlation was found between yield strength and grain or cell size. Instead, there was an excellent correlation between yield strength and grain aspect ratio (grain length, L, divided by grain width, ℓ), whereby the yield strength increased linearly with L/ℓ. This correlation held for non-recrystallized Ni-2ThO_2 with very fine elongated grains, as well as recrystallized Ni-2ThO_2 which had very coarse elongated grains. The

same aspect ratio correlation was found for minimum creep rate and 100-hour rupture life. This influence of grain aspect ratio was interpreted in terms of how L/ℓ influenced grain boundary sliding, which appears to be the major mode of tensile yielding and creep at 1093°C. When the stress axis is parallel to the elongated grain direction, increasing L/ℓ lowers the resolved shear stress on boundaries, on average, and this minimizes the overall amount of sliding.

Thus, a fine, stable, very elongated grain structure is optimum for combined room temperature and high temperature strengthening, and this can be achieved in Ni-2ThO_2 bar, but apparently not in Cr-containing alloys. Here recrystallization occurs at high temperatures, sometimes giving fine, nearly equiaxed, grains and sometimes coarse elongated grains.

The role of deformation texture in preventing recrystallization, or in influencing the resultant microstructure when recrystallization does occur, is not completely clear. Extruded Ni-2ThO_2 had a dual <100>-<111> fiber texture with a very strong <100> component, and was resistant to recrystallization. When processed such that the <100> component dropped to ~ 50% of the texture concentration, partial recrystallization occurred at 1200°C. Also the Cr-containing alloys had a less sharp <100> fiber texture than Ni-2ThO_2, and they were susceptible to recrystallization. Thus a strong <100> fiber texture may promote recrystallization resistance. When recrystallization does occur, often the structure consists of coarse elongated grains, and this is sufficient for good high temperature strength, provided the grain aspect ratio is large enough. The anisotropic grain growth which leads to this kind of structure may be related to the deformation texture.

INTRODUCTION

It has been shown by numerous workers that controlled thermomechanical processing (TMP) of dispersion strengthened metals, such as SAP, TD Nickel, DS Nickel, and TD Ni-Cr, can produce improved strength, although different processsing methods are generally required to enhance strength at room temperature as opposed to strength at high temperatures.

It has been the feeling of many that strengthening occurs by particles blocking dislocation motion, and that additional strengthening can be achieved if the particles act during TMP to help develop and pin certain stable dislocation substructures and grain sizes and shapes. The question of whether or not particles promote certain crystallographic textures, with attendant strengthening, has also been raised. Ansell[1] has used the phrase "direct and indirect dispersion strengthening" to describe these effects of particles, and this concept was demonstrated in the case of Ni-2ThO_2 by Wilcox and Jaffee[2], who compared the tensile deformation of TD Nickel bar with that of recrystallized TD Nickel and pure polycrystalline Ni over the temperature range 25-1200^{o}C. It was found that the recrystallized TD Nickel, which had coarse elongated grains and very little dislocation substructure, was stronger than pure Ni and weaker than TD Nickel bar, over the entire temperature range. The strength increment of recrystallized TD Nickel over pure Ni was attributed to direct strengthening via the Orowan mechanism. The even superior strength of TD Nickel bar, which had a fine stable elongated grain and subgrain structure, was hypothesized to be associated with the fine grain size, a higher dislocation density, and possibly a texture effect.

The uncertainty in the indirect strengthening contribution of ThO_2 particles was the basis for the research performed under the present program. The objectives of this program were to gain an understanding of how various TMP

procedures could alter the microstructure of dispersion strengthened Ni alloys, and how the microstructural changes could influence room temperature and elevated temperature mechanical properties. Another feature of this program dealt with the effect of TMP on texture. Many people have speculated that development of certain textures in dispersion strengthened Ni alloys is "beneficial", although to the authors' knowledge this has not been quantitatively demonstrated, nor has the term "beneficial" been satisfactorily explained. One might ask, for example, whether "texture strengthening" is important, or whether the texture developed during TMP affects recrystallization resistance, or in the event that recrystallization does occur whether the subsequent microstructure is determined to some extent by the deformation texture.

In order to examine these aspects of indirect strengthening, six alloys were studied: Ni, Ni-20Cr, Ni-20Cr-10W, with and without 2-volume percent ThO_2. TMP was accomplished by wire drawing and swaging, and the following properties were examined as a function of TMP: microstructure, room and elevated temperature tensile deformation behavior, high temperature creep characteristics, and features of the dual <100>-<111> fiber texture.

MATERIALS AND PROCEDURES

Materials

The six alloys studied in this investigation were obtained from Fansteel Metallurgical Corporation in the form of 0.35 to 0.40 inch (0.89-1.02 cm) diameter extruded bar. The chemical compositions are given in Table 1, and the fabrication procedures used by Fansteel were as follows:

(1) Hydrostatically compact powders to billets at 60,000 psi (414 MN/m^2)

TABLE 1. COMPOSITION OF EXPERIMENTAL ALLOYS (Weight-percent)

Alloy	ThO_2	Cr	W	C	S	N
Ni	--	--	--	0.0010	0.0062	--
Ni-2ThO_2	2.9	--	--	0.0024	0.0022	0.010
Ni-20Cr	--	19.7	--	0.0278	0.0019	--
Ni-20Cr-2ThO_2	2.0	20.2	--	0.0249	0.020	0.0051
Ni-20Cr-10W	--	20.4	8.6	0.0310	0.0063	--
Ni-20Cr-10W-2ThO_2	2.8	20.8	9.9	0.0271	0.0035	--

(2) Can in mild steel, 2 inch (5.08 cm) outside diameter

(3) Sinter under flowing hydrogen to 1177°C maximum temperature

(4) Cool, evacuate and seal can

(5) Extrude from 2 inch (5.08 cm) diameter to 1/2 inch (1.27 cm) diameter at 1093°C

(6) Decan

(7) Centerless grind to cleanup.

The Ni, Ni-2ThO_2, Ni-20Cr, and Ni-20Cr-2ThO_2 alloys were shipped from Fansteel in the as-extruded condition. However, the two tungsten containing alloys were annealed by Fansteel (1 hour, 1316°C, air) prior to cleanup and shipping. The as-extruded microstructures varied from recrystallized for the pure Ni to fine elongated grains in the Ni-2ThO_2 alloy. Details of the various microstructures are discussed later.

Particle sizes and spacings were determined in the ThO_2-containing alloys using techniques described previously[2,3]. A Zeiss Particle Size Analyzer was used to measure 2000 particle diameters from transmission electron micrographs, and the particle size distributions are shown in Figure 1, and Table 2. In Figure 1 the distribution is expressed as volume percent of the total ThO_2 content. Using the data in Figure 1 the mean planar center-to-center particle spacing, d, was determined by developing the expression[4]

$$d^2 = 1/N_s \quad , \tag{1}$$

where N_s = number of particles intersecting a unit area. Transforming this expression into the appropriate particle parameters, and including the particle size distribution leads to the following relation[2], from which d values were calculated:

$$d^2 = \frac{2\pi}{3 \sum_i (f_i / r_{v_i}^2)} \quad . \tag{2}$$

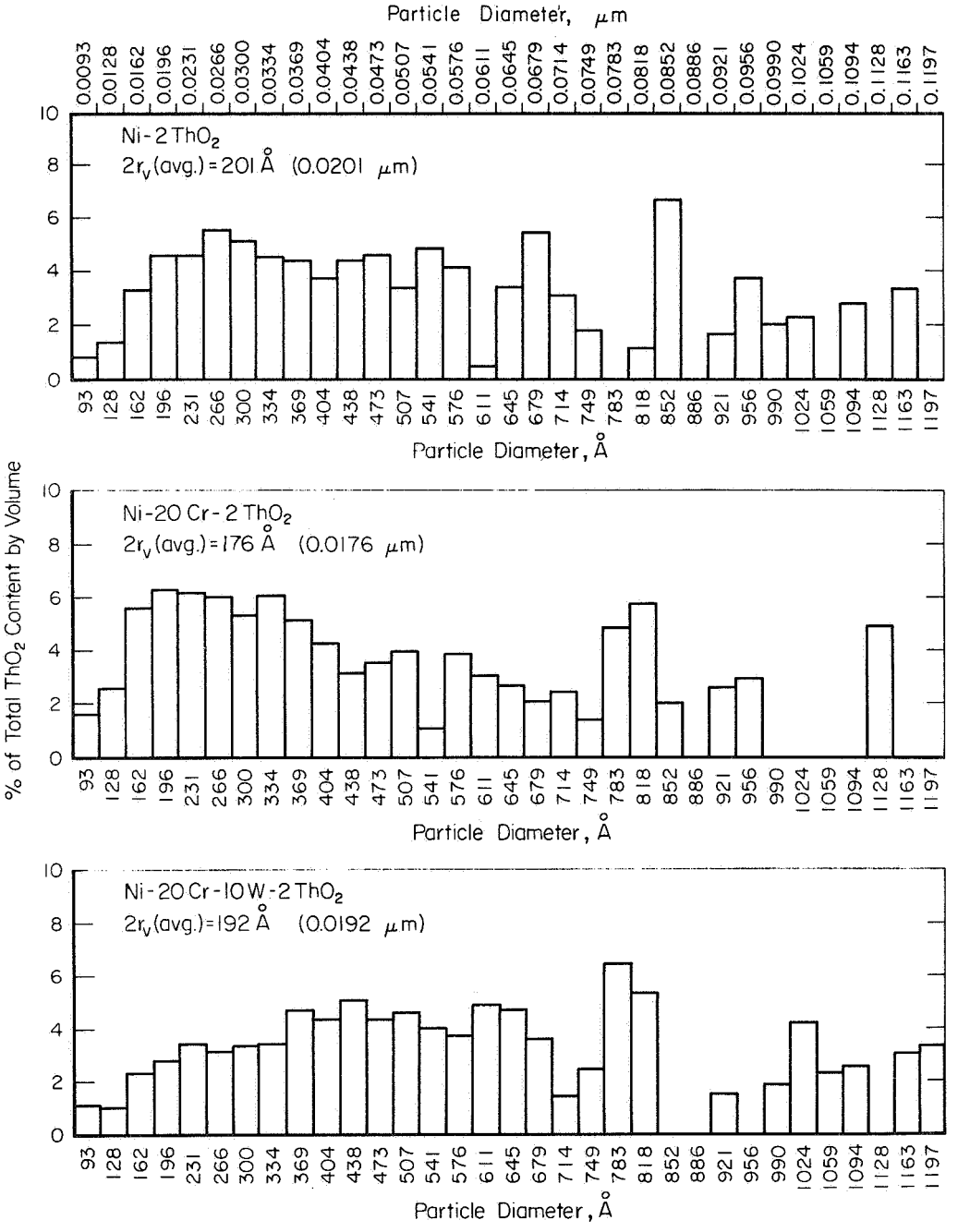

FIGURE 1. Particle size distributions of experimental ThO_2-containing alloys, expressed as volume percent of the total ThO_2 content.

TABLE 2. ThO_2 PARTICLE SIZES AND SPACINGS IN EXPERIMENTAL ALLOYS

Alloy	Analyses				Range[(a)] of Particle Dia., μm	Avg. Particle Dia., μm	Mean Planar Center-to-Center Particle Spacing, μm
	Wt.% Cr	Wt.% W	Wt.% ThO_2	Vol.% ThO_2			
Ni-2ThO_2	--	--	2.9	2.58	0.0093-0.1163	0.0201	0.1505
Ni-20Cr-2ThO_2	20.2	--	2.0	1.70	0.0093-0.1128	0.0176	0.1595
Ni-20Cr-10W-2ThO_2	20.8	9.9	2.8	2.51	0.0093-0.1197	0.0192	0.1670

(a) 2000 particles measured from transmission electron micrographs using a Zeiss Particle Size Analyzer.

Here f_i is the volume fraction of particles in a limited size range having an average particle radius, r_{v_i}. Table 2 shows that the three ThO_2-containing alloys had an average particle size of ~0.02 μm and a mean planar center-to-center particle spacing of ~ 0.16 μm.

Procedures

Thermomechanical Processing

Two types of working, drawing and swaging, were used to process the alloys. Two working procedures were employed, one with no intermediate anneals (hereafter referred to as Procedure A) and the other with intermediate anneals for 1 hour at 1200°C in a hydrogen atmosphere (hereafter referred to as Procedure B). Only wire drawing was used to process the Ni and Ni-2ThO_2 materials, but swaging was used for some of the Cr-containing alloys which proved to be very difficult to work by drawing. Summarized below are the TMP conditions employed for each of the alloys.

Ni and Ni-2ThO_2

Drawing by Procedure A (no intermediate anneals)

Drawing by Procedure B (intermediate anneals after each 50% reduction)

Ni-20Cr and Ni-20Cr-2ThO_2

Drawing and swaging by Procedure A (no intermediate anneals)

Drawing and swaging by Procedure B (intermediate anneals after each 25% reduction)

Ni-20Cr-10W and Ni-20Cr-10W-2ThO_2

Swaging by Procedure B only (intermediate anneals after each 25% reduction).

Both drawing and swaging were done on materials preheated to 200°C. It was found that teflon proved to be the most satisfactory lubricant for wire drawing. Only a limited amount of the Ni-20Cr-10W-2ThO_2 was obtained, so TMP of this alloy (and the Ni-20Cr-10W alloy as well) was confined to swaging by Procedure B. The starting point for Procedure B was extruded plus annealed material. For the alloys drawn or swaged by Procedure B, all examinations (microstructure, tensile and creep tests, and texture) were made after annealing.

Metallography

An integral part of this investigation concerned correlating mechanical properties with microstructure. The major metallographic procedures consisted of optical and transmission electron microscopy (TEM), with selected replica electron microscopy studies. The metallographic and thinning procedures for TEM used in this study were standard, and have been described previously[2,3,5].

Tensile and Creep Testing

All tensile testing was done in an Instron at a strain rate of 0.01 min^{-1}. Two test temperatures, 25 and 1093°C, were used and the high temperature tests were done in a vacuum Brew furnace attached to the Instron. The specimens had threaded ends, and those machined from rod of $\geqslant$ 0.25 inch (0.635 cm) diameter had a 1 inch (2.54 cm) gage length. Specimens machined from smaller diameter rods (to 0.096 inch [0.244 cm] diameter) had a 1/2 inch (1.27 cm) gage length. Axial alignment of all tests was assured by universal joints.

Tension creep tests were made on only the three ThO_2-containing alloys, and at only one temperature, 1093°C. The creep specimens had the same configuration as tensile specimens, and they were tested in a vacuum of 10^{-5} torr ($1.33 \times 10^{-3} N/m^2$) under

constant stress conditions. Additional details of the creep testing procedures have been reported previously[3,6,7].

Texture Measurements

All texture measurements were made at the University of Birmingham, and consisted of measuring complete <200> and <111> pole distributions. From these, the concentrations of the <100> and <111> fiber texture components were determined.

Rods of the thermomechanically processed alloys were mounted in epoxy resin in square section troughs with the specimen axes accurately aligned along the troughs. The composites were transferred to a jig which had slots machined in it at 45° to the long axis of the composite. Slices were then cut through the composite using a jeweller's saw guided within the slots. The slices were ground on one side, polished metallographically and etched in aqua regia to remove all traces of deformation. The final specimens thus had the normal to the prepared surface at 45° to the axis of the bar.

To determine texture in an axi-symmetric material, one requires to know the variation of pole intensity for given crystallographic planes from the axial direction to the radial direction. The specimens prepared as above were mounted on a Siemens texture goniometer so that the specimen could be tilted about an axis which was the radial direction (of the bar) lying in the plane of the section. By tilting the specimen ± 45° about the symmetrical position, the diffracting plane normal was thus varied from the axial to the radial direction. The width of the divergence slits was made great enough so that at any angle of inclination from 0° to 45°, the same total intensity of radiation was incident upon the specimen. The θ and 2 θ angles of the goniometer were set as required for the {111} or {200} reflections using filtered copper Kα radiation. It was observed that as a result of the extreme sharpness of the diffraction peaks on

the axis, deviations of only one or two degrees of alignment of the specimen could lead to large errors in the measured peak height. For this reason, all specimens were finally aligned to give maximum intensity on a sharp axial diffraction peak. The necessary adjustment was never more than three degrees, and typically under one degree. Counts of diffracted intensity were made at 5° intervals of the angle of inclination for periods of 10 seconds while oscillating the specimen in the beam. The background level was measured accurately and subtracted from all measurements.

It may be simply shown that a measured diffracted intensity, I, at an angle, ϕ, to the axial direction represents a volume of material proportional to I Sin ϕ. Thus by summing the value of I Sin ϕ from $\phi = 0^{\circ}$ to $\phi = 90^{\circ}$ and dividing all measurements by this sum, the values are normalized to multiples (and submultiples) of a true random value. This procedure was adopted in the present work. It should perhaps be stressed that the methods described above make no assumption of the existence of fiber textures. It is only assumed that, averaged over the whole specimen, the texture has axial symmetry.

Since the peak intensity values along the axis are very susceptible to error and since, because of the nature of the I Sin ϕ expression, they represent a vanishingly small volume of the material, other quantitative measures of the texture have also been derived. By summing the normalized values of I Sin ϕ between $\phi = 0^{\circ}$ and 10° or 20°, and multiplying by p/2 (where p is the multiplicity of the crystal planes diffracting), one obtains the fraction, or percentage, of material for which the axis lies within 10° or 20° of the crystallographic direction. For example, the value of <111>, 20° indicates the percentage of material for which the axis lies within 20° of <111>.*

---

* For a random sample, <200>, 10° = 4.5%; <200>, 20° = 18%; <111>, 10° = 6%; <111>, 20° = 24%.

In order to study the texture at different depths within the wires, back reflection diffraction patterns were recorded photographically on selected specimens. These were done at the surface and center line positions, or at three intermediate positions. Several specimens were also chemically thinned to 0.01 inch (0.025 cm) diameter, and forward reflection photographs taken to check qualitatively the texture components present at the very center of the wires.

RESULTS AND DISCUSSION

In the discussion of results which follows, it is more convenient to review the Ni and Ni-2ThO_2 results first, followed by a discussion of the four Cr-containing alloys. A General Discussion Section at the end relates all of the observations. In each of the following two sections the discussions center around observations dealing with: microstructure, tensile deformation, creep and creep rupture, and texture.

Ni and Ni-2ThO_2

Microstructure

The microstructures of as-extruded Ni and Ni-2ThO_2 are shown in Figures 2 and 3 respectively.* On cooling from the extrusion temperature of 1093°C, the pure Ni obviously recrystallized (Figure 2a). However, transmission electron microscopy showed that a considerable amount of dislocation substructure still

---

* All of the micrographs in this report are from longitudinal sections. When microstructures appear elongated, the rod axis is parallel to the direction of elongation.

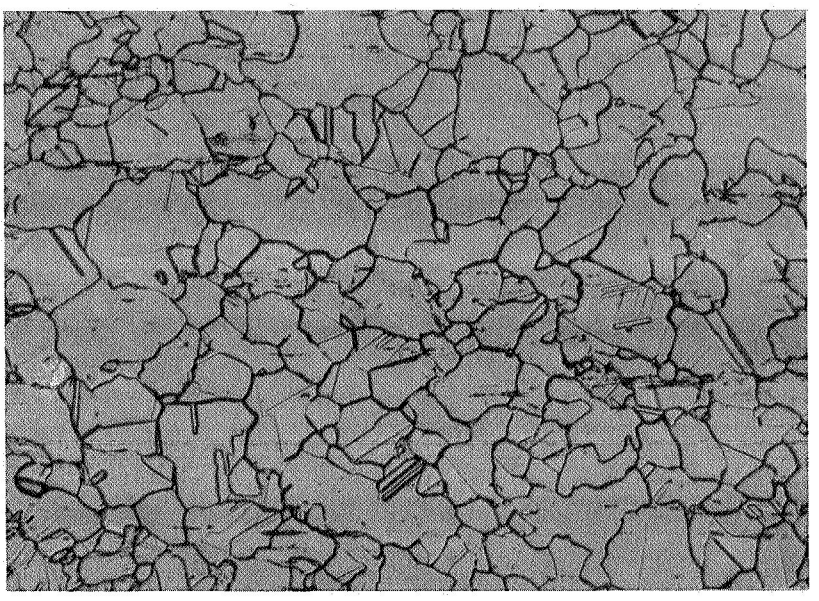

(a) 200X

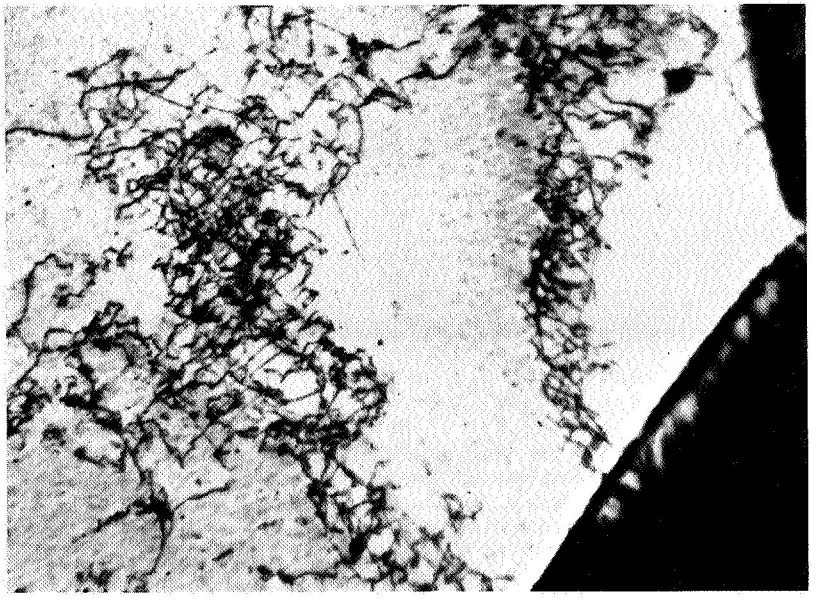

(b) 30,000X

FIGURE 2. Microstructure of as-extruded Ni; (a) optical micrograph, (b) transmission electron micrograph.

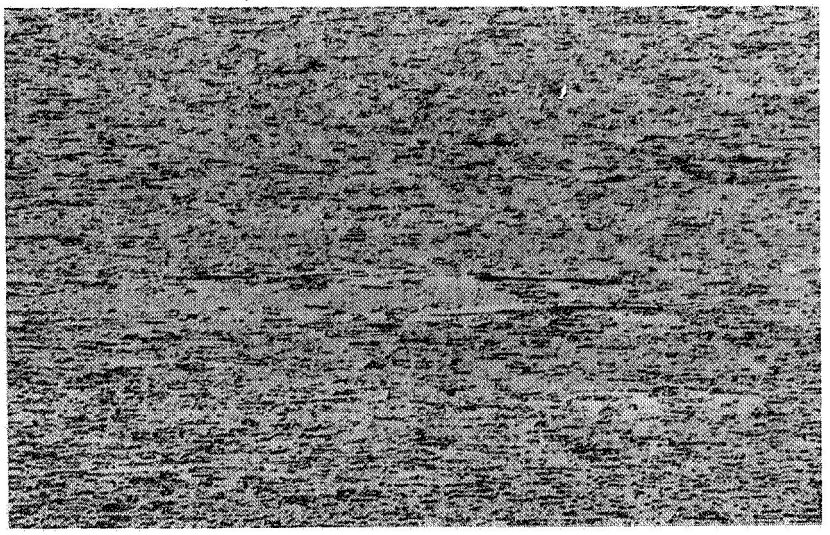

(a) 200X

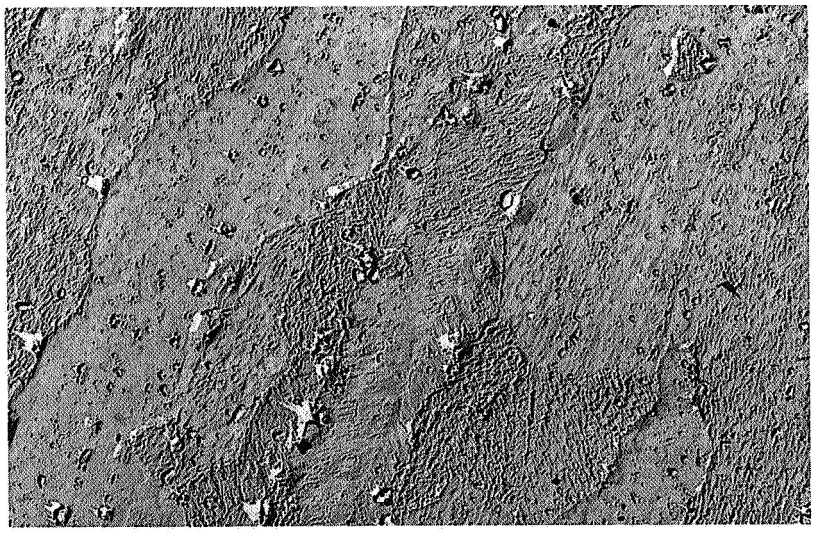

(b) 12,000X

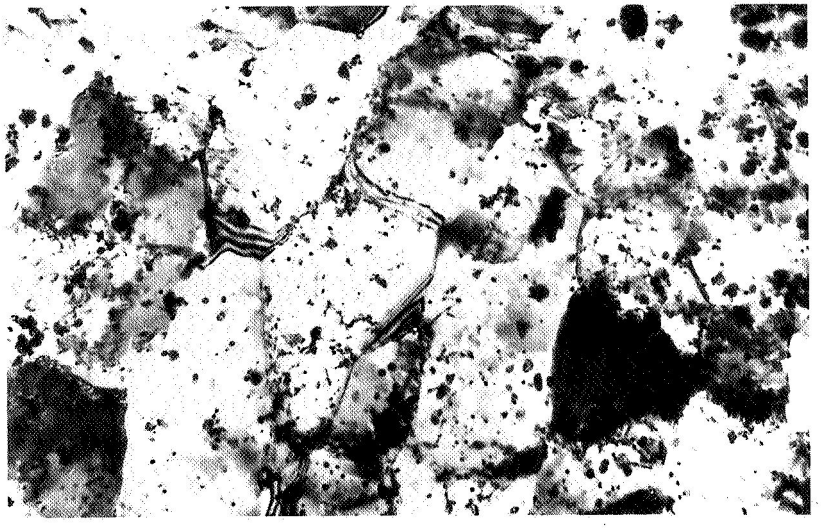

(c) 30,000X

FIGURE 3. Microstructure of as-extruded Ni-2ThO_2; (a) optical micrograph, (b) replica electron micrograph, (c) transmission electron micrograph.

remained (Figure 2b). The as-extruded Ni-2ThO_2 microstructure contained fine, somewhat elongated grains (Figure 3), but the degree of grain elongation in this Ni-2ThO_2 bar was considerably less than that in commercial 1/2-inch (1.27 cm) diameter TD Nickel bar.

After annealing the extruded Ni and Ni-2ThO_2 (the starting point for drawing Procedure B) the resulting microstructures were those shown in Figures 4 and 5. The annealing coarsened the pure Ni grain size somewhat and reduced the amount of dislocation substructure (Figure 4b compared with Figure 2b). TEM showed that many grains in the annealed Ni had no dislocation substructure whatsoever. The transmission micrograph in Figure 5c shows that the anneal coarsened, i.e., recovered, the structure of the Ni-2ThO_2 alloy somewhat, but the optical and replica micrographs in Figure 5 reveal that recrystallization did not occur.

During drawing of the Ni and Ni-2ThO_2 by Procedure A, the grains became increasingly elongated with increasing drawing strain and the spacing between the elongated tangled dislocation cell walls decreased. When the pure Ni was drawn by Procedure B, recrystallization occurred after each anneal, and the resulting grain size varied somewhat with the total drawing strain. After annealing Ni-2ThO_2 specimens drawn by Procedure B, it was found that the cell width remained relatively constant with increasing total drawing strain, which indicates that the worked structure recovered during annealing. The Ni-2ThO_2 drawn 92.5% by Procedure B partially recrystallized ($\sim$ 30%) after the final anneal. The grain sizes and cell diameters are listed in Table 3 as a function of drawing strain for both Ni and Ni-2ThO_2 drawn by Procedures A and B, and representative microstructures in Figures 6-10 illustrate the following features:

Figure 6: Optical micrographs showing increasing cold work as Ni was drawn by Procedure A.

Figure 7: Transmission micrographs showing decreasing cell width as Ni was drawn by Procedure A.

Figure 8. Transmission micrographs showing decreasing grain and cell width as Ni-2ThO_2 was drawn by Procedure A.

Figure 9. Optical micrograph showing recrystallized and non-recrystallized regions of Ni-2ThO_2 drawn 92.5% by Procedure B.

Figure 10. Transmission micrographs showing relative constancy of grain and cell width in Ni-2ThO_2 drawn by Procedure B.

It has been known for a number of years from optical microscopy observations, that deformation causes formation of voids at the interface between coarse particles ($\sim$ 1 μm dia.) and the matrix. In 1966, Palmer and Smith[8] showed by transmission electron microscopy that the same was true for fine particles (0.02-0.04 μm dia.) of SiO2 in Cu, and concurrently Ashby[9] offered a model to account for this behavior. Since then, there have been similar experimental observations of void formation in Ni-2ThO_2[10,11] and Ni-20Cr-2ThO_2[11-13]. In each of these cases the deformations have been fairly heavy, since this is required before the voids are large enough to detect by electron microscopy. A similar observation was made in this study on Ni-2ThO_2 drawn by Procedure A. Figure 11 and Table 4 illustrate how the void length increases with increasing drawing strain. The ratio of void length, X, to particle diameter, 2 r_v, is plotted versus percent reduction by drawing in Figure 12(a) and versus true drawing strain, ϵ_T, in Figure 12(b). The true drawing strain was determined from the usual relation

$$\epsilon_T = \ln[1/(1-RA)] \quad , \tag{3}$$

where RA = fractional reduction in area by drawing. It is seen in Figure 12(b)

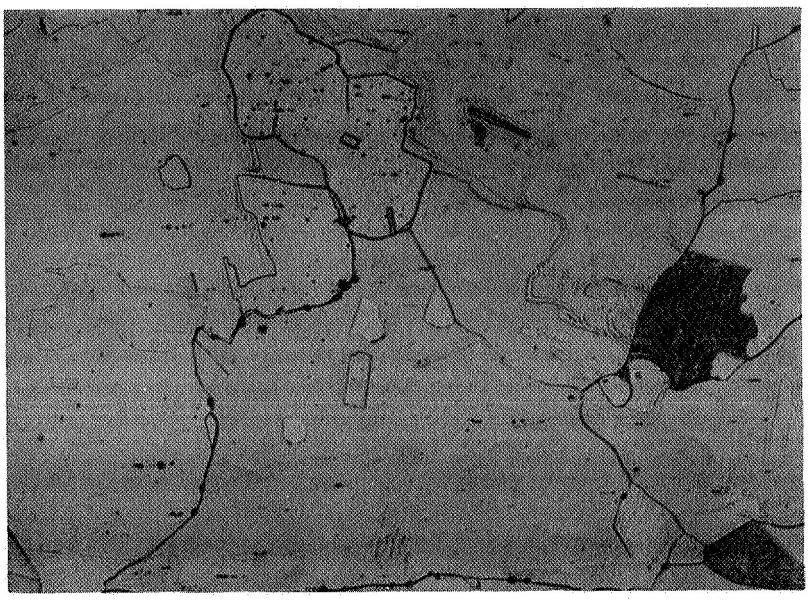

(a) 200X

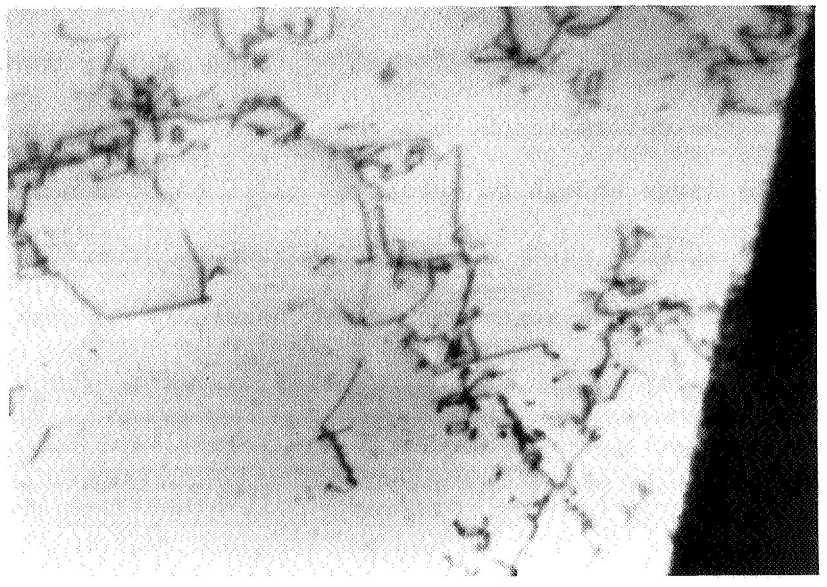

(b) 30,000X

FIGURE 4. Microstructure of extruded-plus-annealed Ni; (a) optical micrograph, (b) transmission electron micrograph.

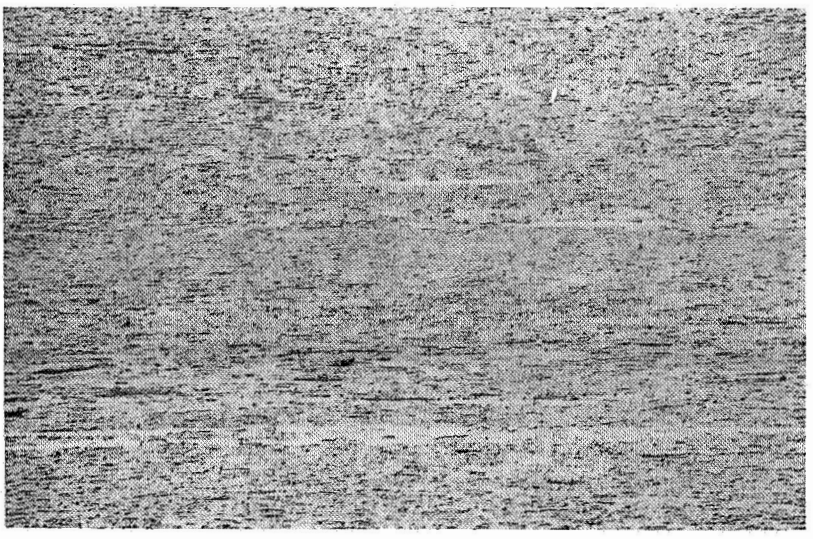

(a) 200X

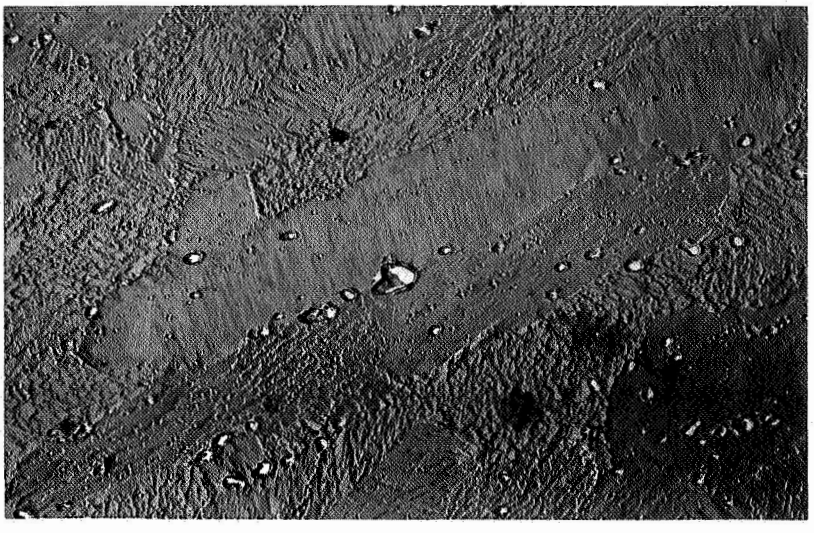

(b) 12,000X

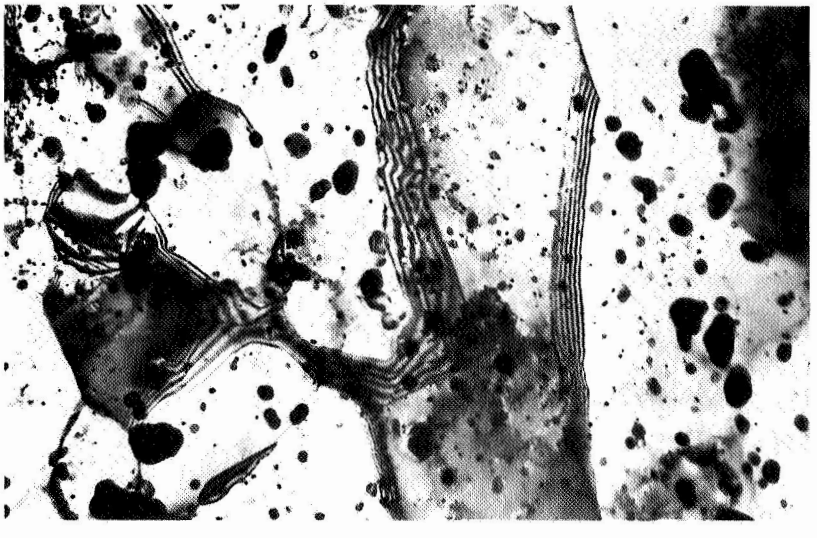

(c) 30,000X

FIGURE 5. Microstructure of extruded-plus-annealed Ni-2ThO_2; (a) optical micrograph, (b) replica electron micrograph, (c) transmission electron micrograph.

TABLE 3. GRAIN SIZE OR CELL SIZE OF Ni AND Ni-2ThO_2 AS A FUNCTION OF DRAWING BY PROCEDURES A AND B

Drawing Procedure	Total Reduction by Drawing, %	Grain or Cell Dia., ℓ, μ m [d]	$\ell^{-1/2}$, μ m$^{-1/2}$	Comments
		Nickel		
As-Extruded	0	2 to 3 [c]	0.71 to 0.58	Recrystallized [c]
A [a]	53.4	0.37	1.64	Not recrystallized, ℓ = cell dia.
A	76.7	0.29	1.85	"
A	88.5	0.23	2.09	"
A	93.4	0.21	2.19	"
Extruded + Ann.	0	70.1	0.12	Recrystallized, ℓ = grain dia.
B [b]	53.4	36.1	0.17	"
B	76.7	23.8	0.21	"
B	88.5	25.9	0.20	"
B	93.4	22.3	0.21	"
		Nickel - 2ThO_2		
As-Extruded	0	0.95	1.02	Not recrystallized, ℓ = cell dia.
A [a]	49.4	0.34	1.71	"
A	73.3	0.26	1.96	"
A	86.8	0.21	2.17	"
A	92.5	0.20	2.24	"
Extruded + Ann.	0	1.13	0.94	"
B [b]	46.5	0.82	1.10	"
B	73.3	0.80	1.12	"
B	86.8	0.80	1.12	"
B	92.5	0.71	1.19	30% recrystallized, ℓ = cell dia. in unrecrystallized region

(a) Drawing Procedure A: Draw at 200°C to indicated total reductions, with no intermediate anneals.

(b) Drawing Procedure B: Draw at 200°C, with intermediate anneals (1200°C, 1 hour, H_2 atm.) after each 50% reduction. Grain and cell size measurements were made on annealed specimens.

(c) This specimen was recrystallized, but had a substantial dislocation cell structure. Here ℓ was taken as the cell diameter.

(d) In heavily drawn material, the "cell size" was taken to be the spacing between the elongated closed cells, or in other words, the diameter of the cell, normal to the rod or wire axis.

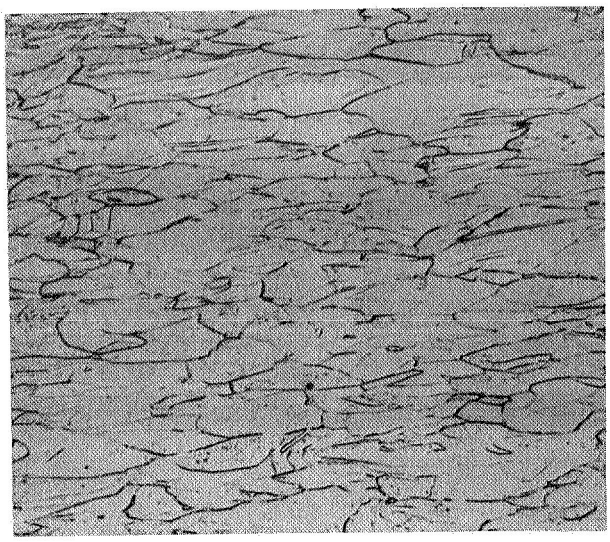

(a) Drawn 53.4% 200X

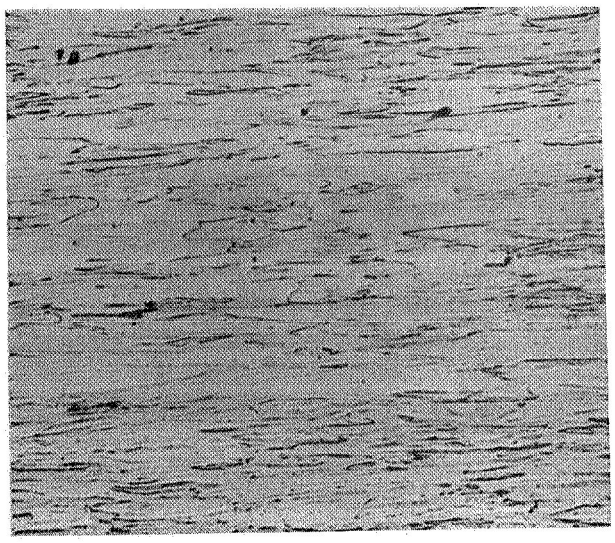

(b) Drawn 76.7% 200X

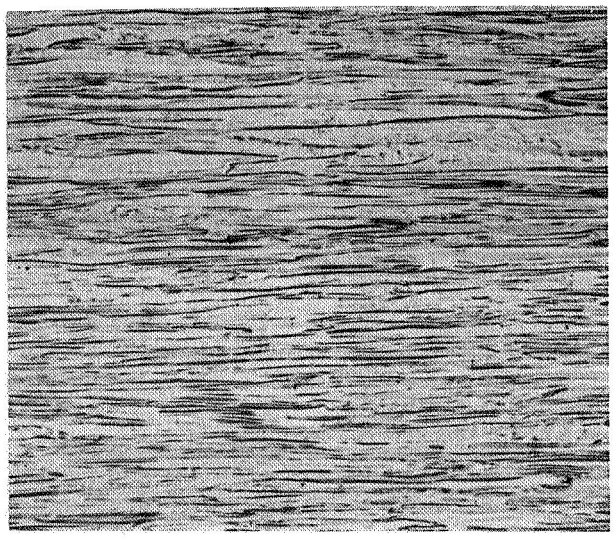

(c) Drawn 88.5% 200X

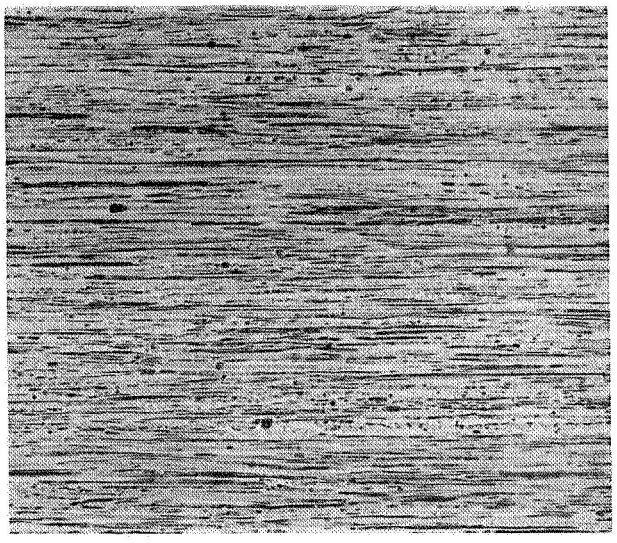

(d) Drawn 93.4% 200X

FIGURE 6. Optical micrographs of Ni drawn by Procedure A (no intermediate anneals).

(a) Drawn 53.4% 30,000X

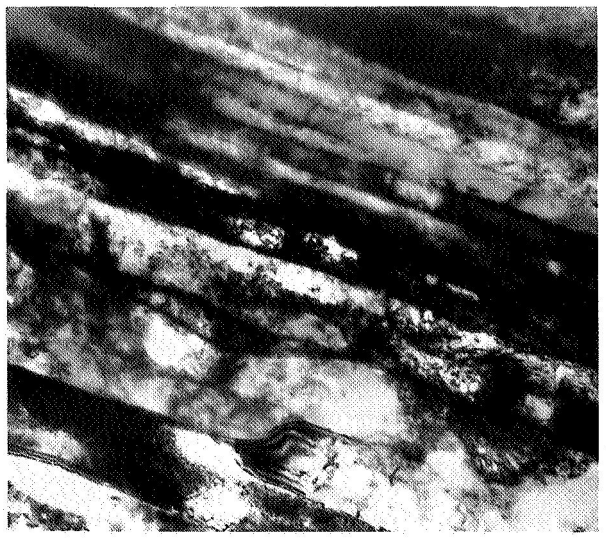

(b) Drawn 93.4% 30,000X

FIGURE 7. Transmission electron micrographs of Ni drawn by Procedure A (no intermediate anneals).

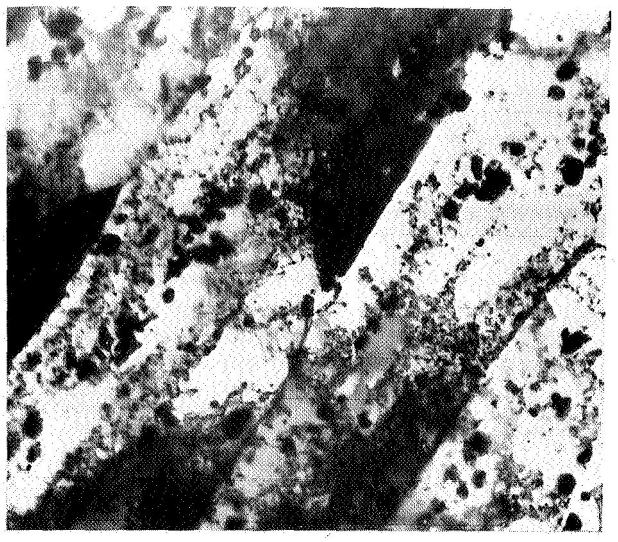

(a) Drawn 49.4% 30,000X

(b) Drawn 92.5% 30,000X

FIGURE 8. Transmission electron micrographs of Ni-2ThO_2 drawn by Procedure A (no intermediate anneals).

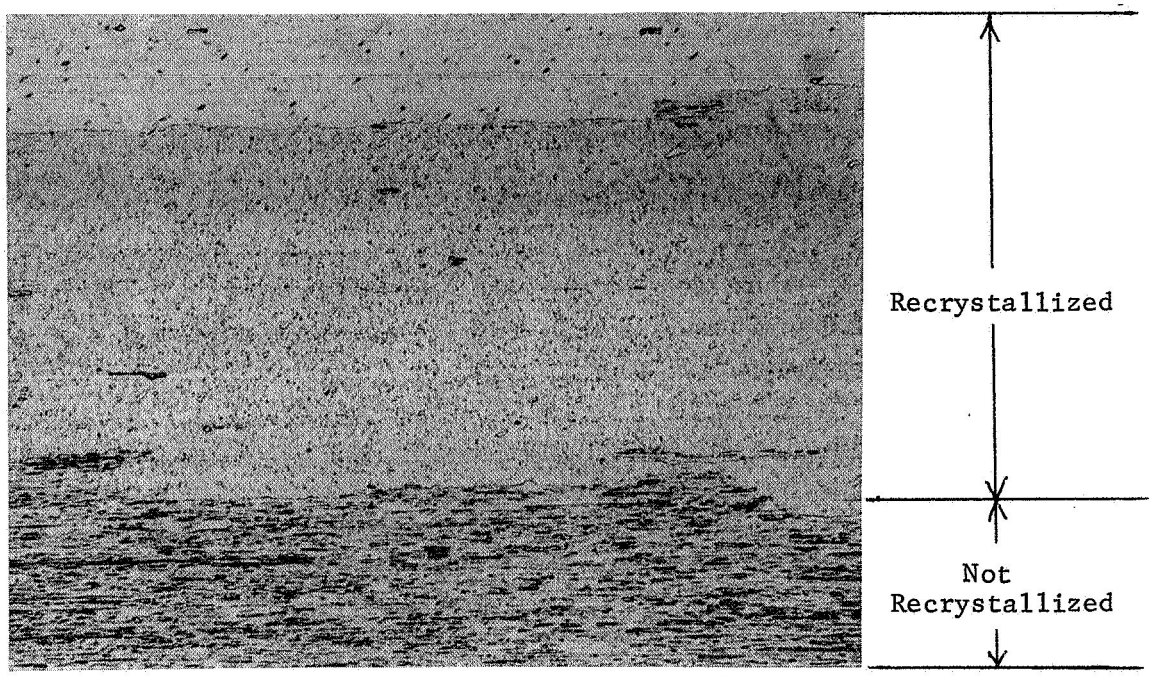

FIGURE 9. Optical micrograph of Ni-2ThO_2, drawn 92.5% by Procedure B. After the final anneal, about 30% of the cross-section had recrystallized.

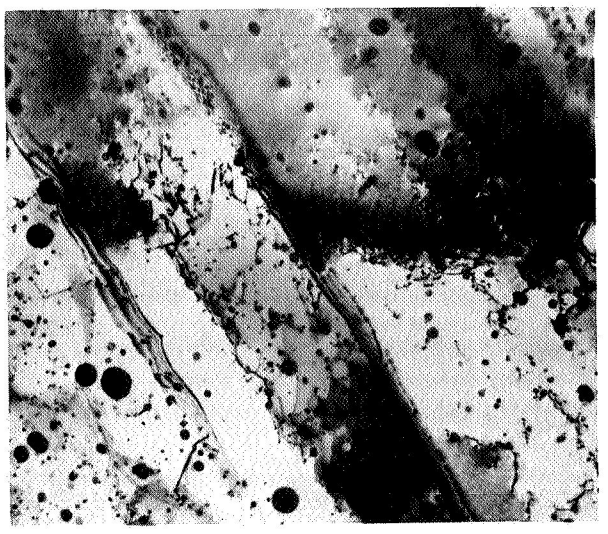

(a) Drawn 46.5% 30,000X

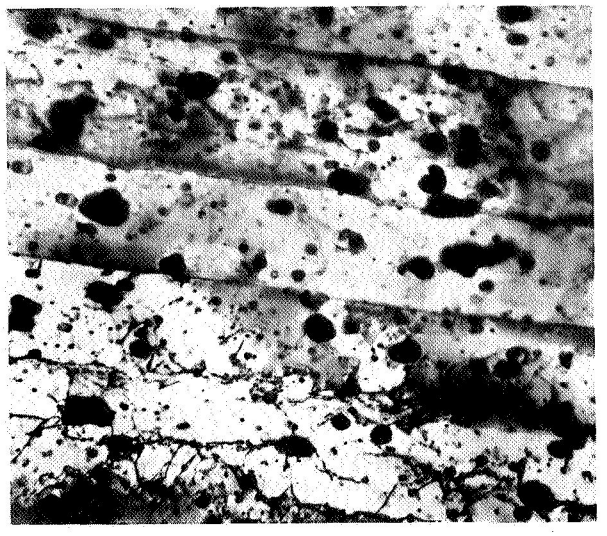

(b) Drawn 92.5% (taken in unrecrystallized region) 30,000X

FIGURE 10. Transmission electron micrographs of Ni-2ThO_2 drawn by Procedure B (intermediate anneals).

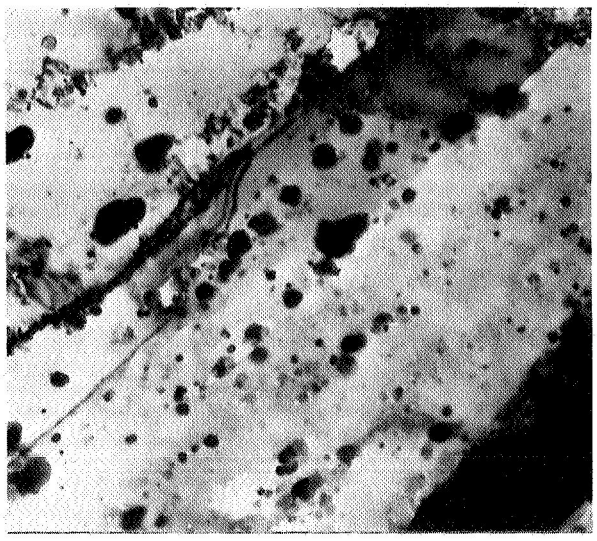

(a) Drawn 46.5% 60,000X

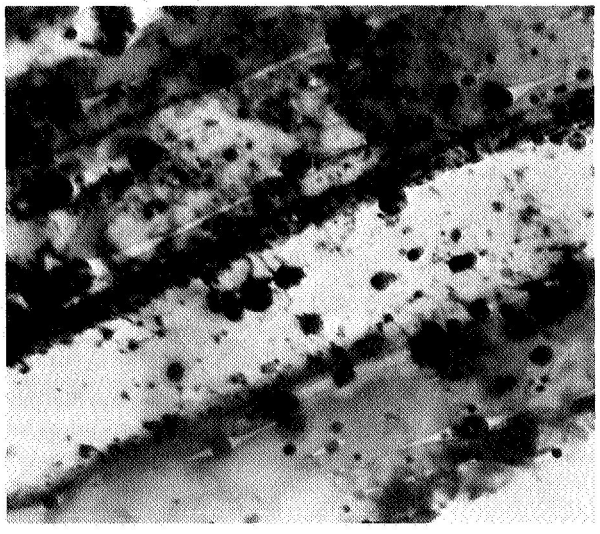

(b) Drawn 86.8% 60,000X

FIGURE 11. Transmission micrographs of Ni-2ThO_2 drawn by Procedure A, illustrating increasing growth of voids at ThO_2 particles with increasing drawing strain.

TABLE 4. AVERAGE RATIO OF VOID LENGTH, X, TO PARTICLE DIAMETER, $2r_v$, IN Ni-2ThO_2 DRAWN BY PROCEDURE A (No intermediate anneals)

Total % Reduction by Drawing	True Drawing Strain	$X/2r_v$ *
As-extruded	0	Voids not detectable by TEM
49.4	0.63	0.47
73.3	1.32	0.55
86.8	2.02	1.43
92.5	2.59	1.69

* Voids were not detected at all of the particles. The $X/2r_v$ values reported are the average of about 50 measurements per condition on those particles which had detectable voids associated with them.

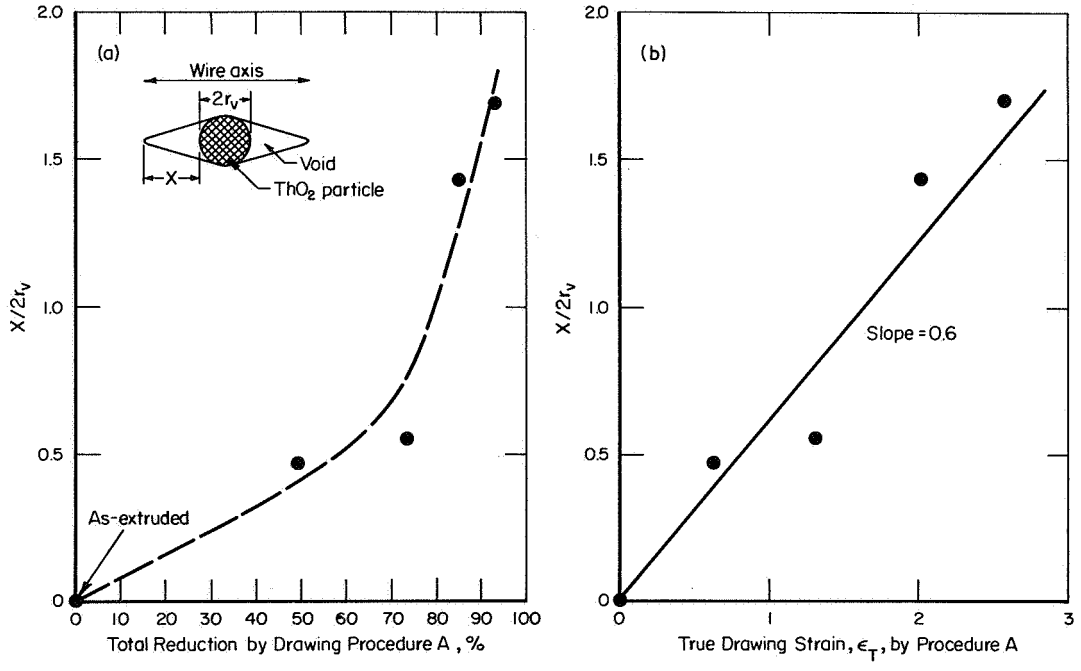

FIGURE 12. Growth of voids at ThO_2 particles during drawing of Ni-2ThO_2 by Procedure A.

that a least-squares straight line can be drawn through the points, which leads to the simple empirical relation

$$X/2r_v = 0.6\ \epsilon_T \quad . \tag{4}$$

In all cases of Ni-2ThO_2 drawn by Procedure B, no voids at the particle-matrix interface were ever detected, e.g., see Figure 10, which indicates that the high temperature anneals were sufficient to heal the voids. This observation is consistent with the fact that particle/matrix voids are not observed in commercial TD Nickel, DS Nickel, or TD Nickel-Chromium. Even though these materials are given repeated deformations during processing, the intermittent and final anneals appear to be sufficient to heal any voids which may have formed, at least to the point where they are not detectable by transmission electron microscopy.

Since there has been no systematic study of the kinetics of void healing in these dispersion strengthened alloys, it is not possible to say what times or temperatures are required to eliminate the voids, or heal them to the point where they are no longer detectable by TEM. Webster[11,13] has suggested that such voids in TD Nickel and TD Nickel-Chromium retard recrystallization and grain growth in these alloys. If the voids heal up rapidly during high temperature annealing, it is likely that they would have no effect whatsoever on recrystallization and grain growth.

Tensile Deformation

The tensile deformation results for Ni and Ni-2ThO_2 are given in Tables 5-8, and strength and ductility are plotted as a function of reduction by drawing in Figures 13-16. Figure 13 shows room temperature tensile results for pure Ni

TABLE 5. TENSILE PROPERTIES OF Ni AT 25 AND 1093°C AFTER DRAWING BY PROCEDURE A
(No intermediate anneals)

Test T, °C	Rod or Wire Dia. in.	Total % Reduction by Drawing	True Drawing Strain	Prop. Lim., psi	0.2% Y.S., psi	U.T.S., psi	RA,%	Uniform Elongation,%	Total Elongation,%
25	0.375 (a)	0	0	27,650	32,250	54,100	71.5	34.9	41.9
25	0.256	53.4	0.76	74,000	82,100	88,500	74.8	0.7	6.1
25	0.181	76.7	1.46	82,000	93,700	94,500	80.6	0.5	11.6
25	0.127	88.5	2.16	86,800	99,000	100,000	75.7	0.6	7.1
25	0.096	93.4	2.72	94,000	106,000	106,000	86.4	0.9	7.3
1093	0.375 (a)	0	0	1,390	1,960	3,200	7.8	5.4	6.3
1093	0.256	53.4	0.76	830	950	1,030	3.4	1.3	3.5
1093	0.181	76.7	1.46	1,170	2,120	2,340	8.2	2.3	8.0
1093	0.127	88.5	2.16	1,760	1,970	2,030	7.4	1.0	6.3
1093	0.096	93.4	2.72	620	780	810	6.7	0.8	9.0

(a) As-extruded.

TABLE 5a. SAME AS TABLE 5, SI UNITS

Test T, °C	Rod or Wire Dia. cm	Total % Reduction by Drawing	True Drawing Strain	Prop. Lim., MN/m^2	0.2% Y.S., MN/m^2	U.T.S., MN/m^2	RA, %	Uniform Elongation, %	Total Elongation, %
25	0.952[a]	0	0	191	221	373	71.5	34.9	41.9
25	0.650	53.4	0.76	512	567	611	74.8	0.7	6.1
25	0.460	76.7	1.46	566	647	653	80.6	0.5	11.6
25	0.323	88.5	2.16	600	684	690	75.7	0.6	7.1
25	0.244	93.4	2.72	649	732	732	86.4	0.9	7.3
1093	0.952[a]	0	0	9.6	13.5	22.1	7.8	5.4	6.3
1093	0.650	53.4	0.76	5.7	6.6	7.1	3.4	1.3	3.5
1093	0.460	76.7	1.46	8.1	14.6	16.1	8.2	2.3	8.0
1093	0.323	88.5	2.16	12.1	13.6	14.0	7.4	1.0	6.3
1093	0.244	93.4	2.72	4.3	5.4	5.6	6.7	0.8	9.0

(a) As-extruded.

TABLE 6. TENSILE PROPERTIES OF Ni AT 25 AND 1093°C AFTER DRAWING BY PROCEDURE B (Intermediate anneals, 1 hour, 1200°C, H_2 atm, after each 50-percent reduction by drawing). All specimens were tested in annealed condition.

Test T, °C	Rod or Wire Dia. in.	Total % Reduction by Drawing	True Drawing Strain	Prop. Lim., psi	0.2% Y.S., psi	U.T.S., psi	RA,%	Uniform Elongation,%	Total Elongation,%
25	0.375[a]	0	0	3,690	5,490	48,000	56.6	34.0	35.6
25	0.256	53.4	0.76	10,800	13,300	41,000	26.9	15.0	15.0
25	0.181	76.7	1.46	13,900	16,750	39,300	44.4	18.0	19.0
25	0.127	88.5	2.16	15,600	19,500	46,000	73.7	27.0	28.5
25	0.096	93.4	2.72	20,600	26,100	49,700	85.1	31.4	36.5
1093	0.375[a]	0	0	--	3,510	3,810	6.0	3.0	5.5
1093	0.256	53.4	0.76	1,140	1,410	1,510	4.4	0.6	1.5
1093	0.181	76.7	1.46	1,900	2,220	2,330	4.5	2.5	3.3
1093	0.127	88.5	2.16	1,490	2,290	2,330	3.6	1.0	3.1
1093	0.096	93.4	2.72	990	1,490	1,680	6.5	1.5	2.7

(a) As-extruded plus annealed.

TABLE 6a. SAME AS TABLE 6, SI UNITS

Test T °C	Rod or Wire Dia. cm	Total % Reduction by Drawing	True Drawing Strain	Prop. Lim., MN/m^2	0.2% Y.S., MN/m^2	U.T.S., MN/m^2	RA,%	Uniform Elongation,%	Total Elongation,%
25	0.952[a]	0	0	25.5	37.8	331	56.6	34.0	35.6
25	0.650	53.4	0.76	74.5	91.8	283	26.9	15.0	15.0
25	0.460	76.7	1.46	95.8	115.0	271	44.4	18.0	19.0
25	0.323	88.5	2.16	108.0	135.0	307	73.7	27.0	28.5
25	0.244	93.4	2.72	142.0	180.0	343	85.1	31.4	36.5
1093	0.972[a]	0	0	--	24.2	26.0	6.0	3.0	5.5
1093	0.650	53.4	0.76	2.9	9.7	10.4	4.4	0.6	1.5
1093	0.460	76.7	1.46	13.1	14.6	16.1	4.5	2.5	3.3
1093	0.323	88.5	2.16	10.3	15.8	16.1	3.6	1.0	3.1
1093	0.244	93.4	2.72	6.8	10.3	11.6	6.5	1.5	2.7

(a) As-extruded plus annealed.

TABLE 7. TENSILE PROPERTIES OF Ni-2ThO_2 AT 25 AND 1093°C AFTER DRAWING BY PROCEDURE A
(No intermediate anneals)

Test T, °C	Rod or Wire Dia. in	Total % Reduction by Drawing	True Drawing Strain	Prop. Lim., psi	0.2% Y.S., psi	U.T.S., psi	RA,%	Uniform Elongation,%	Total Elongation,%
25	0.350 (a)	0	0	56,230	68,460	80,110	74.6	8.8	15.1
25	0.249	49.4	0.68	80,400	98,700	101,000	67.4	1.4	7.6
25	0.181	73.3	1.32	92,000	107,000	112,000	60.1	2.3	14.4
25	0.127	86.8	2.02	97,500	117,500	124,500	62.5	2.3	9.9
25	0.096	92.5	2.59	104,000	122,000	130,000	65.4	1.8	8.2
1093	0.350 (a)	0	0	2,030	4,300	4,990	11.3	3.2	7.6
1093	0.249	49.4	0.68	9,370	11,550	13,000	11.4	1.9	5.2
1093	0.181	73.3	1.32	8,600	11,700	16,400	11.5	1.8	2.9
1093	0.127	86.8	2.02	17,900	20,100	20,900	7.6	1.6	2.0
1093	0.096	92.5	2.59	19,800	22,900	23,500	11.1	0.5	0.8

(a) As extruded.

TABLE 7a. SAME AS TABLE 7, SI UNITS

Test T °C	Rod or Wire Dia. cm	Total % Reduction by Drawing	True Drawing Strain	Prop. Lim., MN/m^2	0.2% Y.S., MN/m^2	U.T.S., MN/m^2	RA,%	Uniform Elongation,%	Total Elongation,%
25	0.889[(a)]	0	0	388	473	562	74.6	8.8	15.1
25	0.632	49.4	0.68	563	680	697	67.4	1.4	7.6
25	0.460	73.3	1.32	635	739	773	60.1	2.3	14.4
25	0.323	86.8	2.02	673	811	858	62.5	2.3	9.9
25	0.244	92.5	2.59	717	841	897	65.4	1.8	8.2
1093	0.889[(a)]	0	0	14.0	29.7	34.5	11.3	3.2	7.6
1093	0.632	49.4	0.68	64.5	79.6	89.7	11.4	1.9	5.2
1093	0.460	73.3	1.32	59.3	80.7	113.0	11.5	1.8	2.9
1093	0.323	86.8	2.02	123.0	139.0	144.0	7.6	1.6	2.0
1093	0.244	92.5	2.59	137.0	158.0	162.0	11.1	0.6	0.8

(a) As-extruded.

TABLE 8. TENSILE PROPERTIES OF Ni-2ThO_2 AT 25 AND 1093°C AFTER DRAWING BY PROCEDURE B (Intermediate anneals 1 hour, 1200°C, H_2 atm., after each 50 percent reduction by drawing). All specimens were tested in annealed condition.

Test T, °C	Rod or Wire Dia. in.	Total % Reduction by Drawing	True Drawing Strain	Prop. Lim., psi	0.2% Y.S., psi	U.T.S., psi	RA,%	Uniform Elongation,%	Total Elongation,%
25	0.350 (a)	0	0	52,970	62,750	77,180	76.9	8.3	15.8
25	0.256	46.5	0.63	54,700	64,500	80,000	80.3	8.4	15.0
25	0.181	73.3	1.32	61,200	71,600	81,000	75.1	7.3	20.5
25	0.127	86.8	2.02	61,000	70,300	82,700	76.1	6.5	16.7
25	0.096 (b)	92.5	2.59	53,600	62,700	78,600	51.3	7.5	13.0
1093	0.350 (a)	0	0	2,460	5,160	5,500	14.9	2.2	8.7
1093	0.256	46.5	0.63	7,380	9,450	9,880	15.4	1.8	3.6
1093	0.181	73.3	1.32	9,070	11,800	13,300	8.7	1.7	4.0
1093	0.127	86.8	2.02	14,600	16,600	17,200	3.6	1.0	2.6
1093	0.096 (b)	92.5	2.59	15,000	17,100	17,400	4.0	0.7	2.2

(a) As-extruded plus annealed.

(b) 30% recrystallized.

TABLE 8a. SAME AS TABLE 8, SI UNITS

Test T, °C	Rod or Wire Dia. cm	Total % Reduction by Drawing	True Drawing Strain	Prop. Lim., MN/m^2	0.2% Y.S., MN/m^2	U.T.S., MN/m^2	RA,%	Uniform Elongation,%	Total Elongation,%
25	0.889[a]	0	0	365	433	531	76.9	8.3	15.8
25	0.650	46.5	0.63	376	445	552	80.3	8.4	15.0
25	0.460	73.3	1.32	422	494	558	75.1	7.3	20.5
25	0.323	86.8	2.02	421	484	570	76.1	6.5	16.7
25	0.244[b]	92.5	2.59	370	432	542	51.3	7.5	13.0
1093	0.889[a]	0	0	17.0	35.6	37.9	14.9	2.2	8.7
1093	0.650	46.5	0.63	51.0	65.2	68.2	15.4	1.8	3.6
1093	0.460	73.3	1.32	62.5	81.5	91.7	8.7	1.7	4.0
1093	0.323	86.8	2.02	101.0	114.0	119.0	3.6	1.0	2.6
1093	0.244[b]	92.5	2.59	103.0	118.0	120.0	4.0	0.7	2.2

(a) As-extruded plus annealed.

(b) 30% recrystallized.

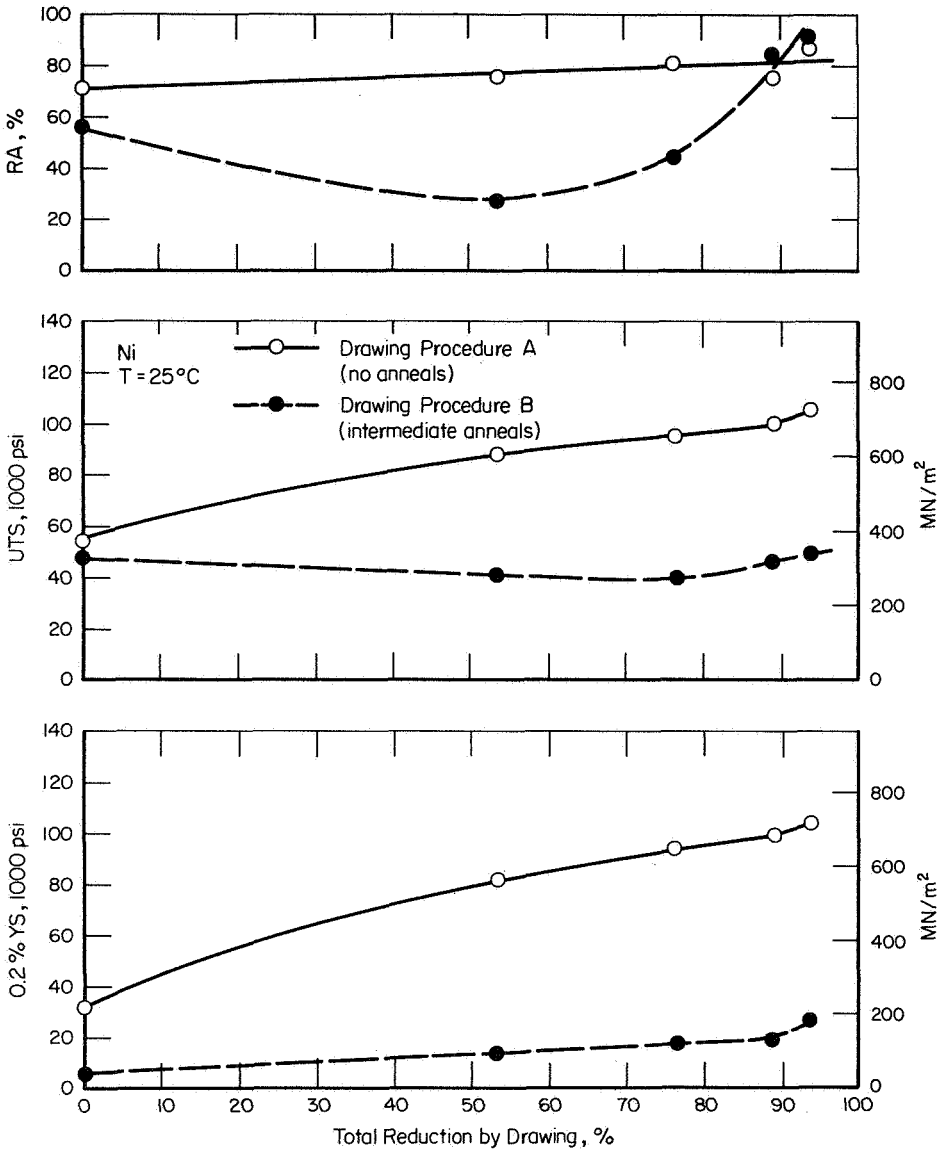

FIGURE 13. Effect of drawing by Procedures A and B on tensile properties of Ni at 25°C.

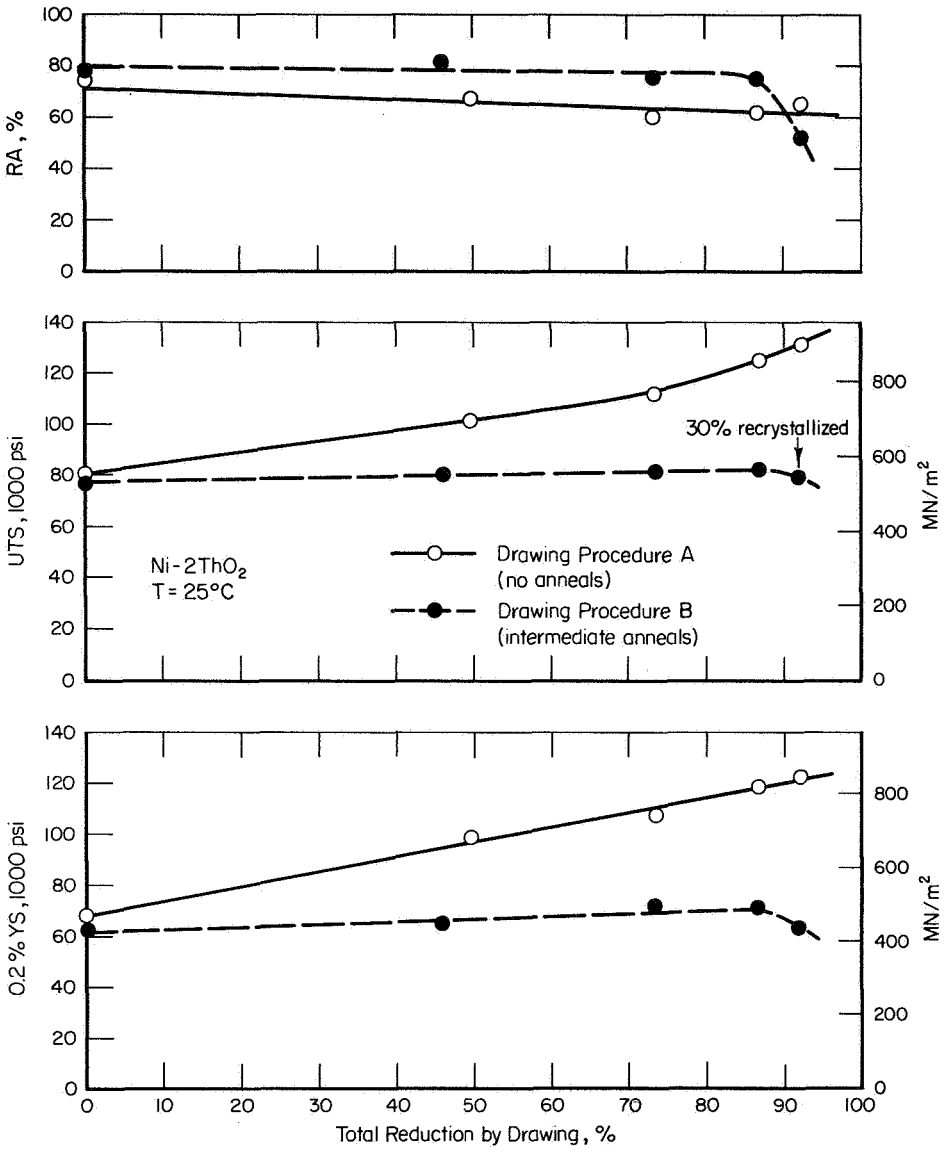

FIGURE 14. Effect of drawing by Procedures A and B on tensile properties of Ni-2ThO_2 at 25°C.

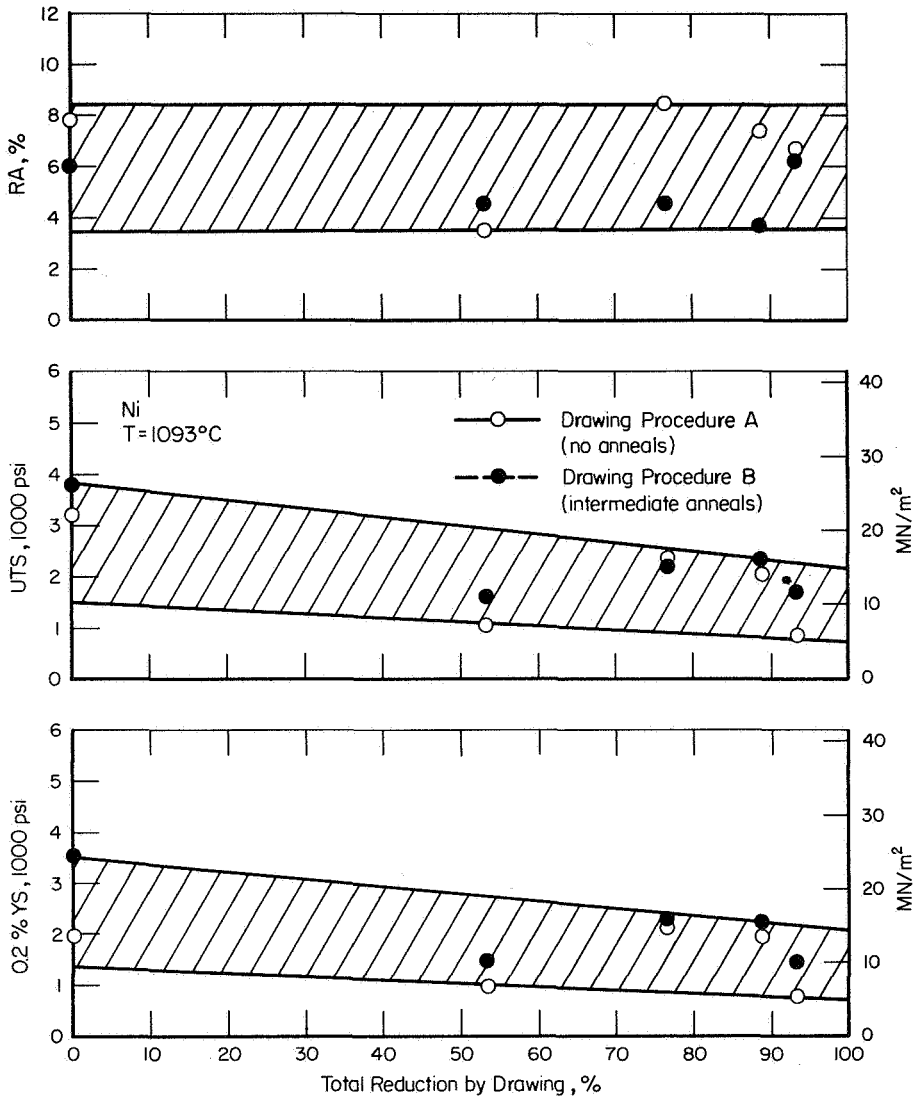

FIGURE 15. Effect of drawing by Procedures A and B on tensile properties of Ni at 1093°C.

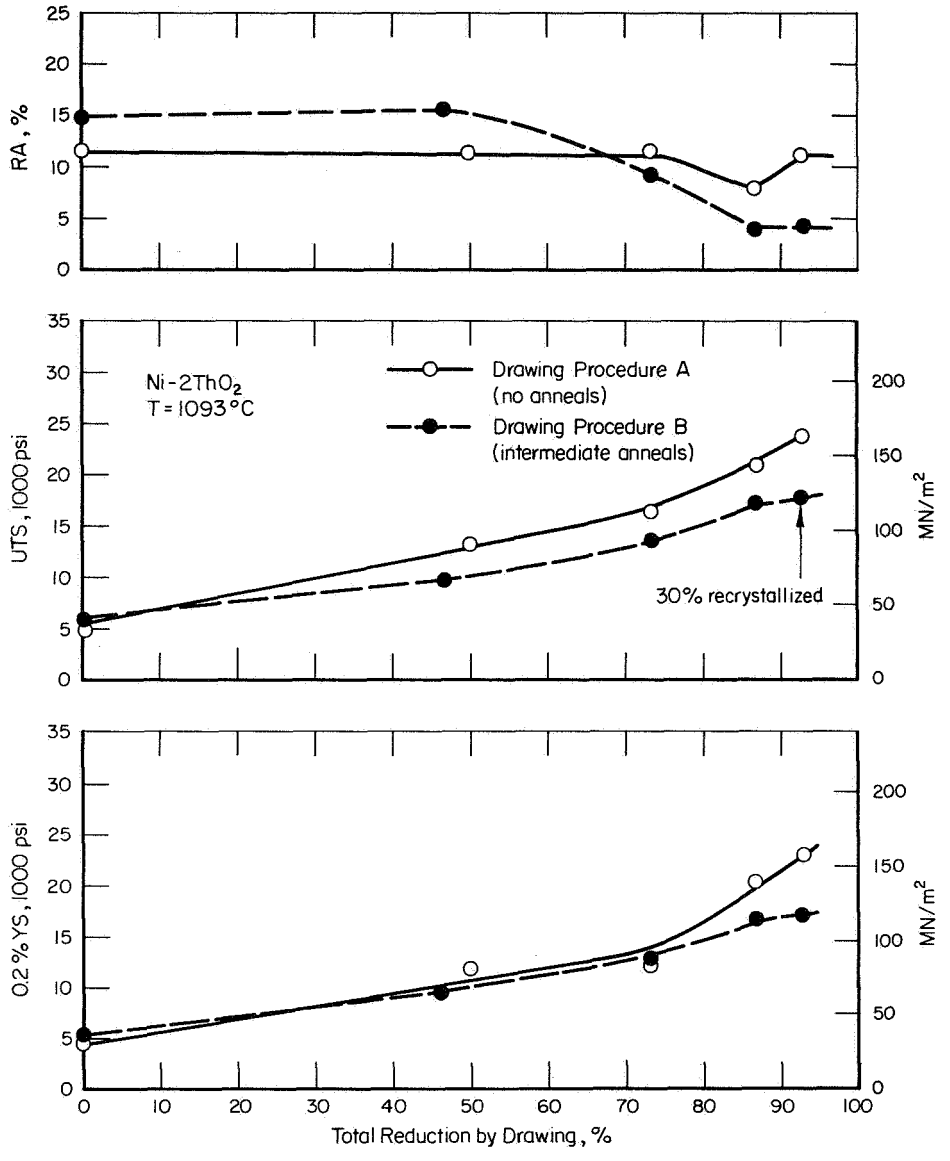

FIGURE 16. Effect of drawing by Procedures A and B on tensile properties of Ni-2ThO_2 at 1093°C.

after having been drawn by Procedures A and B. After drawing by Procedure A (no intermediate anneals) the yield and ultimate strengths increased with increasing drawing strain. This is in accord with previous observations on drawn ferrous alloys[14-17], Mo-TZM[18], and W[19], where it has been shown that the strengthening results from substructure refinement. The same explanation is relevant here, e.g., see Figure 7 and Table 3. When pure Ni was drawn by Procedure B, recrystallization occurred after each anneal, and thus the room temperature strengths in Figure 13 remained relatively constant. The slight variation in yield strength resulted mainly from a variation in the recrystallized grain size.

Figure 14 shows that drawing influenced the room temperature strength of Ni-2ThO_2 in a similar fashion. When drawn by Procedure A the strength increased as the substructure was refined. The same general trend in room temperature strength as a function of drawing strain has been previously reported by Tracey and Worn[20] and Worn and Marton[21] on an experimental Ni-2.5 weight percent ThO_2 alloy. However, when drawn by Procedure B, the intermediate anneals recovered the structure (see Figure 10 and Table 3) such that the spacing between the elongated cells and grains remained relatively constant. Thus, the room temperature strength in Figure 14 was essentially constant. The slight decrease in yield strength after 92.5% drawing reduction was due to the fact that this specimen was about 30% recrystallized, as shown in Figure 9.

Tensile results on pure Ni at 1093°C are shown in Figure 15. There is little difference in strength between material drawn by Procedures A and B, presumably because specimens drawn by Procedure A recrystallized during heat-up to the test temperature and during tensile deformation. In Figure 16 it is seen that the yield and ultimate strength of Ni-2ThO_2 at 1093°C increase with increasing drawing strain after drawing by <u>both</u> Procedures A and B. The highest strengths

were achieved for specimens drawn by Procedure A. The specimen drawn 92.5% by Procedure A was examined metallographically after tensile testing at 1093°C and it had not recrystallized. A somewhat surprising observation in Figure 16 is that the strength of the Ni-2ThO_2 drawn by Procedure B increased with increasing drawing strain, whereas the room temperature strength was relatively constant (Figure 14) and there was no large variation in cell width (Table 3). An explanation of this behavior is given later.

The influence of grain size and cell diameter on the room temperature proportional limit, $\sigma_{P.L.}$, and 0.2% yield strength, $\sigma_{Y.S.}$, of Ni and Ni-2ThO_2 was examined in terms of the Hall-Petch analysis;

$$\sigma = \sigma_o + k\ell^{-1/2} \quad , \tag{5}$$

where ℓ = grain or cell size. The results are plotted in Figure 17 as $\sigma_{P.L.}$ versus $\ell^{-1/2}$ and Figure 18 as $\sigma_{Y.S.}$ versus $\ell^{-1/2}$. Equation (5) is obeyed in both cases, and the slopes, or k values, for the pure Ni plots are greater than the corresponding values for Ni-2ThO_2 in both Figures 17 and 18. Included in these figures are additional results from the literature on pure Ni[2,22-24] and Ni-2ThO_2[2,22].

The convergence of the Ni and Ni-2ThO_2 proportional limit plots in Figure 17 is more pronounced than the corresponding 0.2% yield strength plots in Figure 18. The extrapolated point of convergence in Figure 17 would correspond to $\ell^{-1/2} = 2.8\ \mu m^{-1/2}$, or $\ell = 0.128\ \mu m$, which is close to the mean planar edge-to-edge paeticle spacing of the 0.134 μm in the Ni-2ThO_2 alloy. This result suggests that when the cell spacings of the Ni and Ni-2ThO_2 alloys are of the order of the interparticle spacing of the Ni-2ThO_2 alloy, the strengths of both materials, as measured by the proportional limit, are the same. This result seems eminently

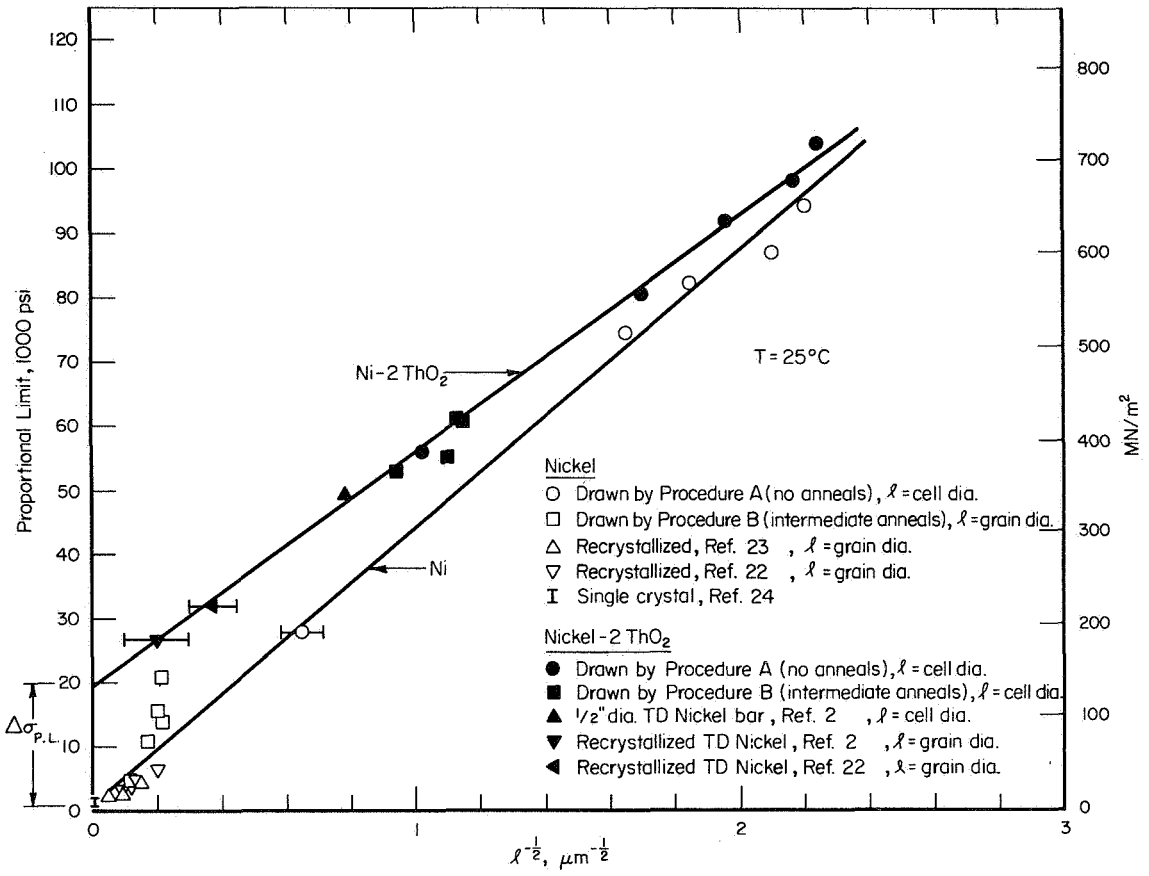

FIGURE 17. Dependence of room temperature proportional limit of Ni and Ni-2ThO_2 on grain size and cell size produced by drawing Procedures A and B. The value of $\Delta \sigma_{P.L.}$ at $\ell^{-1/2} = 0$ is 18,500 psi (128 MN/m^2).

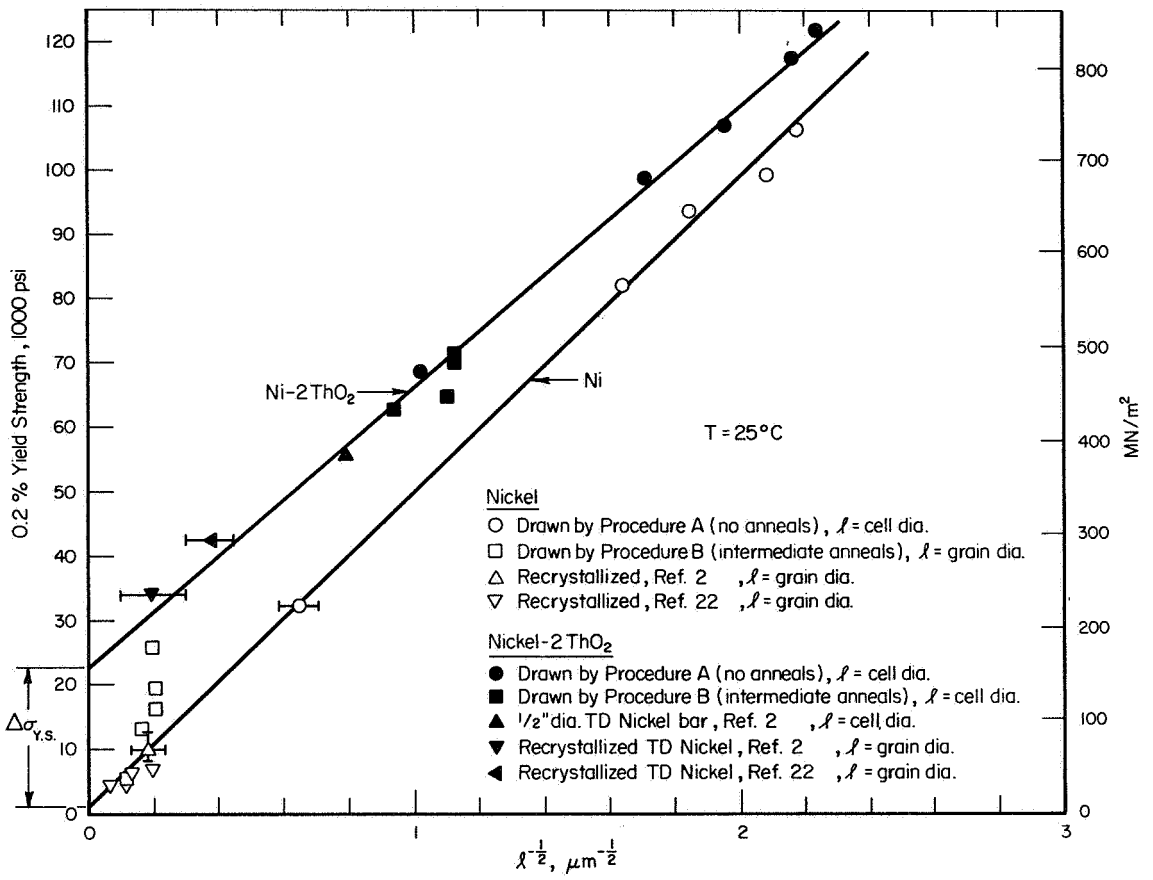

FIGURE 18. Dependence of room temperature yield strength (0.2% offset) of Ni and Ni-2ThO$_2$ on grain size and cell size produced by drawing Procedures A and B. The value of $\Delta \sigma_{Y.S.}$ at $\ell^{-1/2} = 0$ is 21,000 psi (145 MN/m^2).

reasonable, since here the average spacing between barriers to dislocation motion, whether they are particles or cell boundaries, is about the same for both materials.

The 0.2% yield strength versus $\ell^{-1/2}$ plots of Ni and Ni-2ThO_2 in Figure 18 converge at a smaller cell size, $\ell \approx 0.07$ μm, than the corresponding proportional limit plots in Figure 17. A possible explanation is that the particles in Ni-2ThO_2 enhance work hardening, even in the first 0.2% plastic strain and even for material with very closely spaced cell boundaries. The increment in measured stress associated with this enhanced work hardening has the effect of displacing $\sigma_{Y.S.}$ with respect to $\sigma_{P.L.}$ more for Ni-2ThO_2 than for pure Ni. This then causes the yield strength plots to converge at a larger $\ell^{-1/2}$ than the proportional limit plots.

At infinite grain size, i.e., $\ell^{-1/2} = 0$, the increment in strength due to ThO_2 particles is greatest, and the values of $\Delta\sigma_{P.L.}$ and $\Delta\sigma_{Y.S.}$ in Figures 17 and 18 are 18,500 psi (128 MN/m^2) and 21,000 psi (145 MN/m^2), respectively. These values correspond to the level of strengthening expected if the Orowan mechanism of hardening by non-deforming particles were operative. Ashby's[9] model of the Orowan strengthening contribution gives:

$$\tau_p = \frac{0.85\,\varphi\,G\,b}{2\pi\,\lambda}\,\ell n\left[\frac{r_s}{b}\right] . \qquad (6)$$

The definition of terms and the appropriate parameters for the Ni-2ThO_2 alloy are:

τ_p = shear stress increment due to Orowan particle hardening

G = shear modulus of matrix = 11.75 x 10^6 psi (81.1 x 10^3 MN/m^2) at 25°C[25]

b = magnitude of the Burger's vector

r_s = average planar particle radius = $(\sqrt{2/3})$ (r_v) = 82 Å (0.0082 μm)

λ = mean planar edge-to-edge particle spacing = d-2r_s, where d = mean planar center-to-center particle spacing; λ = 1340 Å (0.134 μm)

φ = averaging factor for screw and edge dislocations[26] = 1.23.

After converting to tensile stress, the calculated value of σ_p is 25,400 psi (175 MN/m^2). If the calculation is made for the case of only edge dislocations bowing between particles[9], the result is σ_p = 20,600 psi (142 MN/m^2).

It is of interest to compare the relative room temperature hardening capability of second phase particles with that of grain or cell boundaries. Starting with a single crystal of pure Ni, an increase of 21,000 psi (145 MN/m^2) in the 0.2% tensile yield strength can be achieved by adding 2.58 vol.% of randomly spaced ThO_2 particles having an average particle diameter of 0.02 μm, i.e., a mean planar edge-to-edge particle spacing of 0.134 μm. From Figure 18, it is seen that the same increment in strength can be achieved by grain boundaries or tangled dislocation cells which have a spacing of 5.17 μm; i.e., $\ell^{-1/2} = 0.44\ \mu m^{-1/2}$. Another way of examining this is to determine the expected increase in yield strength of pure Ni if the boundaries had the same spacing as particles in Ni-2ThO_2 (0.134 μm). Extrapolating the pure Ni results in Figure 18 to $\ell^{-1/2} = 2.73\ \mu m^{-1/2}$, it is found that a yield strength increment of 133,500 psi (921 MN/m^2) is realized, compared with the 21,000 psi (145 MN/m^2) achieved by particles which had the same edge-to-edge spacing as the boundaries. Thus, for a given spacing between boundaries or between particles, boundaries are more than six times as potent in raising the room temperature yield strength than are particles.

At this point it is worth examining the concept of additive strengthening mechanisms which has been proposed by Webster[13] and Hansen and Lilholt[27]. Webster considered 0.2% offset yield strength results for Ni, Ni-2ThO_2, Ni-20Cr, and Ni-20Cr-2ThO_2, and Hansen and Lilholt have reviewed the literature for a number of materials, e.g., SAP-type alloys, dispersion strengthened Ni and Ni-Cr alloys, ferrous alloys, and dispersion strengthened Zr. Both came to the conclusion that strengthening at room temperature by dispersions, solid solution

additions, and refinement of grain size and dislocation substructure could be considered additive. This led Hansen and Lilholt to propose the following relation for the 0.2% offset yield strength:

$$\sigma_{0.2\%\ Y.S.} = \sigma_o + \sigma_p + \sigma_{gb} + \sigma_{sol} \quad , \tag{7}$$

where σ_{sol} = strength increment due to solid solution additions, σ_{gb} = strength increment arising from grain or cell boundaries, σ_p = strength increment (Orowan contribution) due to second phase particles, and σ_o can be considered the 0.2% yield strength of a pure base-metal single crystal. Considering, for the moment, Equation (7) without solid solution strengthening effects, the following relation should hold:

$$\sigma_{0.2\%\ Y.S.} = \sigma_o + \sigma_p + k\ell^{-1/2} \quad . \tag{8}$$

Yet, from Figure 18, it is seen that the particle contribution, σ_p, diminishes as $\ell^{-1/2}$ increases, i.e., $\sigma_p = f(\ell^{-1/2})$. Thus, Equation (8) is not strictly valid. However, for grain or cell sizes in the range corresponding to $\ell^{-1/2} \approx 0$ to 1.2 $\mu m^{-1/2}$ Equation (8) is a reasonable approximation. In fact, Webster and Hansen and Lilholt were led to the additivity conclusion by their plots of σ versus $\ell^{-1/2}$ over approximately this $\ell^{-1/2}$ range, where it was possible to draw <u>parallel</u> lines for dispersion-containing and dispersion-free alloys of the same base composition.

In an attempt to ascertain whether the substructure refinement played a similar role in strengthening at high temperatures, the Hall-Petch analysis was applied to the Ni-2ThO_2 results for tensile tests at 1093°C. Figure 19 is a plot of the 0.2% yield strength of Ni-2ThO_2 at 1093°C as a function of $\ell^{-1/2}$. Here it is seen that there is a great deal of scatter, and thus no good correlation between yield strength and $\ell^{-1/2}$.

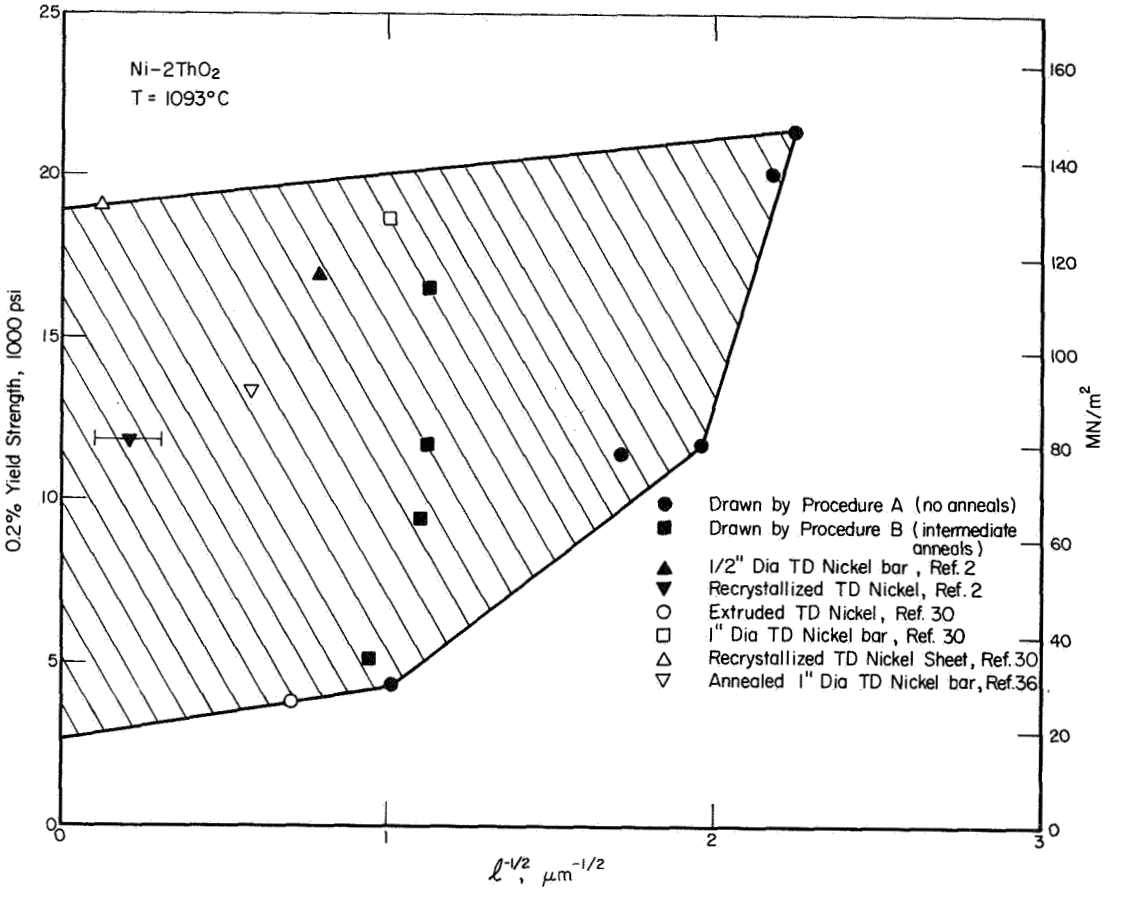

FIGURE 19. Dependence of 0.2% offset yield strength on grain or cell size for Ni-2ThO_2 tested at 1093°C.

It became apparent, however, that the high temperature yield strength did relate to the shape of the grains or cells, and in fact, $\sigma_{Y.S.}$ was proportional to the grain aspect ratio; i.e., ratio of grain or cell length, L, to grain or cell width, ℓ. Table 9 lists values of L/ℓ for some of the Ni-2ThO_2 specimens examined in this study, together with previous results on TD Nickel bar[2,3,30,36] and recrystallized TD Nickel which contained very coarse elongated grains.[2,30] From the available micrographs, it was not possible to determine L/ℓ for all of the Ni-2ThO_2 specimens examined in this program. In particular, if the ratios were $\gtrsim 12$, it was impossible to obtain an accurate measure of the grain length, L. However, the available data are plotted in Figure 20(a) as $\sigma_{Y.S.}$ versus L/ℓ, and an excellent correlation is obtained. Similar correlations with stress-rupture and creep behavior are obtained in Figures 20(b) and (c), respectively, and this will be discussed later.

An important feature of Figure 20(a) is the observation that the two data points for recrystallized TD Nickel fit the curve. These materials had coarse elongated grains[2,30], compared with very fine elongated grains for the other points in Figure 20(a). Thus, in this case, the grain fineness or coarseness is not measurably important as far as influencing the yield strength at 1093°C. Instead, the grain aspect ratio appears to be the dominant factor.

A physical interpretation of Figure 20(a) is that grain boundary sliding plays an important role in high temperature yielding. Wilcox and Clauer[3] previously suggested this to be the case for high temperature creep of TD Nickel bar, and Fraser and Evans[29] and Doble, et al.[30] felt that grain boundary sliding was the predominant mechanism for yielding of Ni-ThO_2 alloys tensile tested at high temperatures. When most of the grain boundaries are parallel to the stress axis, i.e., a highly elongated microstructure, there is, on average,

TABLE 9. 0.2% YIELD STRENGTH, 100 HOUR RUPTURE STRESS, AND STRESS TO GIVE A MINIMUM CREEP RATE OF 10^{-4} hr^{-1} OF Ni-2ThO_2 AT 1093°C AS A FUNCTION OF L/ℓ. L = GRAIN OR CELL LENGTH, ℓ = GRAIN OR CELL DIAMETER

Condition	L/ℓ	0.2% Y.S., psi	Stress to Give a Minimum of Creep Rate of 10^{-4} hr^{-1}, psi	100 Hour Rupture Stress, psi	Means of Determining L/ℓ[a]
As-extruded	1.7	4,300	--	--	TEM, REM
Extruded and annealed (1 hr, 1200°C, H_2 atm)	2.9	5,160	2,180	2,510	TEM, REM
Drawn 49.4% by Procedure A	7.9	11,550	--	--	TEM
Drawn 73.3% by Procedure B	7.8	11,800	7,760	7,730	TEM
Recrystallized TD Nickel Sheet[d] (Refs. 2,28)	8.7	11,900	9,000	--	OM
1/2" dia TD Nickel bar (Refs. 2,3)	12.5 ± 2.5[b]	17,000	16,300	14,000	TEM, REM
Extruded TD Nickel (Ref. 30)	~ 2[c]	3,840	--	--	REM
1" dia TD Nickel bar (Ref. 30)	~ 15[c]	18,650	--	--	REM
Recrystallized TD Nickel Sheet[d] (Ref. 30)	~ 13[c]	~ 19,100	--	--	OM
Annealed 1" dia TD Nickel bar (Ref. 36)	~ 10[c]	13,300	--	--	OM

(a) TEM = transmission electron microscopy; REM = replical electron microscopy; OM = optical microscopy.

(b) Scatter in 1/2" dia TD Nickel bar due to uncertainty in measuring grain length, L.

(c) Values are approximate, since measurements of L/ℓ were made from only one micrograph in paper or report.

(d) When L/ℓ was determined for sheet, the value of ℓ was that measured from micrographs of the longitudinal sheet thickness.

TABLE 9a. SAME AS TABLE 9, SI UNITS

Condition	L/ℓ	0.2% Y.S., MN/m^2	Stress to Give a Minimum of Creep Rate of 10^{-4} hr^{-1} MN/m^2	100 Hour Rupture Stress, MN/m^2	Means of Determining L/ℓ[a]
As-extruded	1.7	29.7	--	--	TEM, REM
Extruded and annealed (1 hr, 1200°C, H_2 atm)	2.9	35.6	15.1	17.3	TEM, REM
Drawn 49.4% by Procedure A	7.9	79.6	--	--	TEM
Drawn 73.3% by Procedure B	7.8	81.3	53.5	53.3	TEM
Recrystallized TD Nickel Sheet[d] (Refs. 2,28)	8.7	82.2	62.1	--	OM
1.27 cm dia. TD Nickel bar (Refs. 2,3)	12.5 ± 2.5[b]	117.0	113.0	96.5	TEM, REM
Extruded TD Nickel (Ref. 30)	~ 2.0[c]	26.5	--	--	REM
2.54 cm TD dia. TD Nickel bar (Ref. 30)	~ 15.0[c]	129.0	--	--	REM
Recrystallized TD Nickel Sheet[d] (Ref. 30)	~ 13.0[c]	~ 132.0	--	--	OM
Annealed 2.54 cm dia. TD Nickel bar (Ref. 36)	~ 10.0[c]	91.7	--	--	OM

(a) TEM - transmission electron microscopy; REM - replica electron microscopy; OM = optical microscopy.

(b) Scatter in 1.27 cm dia. TD Nickel bar due to uncertainty in measuring grain length, L.

(c) Values are approximate, since measurements of L/ℓ were made from only one micrograph in paper or report.

(d) When L/ℓ was determined for sheet, the value of ℓ was that measured from micrographs of the longitudinal sheet thickness.

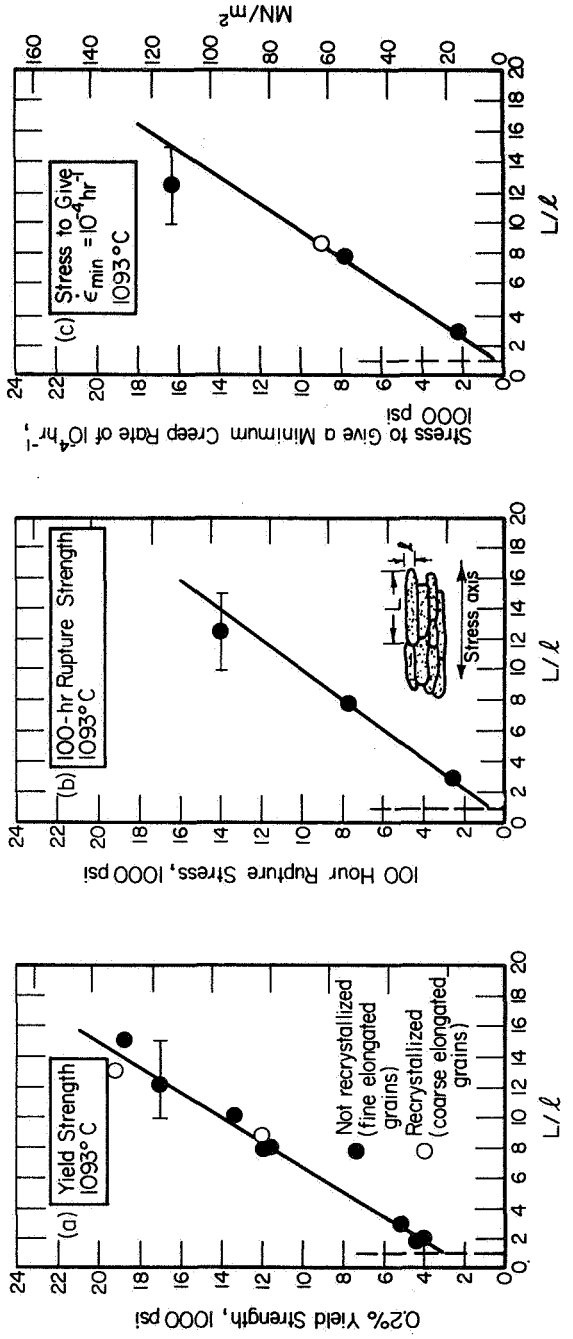

FIGURE 20. The effect of grain or cell aspect ratio, L/ℓ, in Ni-2ThO_2 on strength properties at 1093°C: (a) 0.2% offset yield strength, (b) 100-hour rupture strength, and (c) stress to give a minimum creep rate of $10^{-4}hr^{-1}$. See Table 9 for a description of specimen conditions.

a low resolved shear stress on the boundaries. This minimizes the overall amount of sliding. The maximum sliding would occur when the grain aspect ratio was unity (equiaxed grains). It is probable that a coarse equiaxed structure would have better high temperature strength than a fine equiaxed structure, because having fewer boundaries would reduce the total amount of sliding. Thus, there can be a grain size effect at high temperatures. The observation that the two recrystallized TD Nickel data points fit the $\sigma_{Y.S.}$ versus L/ℓ plot in Figure 20(a) suggests that any grain size difference here has a second order effect on the yield strength, compared with the influence of the grain aspect ratio. The grain elongation effect should be apparent at temperatures above $\sim 0.5\ T_m$ ($\sim 600^{\circ}C$ for Ni-2ThO_2) since here there can be a significant contribution of grain boundary sliding to the total deformation.

At $1093^{\circ}C$ it appears that sliding plays a dominant role, although certainly accommodation deformation* within grains must occur. At lower temperatures, approaching $0.5T_m$, or at much higher strain rates, it is expected that there would be a larger relative contribution of grain interior deformation to macroscopic yielding. Although there are not enough data presently available to quantitatively assess this in the case of Ni-ThO_2 alloys, Figure 21 schematically depicts the anticipated behavior. Here L/ℓ is plotted horizontally, but it is assumed that the grain width, ℓ, is constant. If this assumption were not made, then complications would arise because at higher rates and lower temperatures grain size strengthening would be superimposed on the grain aspect ratio effect. The interplay between grain size strengthening and deformation due to grain boundary sliding might be similar to the effects observed in dispersion strengthened zinc by

---

* It is assumed that diffusional accommodation processes are too slow to be important during yielding.

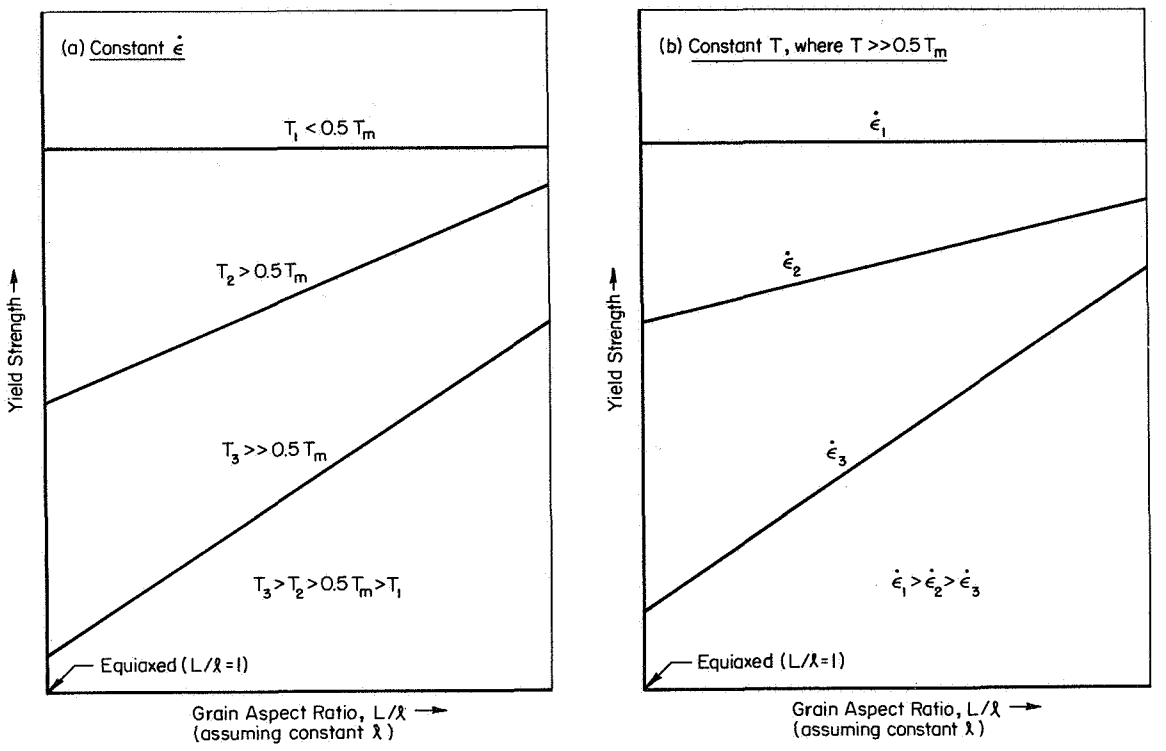

FIGURE 21. Schematic plots showing how test temperature and strain rate may influence the relation between yield strength and grain aspect ratio, L/ℓ, in Ni-ThO_2 alloys.

Tromans and Lund[31]. In Figure 21(a), there is no influence of aspect ratio at $T_1 < 0.5\ T_m$. This curve would be shifted to higher stresses as temperature is further lowered, or as ℓ was decreased at constant T and constant L/ℓ; i.e., the usual Hall-Petch strengthening. At $T_2 > 0.5\ T_m$ grain boundary sliding assumes some importance in yielding, and here there is an effect of grain aspect ratio. At still higher temperatures $T_3 \gg 0.5\ T_m$, grain boundary sliding contributions to yielding become much more important, and the influence of L/ℓ on the yield

strength is more pronounced. At these very high temperatures (1093°C in the case of Ni-2ThO_2) grain width, ℓ, is not significantly important from the Hall-Petch strengthening point of view, since most of the macroscopic yielding occurs by boundary sliding.

Similarly, Figure 21(b) reveals the anticipated effects of strain rate at $T \gg 0.5\ T_m$. For very high rates of deformation, $\dot{\epsilon}_1$, grain boundary sliding may not occur, and hence there is no effect of aspect ratio on yield strength. Here there would be an effect on strength due to grain width, ℓ. At progressively lower strain rates, $\dot{\epsilon}_2$ and $\dot{\epsilon}_3$, sliding would become more pronounced, and there would be a larger influence of aspect ratio on yield strength.

The conclusion that an elongated grain structure is desirable for high temperature strength is not new. For example, workers in the lamp filament industry have known for many years that doped tungsten, which recrystallizes to a coarse elongated grain structure, is far superior to undoped tungsten, which recrystallizes with an equiaxed grain structure. The benefit of doping is derived in part from enhanced creep resistance due to the elongated grain structure. Also, Ver Snyder and Guard[32] obtained directional grain structures in a cast Ni-Cr-Al alloy, and found improved high temperature ductility and creep rupture behavior compared with the same alloy having an equiaxed grain structure. Bourne, et al[72] dispersion strengthened Pt and Pt alloys with a number of oxides and carbides. They produced stable elongated grains by thermomechanical processing, with grain aspect ratios as high as 12.5, and they found that high temperature creep rupture life, t_r, increased with increasing L/ℓ. For example, in a thermomechanically processed Pt-0.04% TiC alloy they found the following results: at 1400°C and 700 psi (4.8 MN/m^2) t_r = 800 hours for $L/\ell = 5$ and t_r = 1200 hours for $L/\ell = 12.5$. Recently, Benjamin[33] and Benjamin and Cairns[34] reported a new superalloy development involving "mechanical

alloying" which allowed them to combine γ' hardening for low temperature strength with oxide dispersion strengthening for high temperature strength. Their material was hot extruded, and when recrystallized it had a coarse, very elongated grain structure. In this condition, the ultimate tensile strength at 1093°C was equivalent to that of TD Nickel bar. Prior to this development, Cook, et al.[35], produced in sheet form a Ni-base alloy strengthened by γ' which also contained ThO_2 particles. Their material had low temperature strength equivalent to Nimonic 80-A in the heat-treated condition, but at high temperatures ($\gtrsim$ 950°C), the usual ThO_2 particle strengthening was not achieved. The microstructure contained fine, nearly-equiaxed grains, and the primary mode of deformation at high temperatures was probably grain boundary sliding. Because pronounced sliding took place at relatively low stresses, compared with that required to produce macroscopic matrix yielding, the potential ThO_2 strengthening was not utilized.

At this point it is relevant to compare the present results on Ni-ThO_2 with the work of previous investigations[20,29,30] which have related thermomechanical processing by drawing and swaging to room temperature and high temperature strength properties. This is done in Figure 22, which shows plots of ultimate strength at 25, 871, and 1093°C as a function of reduction by drawing or swaging. Ultimate strength, rather than yield strength, is plotted since several of the previous investigations reported only this property. Also included in Figure 22 are results from the present study and from the work of Fraser and Evans[29] on the influence of drawing on grain and cell size. The room temperature strength of Ni-2ThO_2 drawn by Procedure A increases with increasing drawing strain in the same general fashion as the earlier work of Tracey and Worn[20], and this is associated with substructure refinement. However, the strength at 871°C[29] and 1093°C[30] behaves somewhat differently from the results obtained on this program.

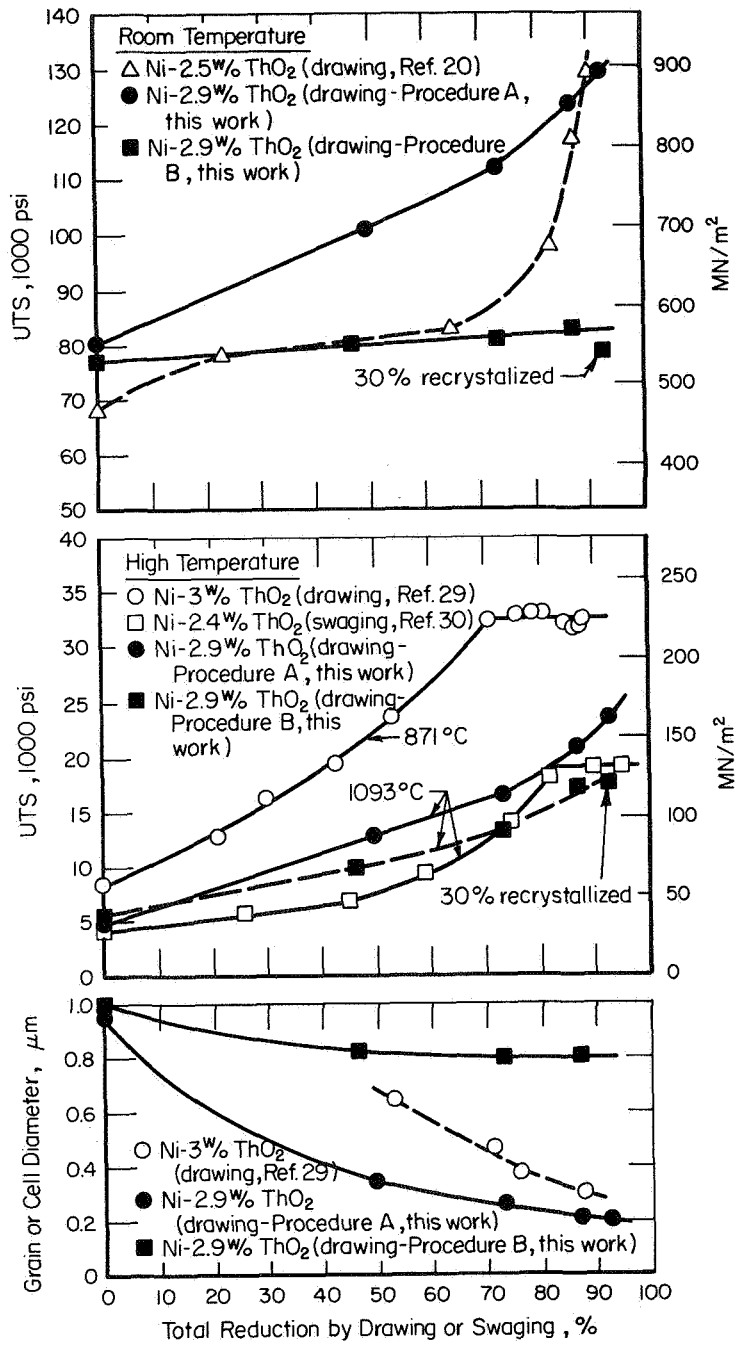

FIGURE 22. Room temperature and high temperature strength, and grain size of Ni-2ThO_2 alloys as a function of reduction by drawing or swaging. Results of this work are compared with those of previous investigators, and in each case the starting material was extruded bar.

Figure 22 shows that after ~ 70% reduction by drawing, the strength at 871°C remains constant with further working. Also, after swaging, the strength at 1093°C remains constant for strains greater than ~ 85%. However, the strengths at 1093°C of Ni-2ThO_2 drawn by Procedures A and B in this study continue to increase with increasing drawing strains up to ~ 93%. A possible explanation for this difference is that Fraser and Evans[29] and Doble, et al.[30], reached a constant grain aspect ratio at high working reductions, but this did not occur in the present study.

In a previous study, Wilcox and Jaffee[2] found that ThO_2 particles in recrystallized TD Nickel produced an increase in yield strength, compared with pure polycrystalline nickel, over the entire temperature range 25 to 1200°C. The increase in $\sigma_{0.2\%\ Y.S.}$ above that of pure Ni was 22,000 (152 MN/m^2) psi at 25°C and 9000 psi (62.1 MN/m^2) at 1200°C. The recrystallized TD Nickel had coarse elongated grains, with an $L/\ell = 8.7$ (Table 9). Wilcox and Jaffee rationalized the increase in yield strength over the entire temperature range in terms of the Orowan mechanism. They used Equation (6) to calculate τ_p and found good agreement between the experimental and calculated results. However, based on the findings of this research program, it now appears that above ~ 600°C, where grain boundary sliding becomes important, the agreement with the Orowan mechanism may have been fortuitous. For example, if the recrystallized TD Nickel had a drastically different grain aspect ratio, say $L/\ell = 2$, then the yield strength would have been ~ 67% lower at 1093°C (Figure 20a), and agreement with the Orowan mechanism at this temperature would not have been realized.

The observation that grain aspect ratio is important in high temperature yielding of Ni-ThO_2 alloys, can be used to explain the difference in results between the work of Wilcox and Jaffee[2] and Doble and Quigg[36]. The following results were found by these investigators:

Material	L/ℓ	0.2% Y.S. at 1093°C psi	0.2% Y.S. at 1093°C MN/m^2	Reference
1/2" (1.27 cm) dia. TD Nickel bar	12.5 ± 2.5	17,000	117	(2)
Recrystallized TD Nickel	8.7	11,900	82.1	(2)
1" (2.54 cm) dia. TD Nickel bar (Ann. 1 hr, 1371°C)	~ 10.0	13,300	91.8	(36)
Recrystallized TD Nickel	?	14,600	101.0	(36)

At 1093°C, Wilcox and Jaffee found a reduced yield strength after recrystallization and this is now attributed to a lower grain aspect ratio than that in the 1/2 inch (1.27 cm) diameter TD Nickel bar. The similarity in yield strength results of the 1 inch (2.54 cm) diameter TD Nickel bar and the recrystallized TD Nickel, obtained by Doble and Quigg, may possibly be due to the fact that both materials had similar grain aspect ratios.

The above discussion should not be construed to indicate that dispersion (or even substructure) strengthening is not important at high temperatures. However, the grain aspect ratio must be large (preferably > 10) before these strengthening mechanisms can be effectively utilized to make matrix yielding more difficult. For optimum high temperature strength, it would be desirable to have $L/\ell \gtrsim 15$.

Creep and Creep Rupture

In this phase of the program only the dispersion strengthened alloy, Ni-2ThO_2, was creep tested, and all tests were performed at 1093°C. Only material drawn by Procedure B was extensively tested, since this method of working more closely approximated commercial practice. In addition, it was expected that the microstructure would be stable as a result of recovery during the final 1200°C anneal, whereas recovery or even recrystallization of material drawn by Procedure A could occur during creep testing. However, one comparison was made

between specimens of Ni-2ThO_2 drawn by Procedures A and B, and the results are shown in Figure 23. The specimens had a total reduction by drawing of ~ 50% and were creep tested at 4000 psi (27.6 MN/m^2). The specimen drawn by Procedure B (intermediate anneals) had a longer primary creep range, a lower minimum creep rate, and a longer time to rupture than the specimens drawn by Procedure A.

All of the creep results on Ni-2ThO_2 are listed in Table 10. The data are plotted in Figure 24 as log $\dot{\epsilon}_{min}$ versus log σ, and in Figure 25 as log t_r versus log σ, where $\dot{\epsilon}_{min}$ = minimum creep rate, σ = applied stress, and t_r = time to rupture. In both Figures 24 and 25, linear relations are apparent, which lead to the proportionalities

$$\dot{\epsilon}_{min} \propto \sigma^n \tag{9}$$

$$t_r \propto \sigma^{-m} \quad . \tag{10}$$

Increasing the amount of total reduction by drawing Procedure B had two effects: (1) the plots are shifted to higher stresses for a given $\dot{\epsilon}_{min}$ or t_r, and (2) the slopes, or n values, increase. The exponents increased from 6.7 to 22.0 for minimum creep rate (Figure 24) and from 7.8 to 19.6 for rupture life (Figure 25). Although stress exponents of n = 4 to 5 are common for creep of single crystals and pure polycrystalline metals, very high stress exponents are common for complex materials such as dispersion strengthened nickel alloys[3,5-7,34]. The qualitative argument that has been used to explain this behavior is that these complex alloys have a very high internal stress, σ_i. Thus the effective stress, σ_e, acting on dislocations is a small fraction of the applied stress, σ, since $\sigma_e = \sigma - \sigma_i$. Even if grain boundary sliding accounted for a large fraction of the total creep strain, the above argument would hold if accommodation deformation by dislocation glide or climb within grains were the rate controlling creep process.

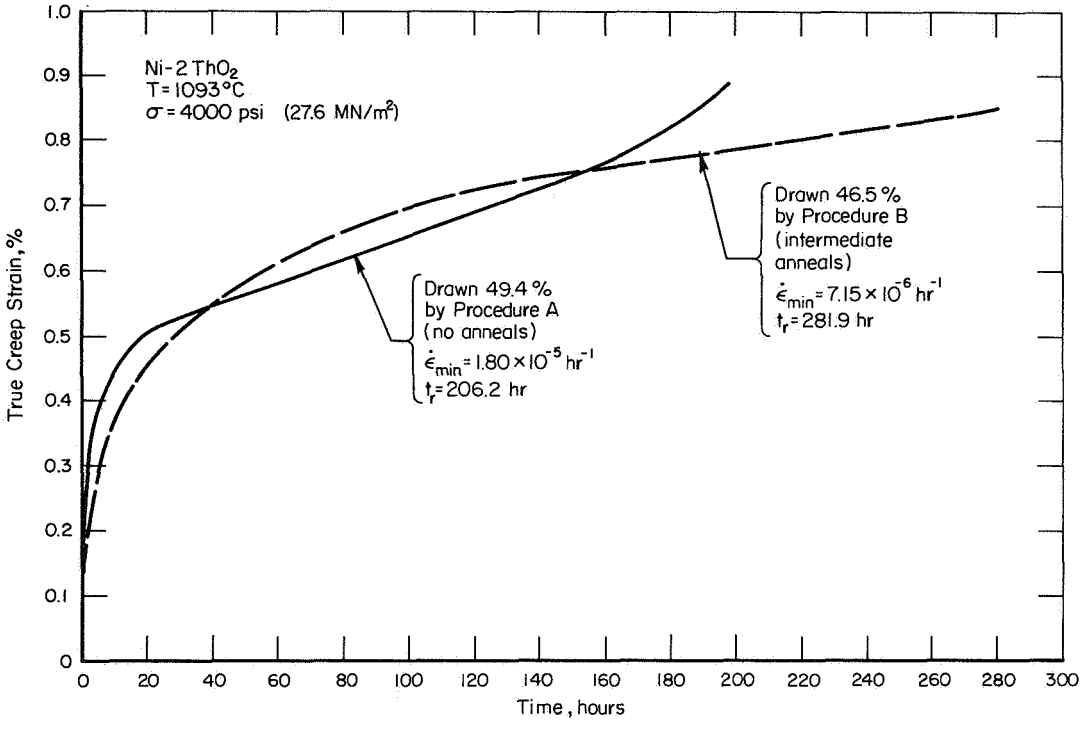

FIGURE 23. Creep curves of Ni-2ThO_2 specimens drawn by Procedures A and B.

TABLE 10. CREEP PROPERTIES OF Ni-2ThO_2 AT 1093°C AS A FUNCTION OF DRAWING BY PROCEDURE B (intermediate anneals at 1200°C). Each specimen was tested in the annealed condition, unless otherwise specified.

Rod or Wire Dia., in.	Rod or Wire Dia., cm	Total % Red. by Drawing	Stress, psi	Stress, MN/m_2	Min. Creep rate, $\dot{\epsilon}_{min}, hr^{-1}$	Time to rupture, t_r, hr	$(\dot{\epsilon}_{min})(t_r)$	Elong.	% R.A.
0.350	0.889	0	2,000	13.8	3.20×10^{-5}	> 550[a]	> 1.76×10^{-2}	--	--
0.350	0.889	0	3,000	20.8	5.52×10^{-4}	20.1	1.11×10^{-2}	1.0	9.1
0.350	0.889	0	4,000	27.6	2.73×10^{-3}	3.0	0.82×10^{-2}	1.9	9.1
0.249	0.632	46.5	4,000	27.6	7.15×10^{-6}	281.9	0.20×10^{-2}	1.9	2.6
0.249	0.632	46.5	5,000	34.5	5.00×10^{-4}	21.5	1.08×10^{-2}	1.9	4.8
0.249	0.632	46.5	7,000	48.3	4.10×10^{-2}	0.28	1.56×10^{-2}	4.9	8.3
0.249	0.632	46.5	9,000	62.1	--[b]	0.042	-	7.4	17.5
0.181	0.460	73.3	7,500	51.7	6.50×10^{-5}	163.7	1.06×10^{-2}	2.8	1.8
0.181	0.460	73.3	8,000	55.2	2.42×10^{-4}	52.7	1.28×10^{-2}	1.9	3.8
0.181	0.460	73.3	8,500	58.7	2.60×10^{-4}	26.5	0.69×10^{-2}	3.9	0.7
0.181	0.460	73.3	9,000	62.1	6.20×10^{-3}	6.1	3.78×10^{-2}	6.0	1.1
0.127	0.323	86.8[c]	9,500	65.5	2.75×10^{-4}	21.9	0.60×10^{-2}	3.9	9.1
0.127	0.323	86.8[c]	11,000	75.8	5.00×10^{-4}	9.8	0.49×10^{-2}	4.7	9.1
0.127	0.323	86.8[c]	12,000	82.7	8.75×10^{-4}	6.3	0.55×10^{-2}	1.9	5.4
0.096[e]	0.244	92.5	11,000	75.8	1.38×10^{-4}	30.1	0.42×10^{-2}	1.0	4.8
0.096[e]	0.244	92.5	12,000	82.7	8.33×10^{-4}	6.2	0.52×10^{-2}	3.9	10.2
0.096[e]	0.244	92.5	13,000	89.6	3.70×10^{-3}	0.9	0.33×10^{-2}	5.0	4.4
0.249	0.632	49.4[d]	4,000	27.6	1.80×10^{-5}	206.2	0.37×10^{-2}	1.0	1.7

(a) Test stopped after 550 hours.

(b) Specimen deformed too fast to allow creep measurements.

(c) Results from these specimens were anomalous, and thus are not plotted in Figures 24 and 25.

(d) This specimen drawn by Procedure A (no intermediate anneals).

(e) 30% recrystallized.

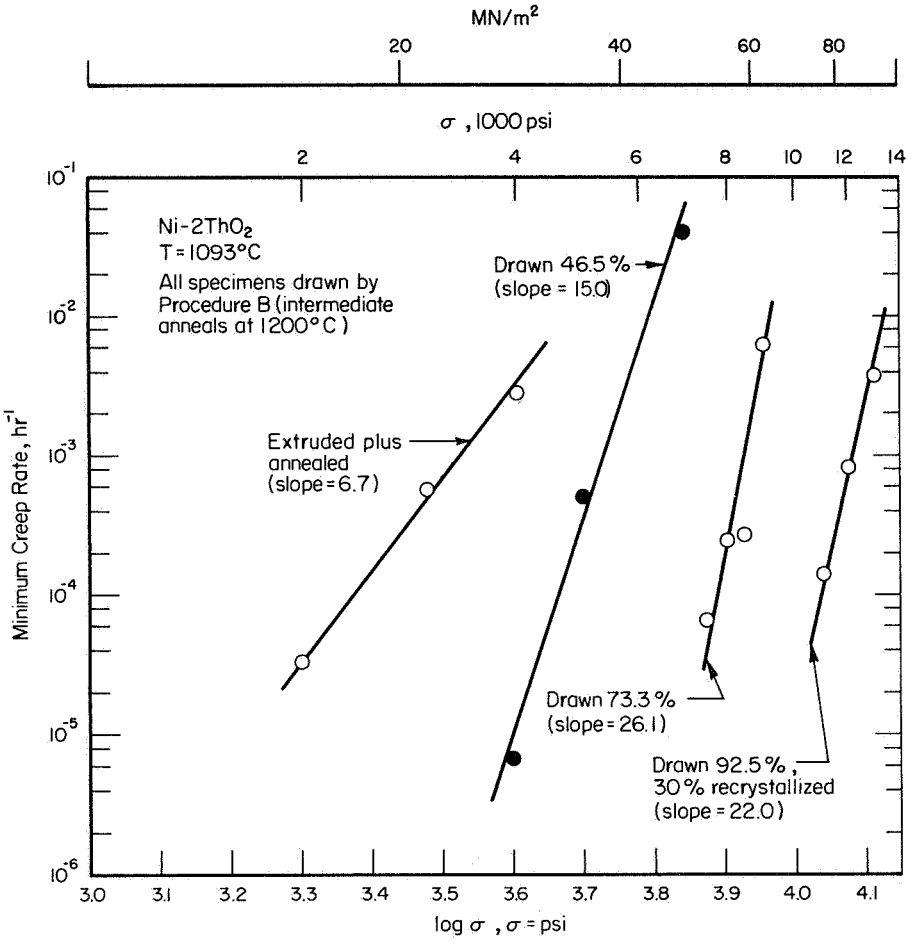

FIGURE 24. Effect of drawing by Procedure B (intermediate anneals) on minimum creep rate of Ni-2ThO_2 at 1093°C.

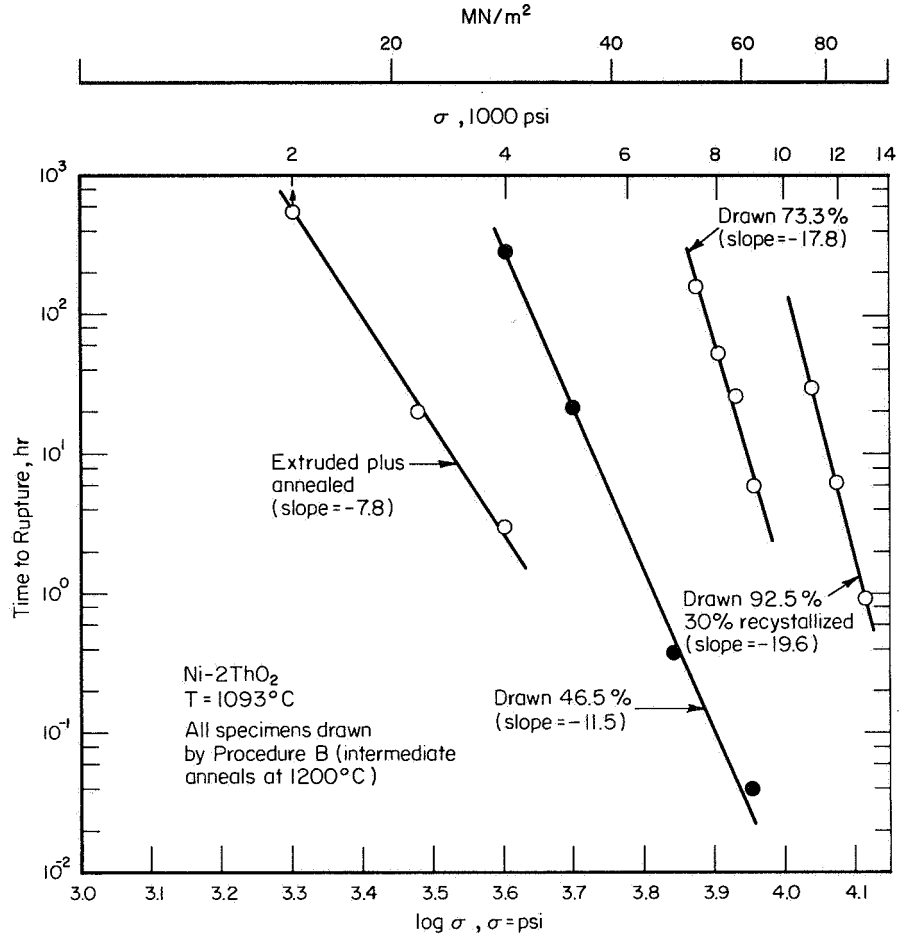

FIGURE 25. Effect of drawing by Procedure B (intermediate anneals) on creep rupture life of Ni-2ThO_2 at 1093°C.

Unfortunately, in materials such as these it has not been possible to identify a rate controlling creep process, although at high temperatures grain boundary sliding certainly appears to be the major mode of deformation.

The most important feature of Figures 24 and 25 is that Ni-2ThO_2 becomes more creep resistant at higher total reductions by drawing Procedure B. This is illustrated in a different way in Figure 26. In this figure, the stress to cause a minimum creep rate of 10^{-4} hr^{-1} and the stress to cause rupture in 100 hours at 1093°C are plotted as a function of total reduction by drawing. It is seen that material drawn 92.5% is about five times "stronger" than extruded plus annealed material.

Also included in Figure 26 are typical 100 hour rupture life data from Fansteel Metallurgical Corporation[37] for TD Nickel bar and sheet. The Ni-2 ThO_2 drawn 92.5% has a 100 hour rupture life comparable to the best commercial sheet and to 1-1/4 inch diameter TD Nickel bar, but is about 4000 psi (27.6 MN/m^2) "weaker" than commercial 1/2 inch (1.27 cm) diameter TD Nickel bar at 1093°C.

The values of minimum creep rate times rupture life ($\dot{\epsilon}_{min} \cdot t_r$) are listed in Table 10 for Ni-2ThO_2 drawn various amounts by Procedure B. For a given drawing reduction, the usual empirical relation[38] is approximated:

$$\dot{\epsilon}_{min} \cdot t_r \approx C \quad . \tag{11}$$

The average value of C decreases from $\sim 1.2 \times 10^{-2}$ for extruded plus annealed material to $\sim 0.4 \times 10^{-2}$ for material drawn 92.5%. The average value for C, from all tests is $\sim 10^{-2}$. Thus, for example, a rough estimate of the minimum creep rate for material which ruptures after 100 hours at 1093°C, would be $\dot{\epsilon}_{min} = 10^{-4}$ hr^{-1}. Figure 26 shows that the stress required to give a creep rate of 10^{-4} hr^{-1} is approximately the same as that required to cause failure in 100 hr.

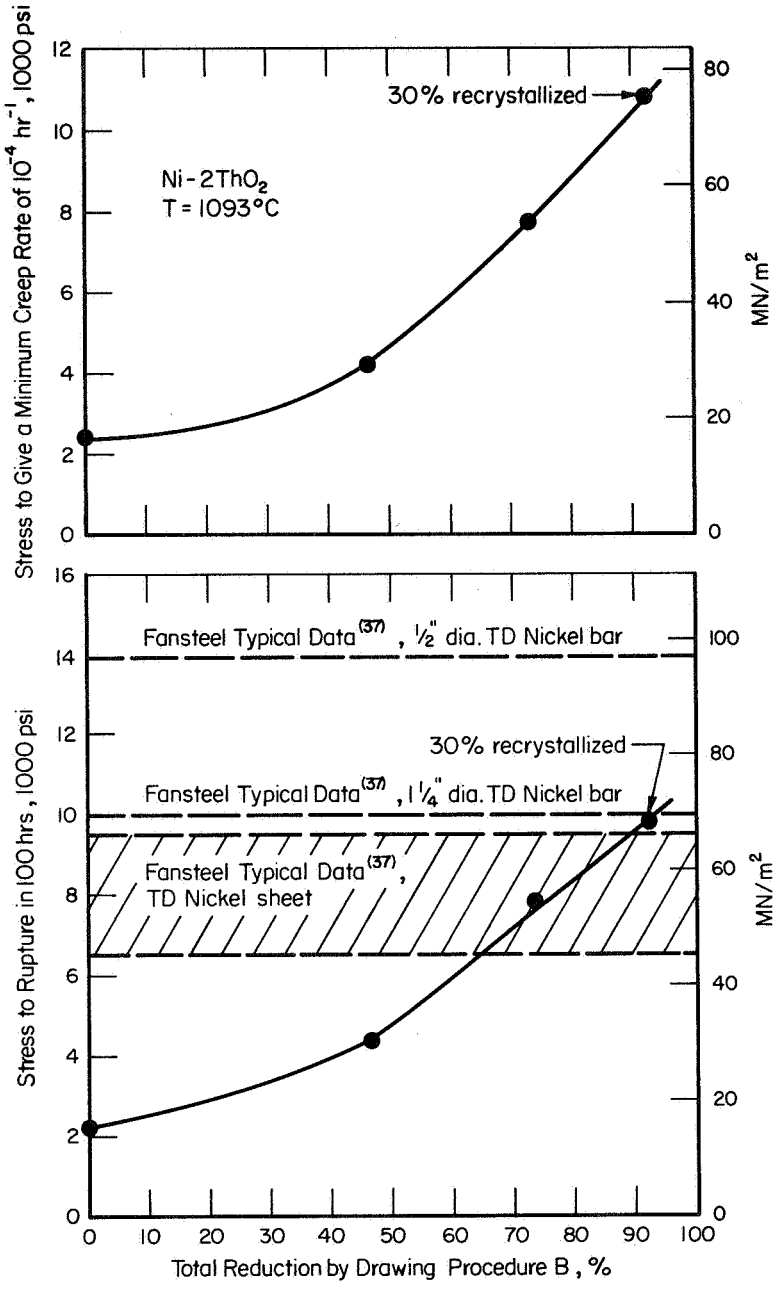

FIGURE 26. Influence of drawing Ni-2ThO_2 by Procedure B (intermediate anneals) on stress to cause a minimum creep of $10^{-4}hr^{-1}$ and stress to cause rupture in 100 hr at 1093°C.

Returning to Figure 20(b) and Figure 20(c), it is seen that the grain aspect ratio has the same effect on rupture life and creep strength as it did on yield strength. As the aspect ratio is increased, the 100-hour rupture stress and the stress required to give a minimum creep rate of 10^{-4} hr^{-1} increase. The explanation again involves grain boundary sliding. The more elongated the structure, the less sliding and the lower the creep rate at a given stress, or alternately the higher the stress required to produce a given minimum creep rate. The comparison in Figure 26 suggests that the Ni-2ThO_2 drawn 92.5% has an effective L/ℓ about the same as the best TD Nickel sheet and the 1-1/4 inch (3.18 cm) diameter TD Nickel bar, but a lower grain aspect ratio than the 1/2 inch (1.27 cm) diameter TD Nickel bar. It is anticipated that the aspect ratio effect on creep behavior would be more important at lower temperatures than the effect of L/ℓ on yield strength. This is because creep rates are generally slower than normal tensile strain rates, and thus the rate effects in Figure 21(b) would be important.

Ashby and Raj[39] have treated continuum aspects of grain boundary sliding and diffusional creep. They considered the cases where sliding was accommodated by: (1) elastic strain, (2) diffusive flow of matter, and (3) plastic flow by dislocation motion. In their most detailed model they examined diffusional accommodation of grain boundary sliding for grains with a large aspect ratio, a situation which is relevant to the present Ni-2ThO_2 materials. The result of their analysis gives the shear strain rate, $\dot{\gamma}$, in creep as:

$$\dot{\gamma} \simeq \frac{16\ \tau_a\ \Omega}{kT} \cdot \frac{1}{x^2}\left[\frac{D_v}{R} + \frac{\delta\ D_b}{x\ R^{1/2}}\right] , \qquad (12)$$

where τ_a = applied shear stress on the boundary

Ω = atomic volume

k = Boltzmann's constant

T = absolute temperature

x = effective grain size = $(L \cdot \ell)^{1/2}$

D_v = volume diffusivity

D_b = grain boundary diffusivity

R = grain aspect ratio = L/ℓ

δ = grain boundary thickness.

This relation says that creep rate is proportional to τ_a and that some combinations of volume and grain boundary diffusion influences the creep rate; i.e., the activation energy for creep, Q_c, should be $Q_v \gtrsim Q_c \gtrsim Q_b$ where Q_v = activation energy for volume diffusion, and Q_b = activation energy for grain boundary diffusion. Yet for TD Nickel bar creep tested from 700-1100°C, where $L/\ell \approx 12$, it was found that $Q_c \approx 3\ Q_v$.[3] Also a very high stress exponent, $n = 40$, was found. Similarly, in this work it was found that the stress exponent increased with increasing L/ℓ. Thus the model represented by Equation (12) does not describe the experimental creep results for Ni-2ThO_2 with a high grain aspect ratio.

Ashby and Raj[39] also considered grain boundary sliding where particles in the boundary impede the sliding. Here again, the sliding rate was proportional to τ_a and the activation energy for sliding should be between that for volume and grain boundary diffusion. Thus this model is not directly applicable to the present results.

It appears that a mechanistic interpretation of the high temperature creep behavior of Ni-2ThO_2 having $L/\ell > 1$ is indeed much more complicated. Development of a rigorous model should include the following considerations:

(1) The main mode of deformation at high temperatures is grain boundary sliding.

(2) The creep rate is proportional to the grain aspect ratio, at least for $T \approx 0.8\ T_m$.

(3) It is possible that both diffusional and dislocation deformation accommodation are operative, with the former being more important at higher temperatures and lower stresses and the latter more important at lower temperatures (approaching 0.5 T_m) and higher stresses.

(4) Creep is not Newtonian viscous, but rather very high stress exponents are obtained, and these appear to increase with increasing grain aspect ratio.

(5) Apparent activation energies for creep are very high, say 2 to 3 times the activation energy for volume self-diffusion.[3,34] Such activation energies may not have any direct physical significance, but it would be desirable for any viable model to explain their origin.

Texture

There have been several previous investigations[20,21,30,40-44] on Ni-ThO_2 and Ni-Cr-ThO_2 alloys which included texture determinations on sheet or bar material, and some of these have examined texture as a means of strengthening[42,44] and the possible influence of deformation texture on recrystallization resistance or recrystallization textures[20,30,40,41,43]. Before discussing the results of this program, and the previous texture determinations on dispersion strengthened nickel alloys, it is appropriate to briefly review some aspects of deformation and recrystallization fiber textures in dispersion-free FCC metals and alloys.

It is generally observed that extrusion and drawing operations, which give equivalent deformations, result in similar textures provided that

recrystallization does not occur during extrusion. In pure metals the deformation fiber textures are composed of two main orientations, having <111> or <100> directions parallel to the rod axis[45]. The relative proportions of these orientations vary between different metals and single phase alloys. Chin and English[46] have shown that the ratio of <100>/<111> varies with stacking fault energy, γ, (or more strictly with γ/Gb where G = shear modulus, and b = the magnitude of the relevant Burgers vector). For very low values of γ/Gb the <111> fiber texture predominates, but as γ/Gb increases, the <100> content increases to a maximum and then decreases to a very low value. For metals with high γ's such as aluminum and nickel, the <111> component normally represents 80% to 100% of the volume after heavy drawing. Chin[47] has analyzed in detail the effect of various deformation modes on texture formation and his main conclusions were:

(1) For homogeneous deformation by slip on {111}<110> systems, both <111> and <100> orientations are stable, but from a randomly oriented starting material, the <111> is predicted to become about twice as strong as the <100>.

(2) If cross slip is so easy that the deformation is effectively {hkℓ}<110> slip, then there is very little difference from case (1). In fact, the volume of material which can rotate to <111> is slightly increased.

(3) If gross mechanical twinning occurs, the general picture is rather unclear. However, the <111> orientation is susceptible to twinning during drawing while the <100> is not, and it appears that combinations of twinning and slip should favor the <100> orientation. The intense <100> component in silver is believed to form in this way.

(4) It has been shown experimentally that when crystals of the <100> orientation are drawn, the deformation is often not a homogeneous

slip process. The phenomenon of deformation banding occurs in which separate volumes of the crystal deform in approximately plane strain in different modes such that over the whole specimen the strain is the imposed axi-symmetric strain. It has been shown that this inhomogeneous deformation occurs because it involves less total work than homogeneous deformation of the <100> orientation. The orientations of the metal inside the deformation bands are not stable, but rotate toward <111>. It is important to note that this is the only recognized mechanism by which material in the <100> orientation can rotate away from <100> in metals having moderate or high γ values. In metals with very low stacking fault energies, intrinsic faulting may also achieve such rotation.

The textures formed on deformation of rods or wires are usually greatly modified during recrystallization. Many different recrystallization textures have been observed, the most common being <100>[48], <112>[45], <113>[48,49], <115>[48], and <130>[49]. According to Dillamore and Roberts[45] recrystallization to <100> appears to be favored in a predominantly <111> deformed matrix while <112> is favored in <100>. It is certainly true that the <100> component in extruded aluminum comprises recrystallized grains, and that the accompanying <111> component represents deformed metal[48]. In other work it has been shown that favorable orientation relationships for rapid growth exist between recrystallized grains and the deformation texture.[49] One explanation for the presence of <100> recrystallized grains is that these have the lowest elastic strain energy[50] under the conditions of applied stress in extrusion. It must be concluded, however, that recrystallization fiber textures are not well understood, and seldom predictable.

All of the texture results on Ni and Ni-2ThO_2 are listed in Table 11 and plots of the <100> and <111> texture concentrations as a function of drawing by Procedures A and B are shown in Figures 27 and 28. In Figures 27(a)

TABLE 11. QUANTITATIVE MEASURES OF TEXTURE INTENSITY IN Ni AND Ni-2ThO_2 AS A FUNCTION DRAWING STRAIN

Alloy	Drawing Procedure	Total Reduction by Drawing, %	Specimen No.	Pk_{200} (X Random)	Pk_{111} (X Random)	Pk_{200}/Pk_{111}	Texture Concentration, %, within 10° or 20° of Rod Axis <100>, 10°	<100>, 20°	<111>, 10°	<111>, 20°
Ni-2ThO_2	A[a]	As-Extruded	1	38	2.7	14	64	84	7.5	13
"	A	49.4	2	24	3.9	6.2	48	70	8.6	14
"	A	73.3	3	23	7.9	3.0	36	64	12	21
"	A	86.8	4	23	18	1.5	31	51	22	36
"	A	92.5	5	24	17	1.4	27	46	26	43
Ni-2ThO_2	B[b]	Extruded and Annealed	6	51	1.9	37	77	94	4.7	7.7
"	B	46.5	7	30	3.1	10	58	92	5.0	8.9
"	B	73.3	8	32	2.3	14	39	65	4.7	12
"	B	86.8	9	40	2.0	20	39	60	2.7	13
"	B	92.5	10	41	3.4	12	39	50	15	39
Ni	A[a]	As-Extruded	11	16	1.1	14	24	35	7.4	32
"	A	53.4	12	3.9	4.3	1.1	13	34	17	37
"	A	76.7	13	2.8	9.5	0.3	7.4	20	22	36
"	A	88.5	14	3.0	15	0.2	6.5	18	26	45
"	A	93.4	15	1.3	21	0.06	2.4	5	29	50
Ni	B[b]	Extruded and Annealed	16	20	1.1	18	29	41	8.4	34
"	B	53.4	17	2.6	0.9	2.7	5.5	19	5.7	24
"	B	76.7	18	1.6	0.7	2.3	6.5	25	7.2	22
"	B	88.5	19	1.4	0.7	2.1	5.3	19	5.4	19
"	B	93.4	20	0.7	0.6	1.2	4.1	16	6.4	22

(a) Drawing Procedure A: Draw at 200°C to indicated total reductions; no intermediate anneals.

(b) Drawing Procedure B: Draw at 200°C, with intermediate anneals (1200°C, 1 hr, H_2 atm.) after each 50% reduction. Texture measurements were on annealed specimens.

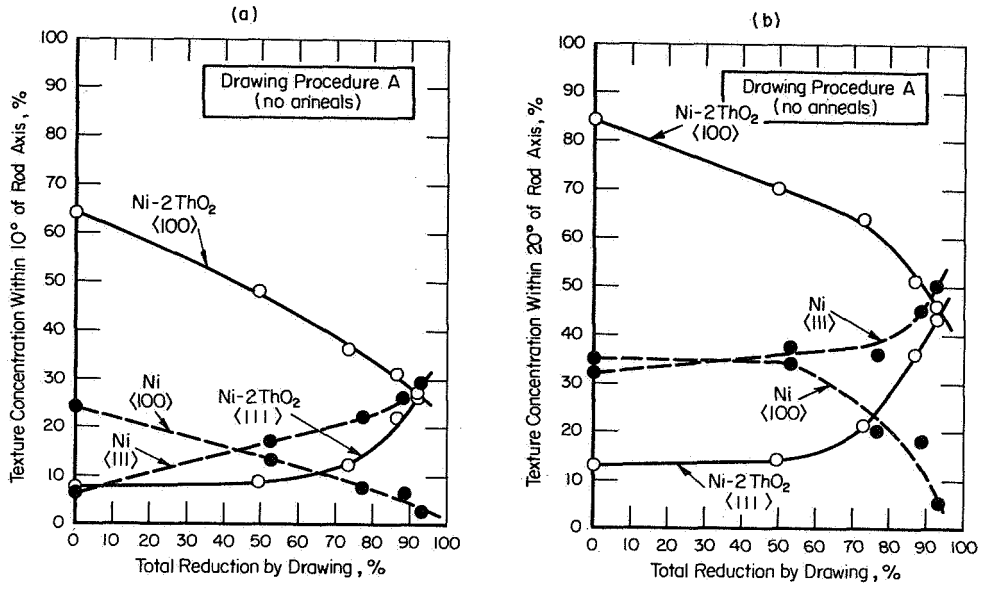

FIGURE 27. Effect of drawing by Procedure A (no intermediate anneals) on the fiber texture of Ni and Ni-2ThO_2. Texture concentrations are (a) within 10° of the rod axis, and (b) within 20° of the rod axis.

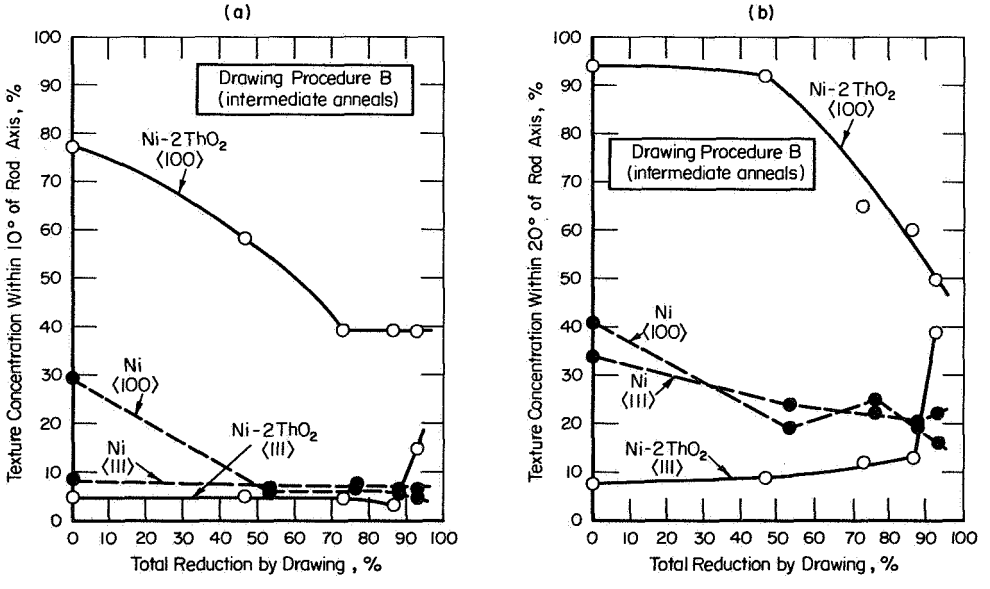

FIGURE 28. Effect of drawing by Procedure B (intermediate anneals) on the fiber texture of Ni and Ni-2ThO_2. Texture concentrations are (a) within 10° of the rod axis, and (b) within 20° of the rod axis.

and 28(a) the texture concentration within 10^{o} of the rod axis is plotted versus drawing strain for both Ni and Ni-2ThO_2 and similar plots are made in Figures 27(b) and 28(b) for the texture concentration within 20^{o} of the rod axis. The specimens in Table 11 are numbered 1-20, and the corresponding graphs of normalized intensity versus angle of inclination for the {111} and {200} reflections are given in Appendix A (Figures 1-A through 20-A) for each specimen.

Prior to the quantitative texture measurements, some selected back reflection photographs were taken on Specimens 1-5 (Ni-2ThO_2, drawn by Procedure A). Specimen (1) showed very similar back reflection patterns at the centerline and at the surface (surface ground and then electropolished after extrusion) although the texture appeared to be a little weaker at the surface. In specimens (3), (4), and (5), the sharp fiber textures were evident at the centerline, but the drawn surface was apparently texture-free, showing continuous Debye rings. In specimen (4), where an attempt was made to chart the texture photographically through the wire, it appeared that at least the outer quarter of the radius showed barely discernible signs of texture. All of the texture components detected on the films corresponded to the quantitative goniometric texture measurements.

The following results on quantitative texture measurements were obtained:

(1) Ni-2ThO_2 drawn by Procedure A; refer to Table 11, Figures 27(a) and (b) and Figures 1-A through 5-A.

The as-extruded Ni-2ThO_2 was very highly <100> textured, but also had a small amount of <111>. With increasing drawing reductions the content of <100> decreased, while still remaining the strongest single component, and the <111> developed continuously. These results are consistent with the previous findings of Tracey and Worn[20]. There was also a <112> component which was particularly

obvious in specimens (4) and (5); see Figures 4-A and 5-A. A manifestation of the <112> component is the peak in the {200} reflection at ~ 65° from the axis. In order to check for the presence of <112> oriented material at the very center of specimen (5) a forward reflection phogograph was taken from a sample thinned to 0.01 inch (0.025 cm) diameter. No trace of <112> orientation could be detected here, although the <100> and <111> components agreed closely with the goniometric measurements. It must be concluded that the <112> component was present at or near the surface of the wires, and probably arose due to shear resulting from surface friction.

(2) Ni-2ThO_2 drawn by Procedure B; refer to Table 11, Figures 28(a) and (b) and Figures 6-A through 10-A.

On annealing the extruded bar there was a very slight increase in the <100>, and decrease in the <111> components. As the processing continued by Procedure B, the <100> became depleted, but not quite as rapidly as in drawing Procedure A. The intermediate anneals prevented to some extent rotation away from <100>. This may be, as suggested by Dillamore[51], because annealing destroys the dislocation arrangement by which deformation bands rotate material from <100>. Thus on further working, rotation back to <100> occurred by homogeneous slip. The most striking difference between drawing Procedures A and B is that the intermediate anneals effectively prevented the formation of the <111> component. On close examination of the subsidiary peaks in specimens (7), (8), (9), and (10) (Figures 7-A through 10-A) it is seen that these are at <114>, <113>, <113> to <112>, and <112> to <223>, respectively. In specimen (10) there was 30% recrystallization so this result should probably be ignored. However, it is clear that a slow rotation process occurred from <100> to <111>. The intermediate anneals acted to delay the rotation process. A possible explanation of this is as follows. The presence of the ThO_2 particles limits the blocks of material

which can rotate to very small volumes. These blocks therefore are highly misoriented small volumes, which on annealing are thermodynamically unstable. Some are therefore swallowed up into the bulk of the texture by short range boundary migration. This, admittedly speculative, explanation accounts for the sense of rotation and the delaying action of the anneals. After a sufficiently large total deformation by Procedure B it would be expected that the <111> orientation would be achieved. An alternative explanation for the subsidiary peaks might be in terms of a surface texture.

(3) Pure Nickel drawn by Procedure A; refer to Table 11, Figures 27(a) and (b) and Figures 11-A through 15-A.

The extruded pure nickel had a fairly strong <100> fiber texture and also a spread of orientations approximately <113> - <112> - <223>. From examination of the grain structure (Figure 2) it is clear that all these components must represent recrystallization textures. During drawing by Procedure A, much of the spread around <112> rotated to <111> which soon became the strongest texture component. The initial <100> component was rapidly depleted, presumably by a deformation banding mechanism, since this orientation should be stable in homogeneous deformation. A very significant <112> texture also developed with increasing strain. However, transmission X-ray photographs from the center of the wires showed no trace of this orientation. Thus, as in the Ni-2ThO_2 alloy, it is assumed to be a surface, or near surface, shear texture.

(4) Pure Nickel drawn by Procedure B; refer to Table 11, Figures 28(a) and (b) and Figures 16-A through 20-A.

Annealing the extruded nickel had very little effect on the texture. This observation is perhaps to be expected since there was little change in the microstructure.* The strong <100> component became a little sharper. After the subsequent deformations and anneals, the texture was almost random. The

---

* The annealed Ni texture specimen was taken from a different part of the extrusion than the metallographic and tensile specimens. The texture specimen showed much less grain growth than is observed in Figure 4a.

fluctuations in intensity shown in Figures 17-A to 20-A are possibly spurious, resulting from the relatively large grain size of this material. The randomizing effect obtained by recrystallization after small strains is a well documented phenomenon.

Because of the considerable differences in microstructure developed in Procedure B, no direct comparison is valid between the Ni and Ni-2ThO_2. The following discussion is therefore limited to drawing by Procedure A. The extrusion textures of the Ni and Ni-2ThO_2 were qualitatively rather similar, although in the pure nickel the subsidiary peak was around <112> rather than <111> as in the Ni-2ThO_2 alloy. The major <100> component was also weaker in the pure nickel.

The most important difference is that on drawing, the initially strong <100> component was reduced to a very low level in the pure nickel, but remained strong (although somewhat depleted in volume) in the Ni-2ThO_2. According to Chin's analysis[47], the only mechanism allowing rotation away from <100> is that of deformation banding. In the presence of fine particles, it would be expected that the difficulty of accommodating strain around the particles would reduce the size of potential deformation bands. In this way the ratio of deformation band surface to volume would be greatly increased. The surfaces of deformation bands are known to be very highly strained, high energy sites[52]. Increasing the proportion of these would be expected to inhibit deformation banding since the feasibility of the process depends on a delicate selection of the lowest energy deformation mechanism.

Extrusion, drawing, or swaging textures in dispersion strengthened nickel and copper have been studied by several workers[20,21,30,53,54], and their results

show some interesting differences compared with pure metals. The previous results on Ni and Ni-ThO_2 alloys are consistent with the present results. Tracey and Worn[20] found that in hot extruded Ni-2.5ThO_2 (~ 98% reduction) the texture was approximately 80% <100> and 10% <111>. They felt that the <100> component arose through recrystallization, although the evidence for recrystallization was not obvious. In three other studies[21,30,53], on extruded dispersion strengthened nickel, the major component was identified as <100> although for a smaller extrusion ratio[30] there was an additional strong <111> component. In addition, Worn and Marton[21] have reported that <111> is strengthened with increasing volume fraction of thoria although it was never observed to become as strong as the <100> component.

The information on drawing textures in Ni-ThO_2 alloys is rather confused by the presence of strong starting textures resulting from prior extrusion. During drawing, the strong <100> starting texture is somewhat weakened, and the <111> increases. This behavior is qualitatively the same as in pure nickel, but with the difference that the <100>/<111> ratio remains much larger (~ 1) than for the pure metal (~ 0.1) drawn in excess of 90% reduction. This condition is observed even when the starting texture is not strongly biased towards <100>[30]. Tracey and Worn[20] observed that on annealing cold drawn Ni-2.5ThO_2, the <100> orientation increased slightly while the <111> decreased. Unfortunately, they did not indicate whether or not gross recrystallization occurred during the anneal. This behavior is similar to that observed in this program on Ni-2ThO_2.

The most thorough study of fiber textures in a dispersion strengthened FCC metal is that of Liesner and Wassermann[54] on the copper-alumina system. These

workers varied the size and volume fraction of particles, and examined the textures after extrusion, drawing, and annealing. The extrusion textures were either <100> or <112>, the <100> being favored by increase in volume fraction of Al_2O_3, and decrease in the size of the particles. The <112> component was explained as being a recrystallization texture while the <100> was stated to be a warm deformation texture, recrystallization being inhibited by the numerous fine particles.* On cold drawing the extruded material, the <100> remained stable (in the presence of particles) while the <112> component rotated in a mixture of <111> and <100>. Subsequent recrystallization caused the <100> to be replaced by <112>, which provides further evidence that this component is a recrystallization texture.

Several results[55-58] have been reported for S.A.P. aluminum which seem to be at variance with the results for nickel and copper based alloys. For S.A.P. it appears that the main extrusion texture is <111>, although <100> may be present to an almost equal degree with low volume fractions of alumina[55]. Increasing the volume fraction of alumina was reported to suppress the <100> component[56].

It was shown earlier in this report that the optimum combination of room temperature and high temperature strengths was achieved by a fine very elongated grain structure. To obtain this structure, recrystallization should be prevented. When recrystallization does occur there is a loss in room temperature strength; yet the high temperature strength may not be decreased, provided the recrystallized grain aspect ratio is high enough. Thus when recrystallization does occur, a high grain aspect ratio is desirable.

---

* The presence of the <100> deformation texture in extrusions is at variance with theoretical predictions, since deformation twinning is the only mechanism known to be capable of producing intense <100> textures. Deformation twinning in copper and nickel during high temperature extrusion does not seem probable.

Although there have been several previous studies on the recrystallization behavior of Ni-2ThO_2 [30,40,41,43,53,59] and Ni-20Cr-2ThO_2 [11], the conditions under which these alloys are susceptible to recrystallization are not well defined. Different workers have found recrystallization temperatures varying from ~ 500°C [40] to > 1300°C [30] for Ni-2ThO_2. Doble, et al. [30], came to the important conclusion that recrystallization was influenced more by the type of working operation and working direction than the amount of working deformation. For example, they noted that rolling TD Nickel transverse to the extrusion axis was much more conducive to recrystallization than rolling parallel to the axis. When rolling TD Nickel bar in one direction, they noted that continued rolling deformation produced a more recrystallization resistant structure in spite of the increased strain hardening.

Doble, et al. [30], and others [41,43] have related recrystallization resistance to the type of texture developed by working. These results provide circumstantial evidence that there may be a connection between preferred orientation and ease of recrystallization. If this is indeed so, then the stabilizing textures appear to be the <100> fiber in rod and the pure metal texture, {123}<142> in sheet. In support of this, it was noted that Ni-2ThO_2 drawn by Procedure B did not begin to recrystallize until 92.5% total deformation, where the <100> component of the texture (within 20° of rod axis) dropped to ~ 50% (see Figure 28b). However, such a simple analysis is not completely satisfactory. Cold rolled TD Nickel specimens with almost identical pure metal textures were found to exhibit widely differing recrystallization behavior [30]. While it is known that deformed single crystals of certain orientations are resistant to recrystallization, all the textures found in dispersion strengthened Ni alloys are too diffuse to consist only of such orientations. In addition, the presence of grain boundaries allows

considerable scope for nucleation modes which are not possible in single crystals. A contributing factor to enhancing recrystallization may be the breakup of the elongated grain structure, as discussed by Petrovic, et al.[59]. This occurs for TD Nickel bar rolled transverse to the bar axis (recrystallization prone) but not for the same material rolled parallel to the bar axis (recrystallization resistant).

In dispersion strengthened metals, the inhibition of recrystallization is largely due to difficulty of nucleation[60]. It seems probable that for good structure stability, several conditions have to be satisfied simultaneously to prevent nucleation. A strong texture will tend to reduce the differences in Schmidt factors between grains, and so the true shear strain and the local stored energy of deformation will be made more homogeneous. For nucleation, a sharp gradient of stored energy is required to allow movement of grain boundaries or subboundaries. The presence of finely dispersed particles is known to homogenize the deformation substructure[61] and to reduce substructure variation between grains of different orientations[62]. The particles can inhibit movement of high and low angle boundaries, the processes by which recrystallized grains must form. A final point is that the grain shape or subgrain shape may possibly be an important factor. It is quite conceivable that a highly elongated worked grain structure represents a rather stable configuration which is resistant to initial boundary movement. This could help to explain the relative stability achieved in drawing, swaging, and rolling parallel to the extrusion direction and the lack of stability on cross-rolling of bar.

Once recrystallization nuclei are formed, growth appears to occur preferentially parallel to the rod axis. For example, the Ni-2ThO_2 specimen drawn 92.5% by Procedure B was 30% recrystallized and the recrystallized portion consisted of coarse, very elongated grains parallel to the rod axis. The recrystallized grain structures in Ni-ThO_2 and Ni-Cr-ThO_2 alloys often are

very directional. The explanation for this directional grain growth may be associated with Gleiter's[63,64] concepts of grain boundary migration where the migration rate of a boundary strongly depends on the boundary orientation and the growth direction. Some amplifications of this model may provide an explanation for the preferential growth of elongated grains in dispersion strengthened nickel alloys.

Ni-20Cr, Ni-20Cr-2ThO_2, Ni-20Cr-10W, and Ni-20Cr-10W-2ThO_2

Microstructure

The microstructures of as-extruded Ni-20Cr and Ni-20Cr-2ThO_2 alloys are shown respectively in Figures 29 and 30.* The Ni-20Cr alloy was recrystallized, although the TEM in Figure 29(b) shows that some subboundaries were present. The optical micrograph of as-extruded Ni-20Cr-2ThO_2 in Figure 30(a) indicates a non-recrystallized structure. However, the annealing twins in Figure 30(b) show that this material was at least partially recrystallized, with the resulting grains being extremely fine. In the optical micrographs of both alloys, there are dark etching stringers. These are probably Cr_2O_3 particles, some of which are very coarse ($\lesssim 1\ \mu m$) and some very fine ($\sim 0.05\ \mu m$). The presence of the finer Cr_2O_3 particles in Ni-20Cr is seen in the TEM in Figure 31. This micrograph was taken from an area of the foil which had been damaged in handling, and there are several examples of dislocation loops around particles. To the authors' knowledge this is the first time such loops have been shown in Ni-base alloys containing hard oxide particles, although such loops have been observed around overaged γ' particles in Ni-base superalloys[9].

---

* Only a limited amount of the Ni-20Cr-10W-2ThO_2 alloy was obtained, and this was in the extruded plus annealed condition. Hence, studies of this alloy and its ThO_2-free counterpart were confined to working by Procedure B only.

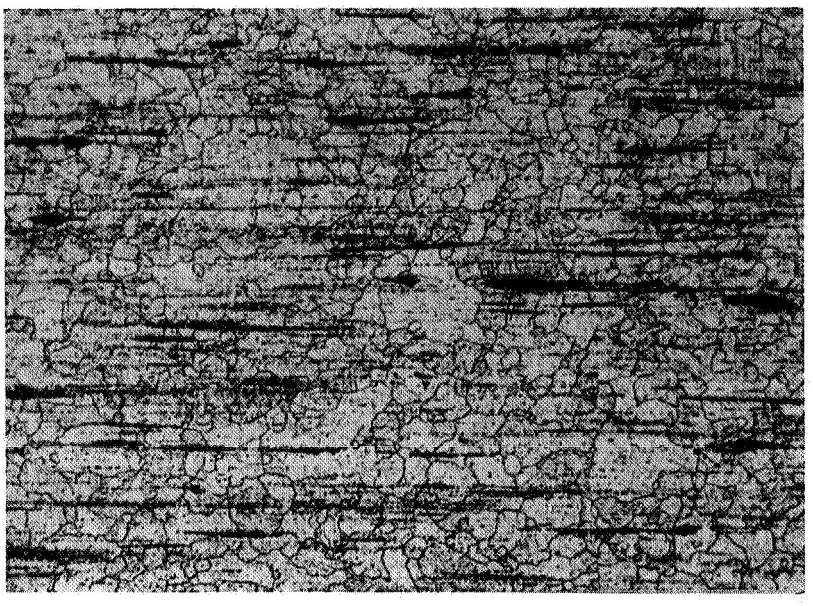

(a) 200X

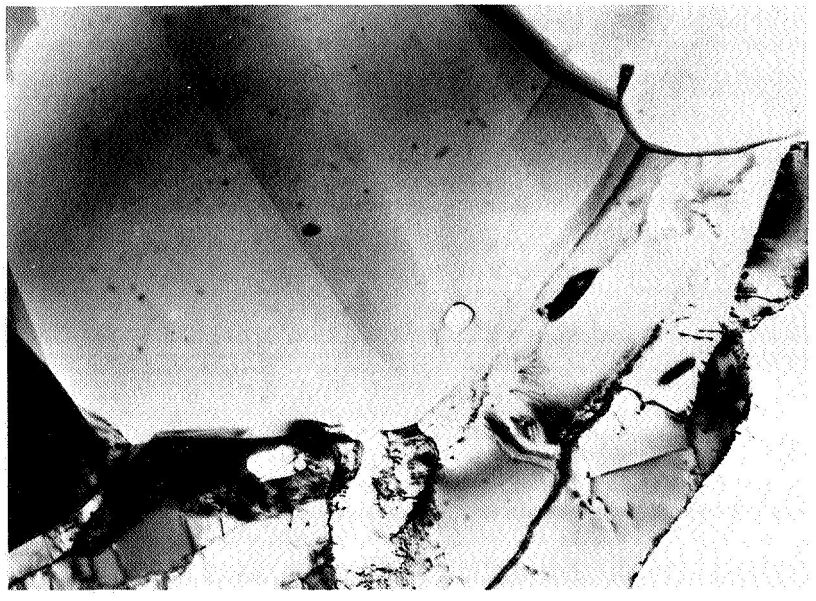

(b) 30,000X

FIGURE 29. Microstructure of as-extruded Ni-20Cr; (a) optical micrograph, (b) transmission electron micrograph.

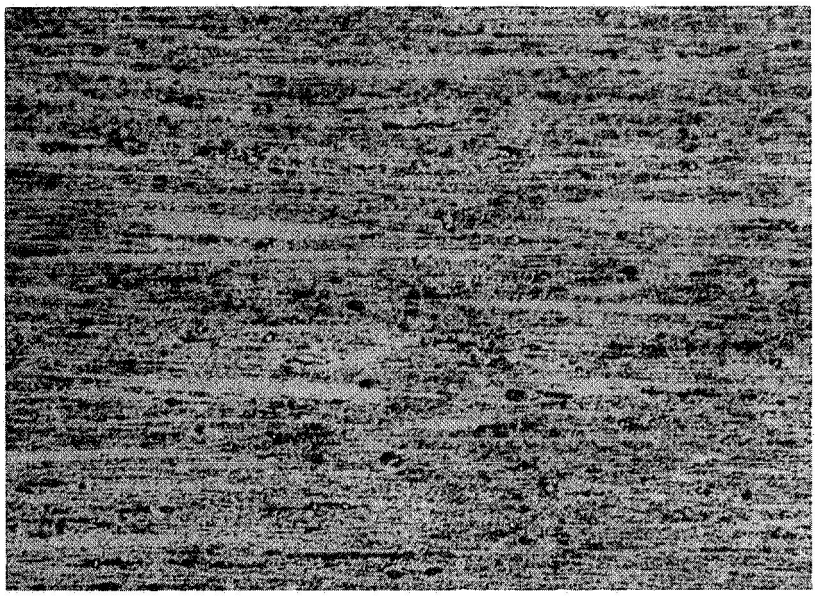

(a) 200X

(b) 30,000X

FIGURE 30. Microstructures of as-extruded Ni-20Cr-2ThO_2; (a) optical micrograph, (b) transmission electron micrograph.

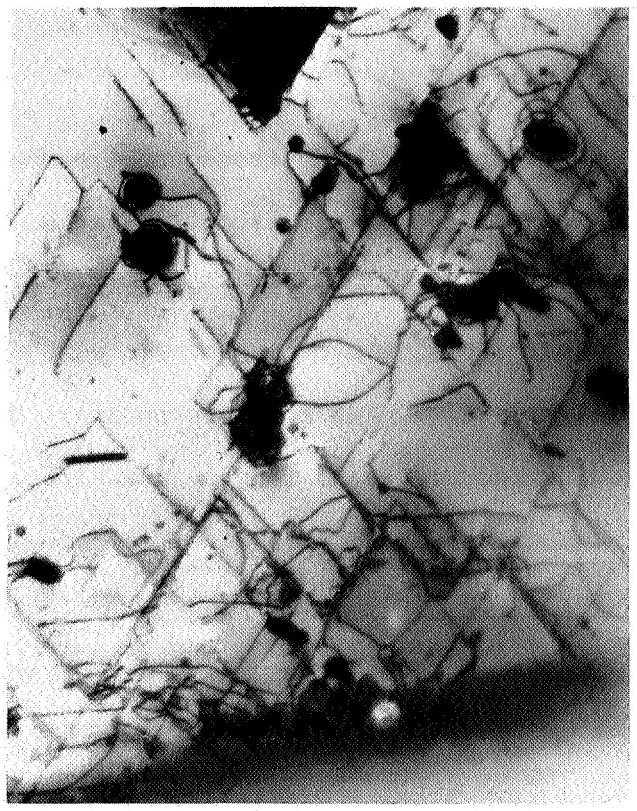

30,000X

FIGURE 31. Dislocation loops around particles (probably Cr_2O_3) in as-extruded Ni-20Cr. Photographs are from region of foil which was damaged in handling.

After annealing these alloys (1 hour, 1200°C in hydrogen), the resulting optical microstructures are those shown in Figure 32(a), Ni-20Cr, and Figure 32(b), Ni-20Cr-2ThO_2. The anneal caused very little change, compared with the as-extruded microstructures. It is somewhat surprising that the Ni-20Cr-2ThO_2 did not recrystallize to a coarse elongated grain structure, which is typical of commercial TD Nickel Chromium.

Drawing these alloys ~ 25% by Procedure A produced a heavily worked structure, with the usual tangled dislocation cells (see Figure 33). However, when the Ni-20Cr and Ni-20Cr-2ThO_2 alloys were worked by Procedure B (either drawing or swaging), the resulting microstructures were always recrystallized, with a fairly fine slightly elongated grain structure. Examples of this are shown in Figure 34 for Ni-20Cr and Figure 35 for Ni-20Cr-2ThO_2. The measured grain or cell sizes for the Ni-20Cr and Ni-20Cr-2ThO_2 alloys are listed in Table 12.

The Ni-20Cr-10W and Ni-20Cr-10W-2ThO_2 alloys were obtained from Fansteel in the extruded plus annealed condition. The treatment employed by Fansteel consisted of a 1 hour anneal in air at 1316°C. This was 116°C higher than the anneals given the other five alloys to begin working Procedure B. Also, the subsequent anneals given the two tungsten containing alloys (swaging Procedure B) were at 1200°C. Both alloys had a substantial amount of Cr_2O_3, elongated in stringers parallel to the extrusion axis. Figure 36(a) shows that the extruded plus annealed microstructure of Ni-20Cr-10W consisted of very fine equiaxed grains. The TEM in Figure 36(b) shows that some dislocation substructure was present, and in addition reveals a particle (presumably Cr_2O_3) blocking a non-coherent twin boundary. The Ni-20Cr-10W-2ThO_2 alloy had coarse, recrystallized, somewhat elongated grains in the extruded plus annealed (1316°C) condition (Figure 37a), but the TEM in Figure 37(b) shows that there were still some

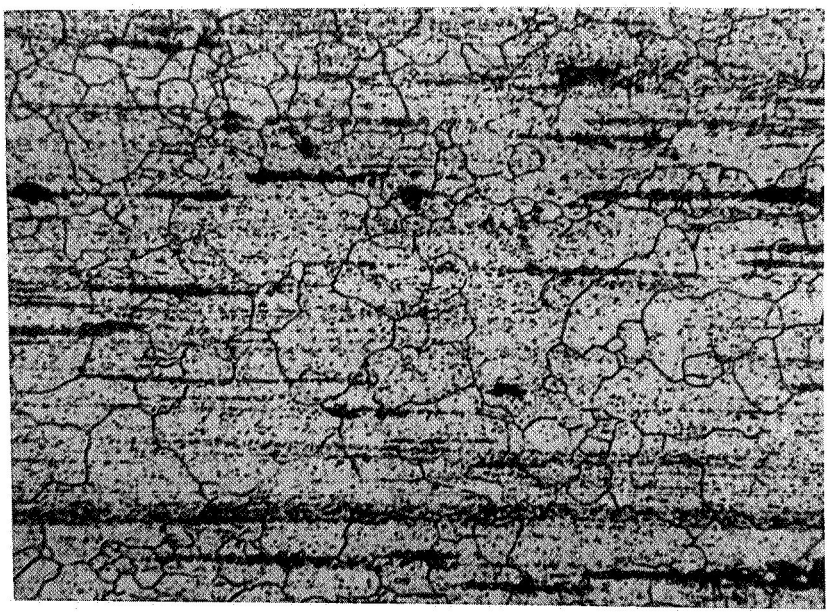

(a) 500X

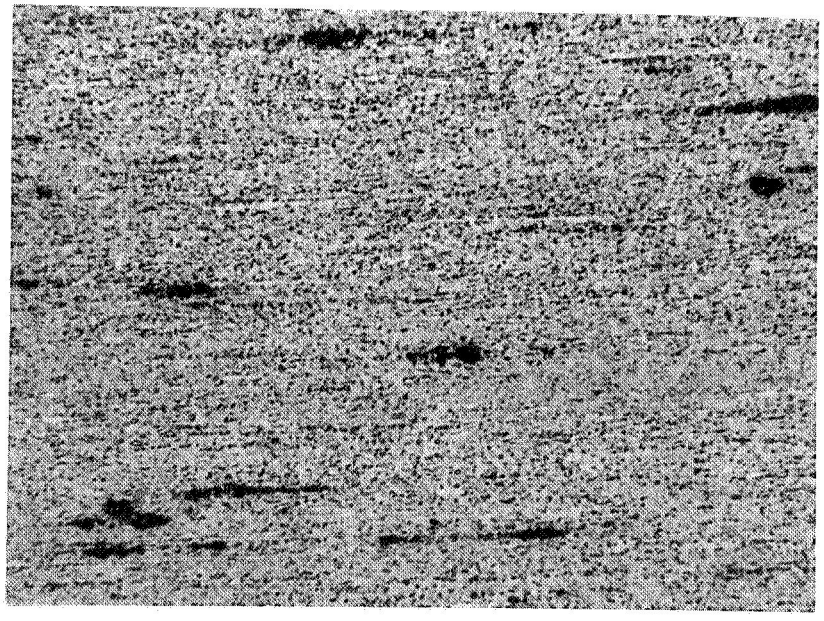

(b) 500X

FIGURE 32. Optical micrographs of (a) extruded plus annealed Ni-20Cr, (b) extruded plus annealed Ni-20Cr-2ThO_2.

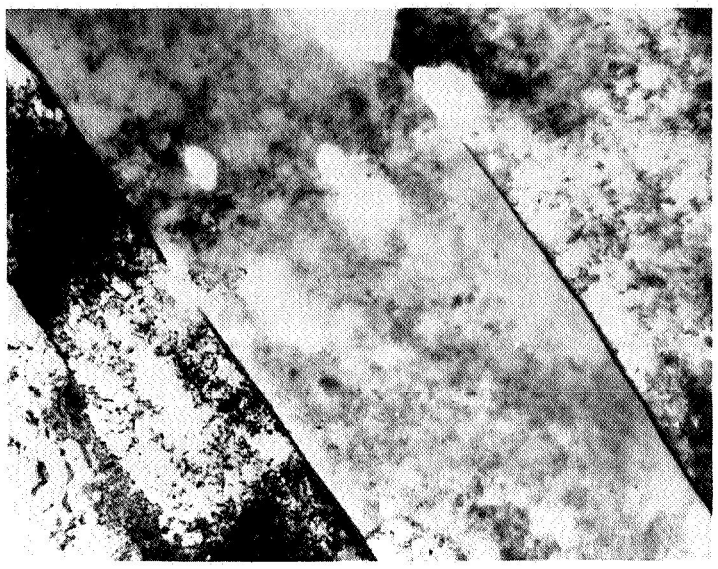

(a) 30,000X

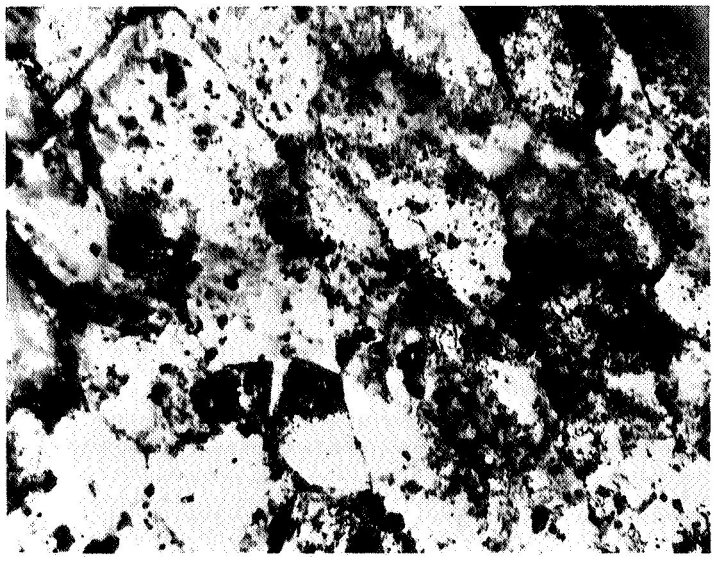

(b) 30,000X

FIGURE 33. Transmission electron micrographs of (a) Ni-20Cr drawn 24.4% by Procedure A, (b) Ni-20Cr-2ThO_2 drawn 23.7% by Procedure A.

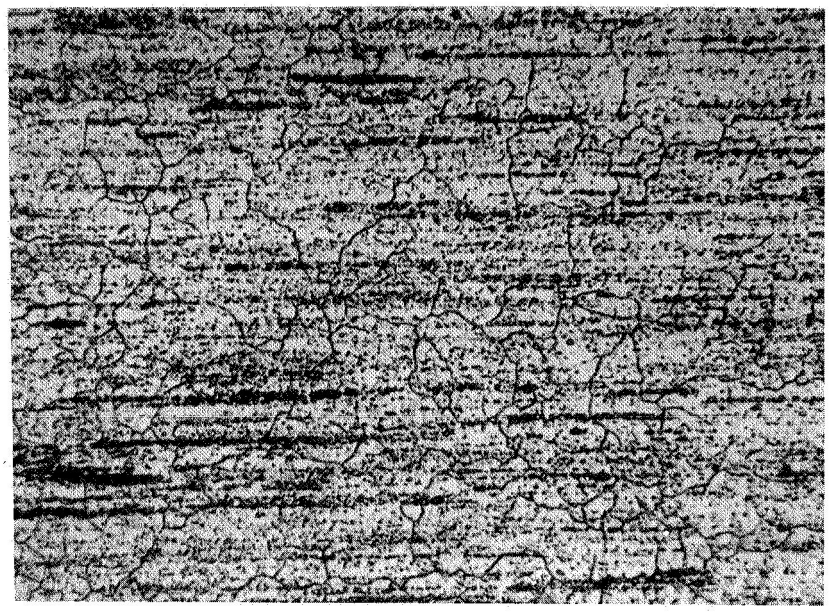

(a) 500X

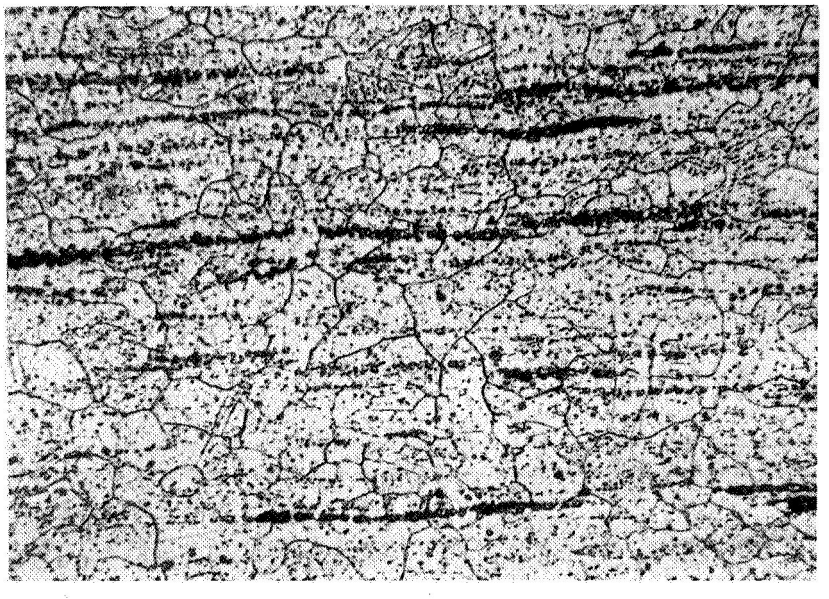

(b) 500X

FIGURE 34. Examples of optical microstructures of Ni-20Cr (a) drawn 24.4% by Procedure B, (b) swaged 49.1% by Procedure B.

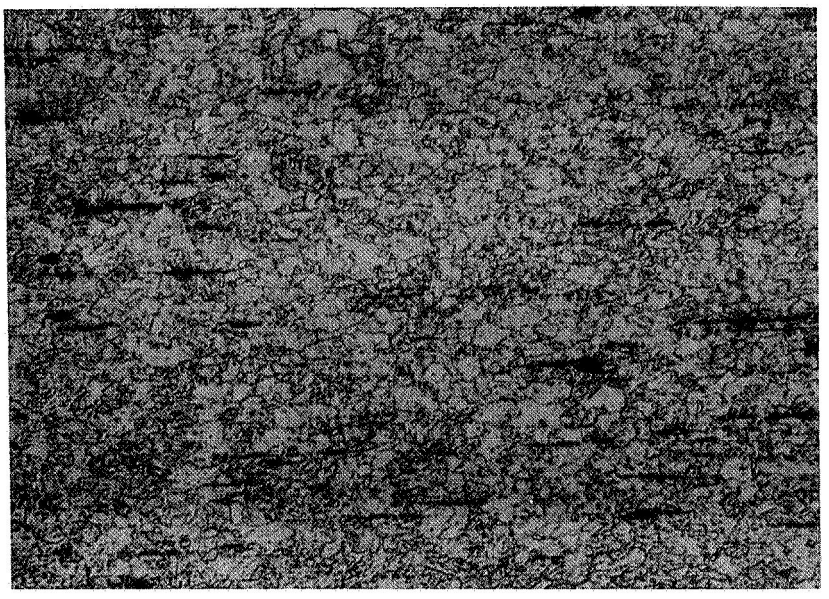

(a) 200X

(b) 30,000X

FIGURE 35. Microstructure of Ni-20Cr-2ThO_2 drawn 25.6% by Procedure B; (a) optical micrograph, (b) transmission electron micrograph.

TABLE 12. GRAIN OR CELL SIZE IN Ni-20Cr AND Ni-20Cr-2ThO_2 AS A FUNCTION OF DRAWING BY PROCEDURES A AND B[2]

Drawing or Swaging Procedure	Total Reduction by Drawing or Swaging,%	Grain or Cell Dia., ℓ, μm	$\ell^{-1/2}$, $\mu m^{-1/2}$	Comments
		Ni-20Cr		
As-extruded	0	18.8	0.231	Recrystallized, ℓ = grain dia.
Drawn - Procedure A	24.4	0.69	1.20	Not recrystallized, ℓ = cell dia.
Extruded + Annealed	0	20.5	0.221	Recrystallized, ℓ = grain dia.
Drawn - Procedure B	24.4	15.4	0.225	Recrystallized, ℓ = grain dia.
Swage - Procedure B	49.1	16.5	0.246	Recrystallized, ℓ = grain dia.
Drawn - Procedure B	58.0	20.0	0.224	Recrystallized, ℓ = grain dia.
		Ni-20Cr-2ThO_2		
As-extruded	0	0.67	1.22	Not recrystallized, ℓ = cell dia.
Drawn - Procedure A	23.7	0.31	1.80	Not recrystallized, ℓ = cell dia.
Drawn - Procedure B	25.6	3.5	0.54	Recrystallized, ℓ = grain dia.
Drawn - Procedure B	53.8	0.71	1.19	Recrystallized, ℓ = grain dia.
Swaged - Procedure B	47.7	1.3	0.87	Recrystallized, ℓ = grain dia.

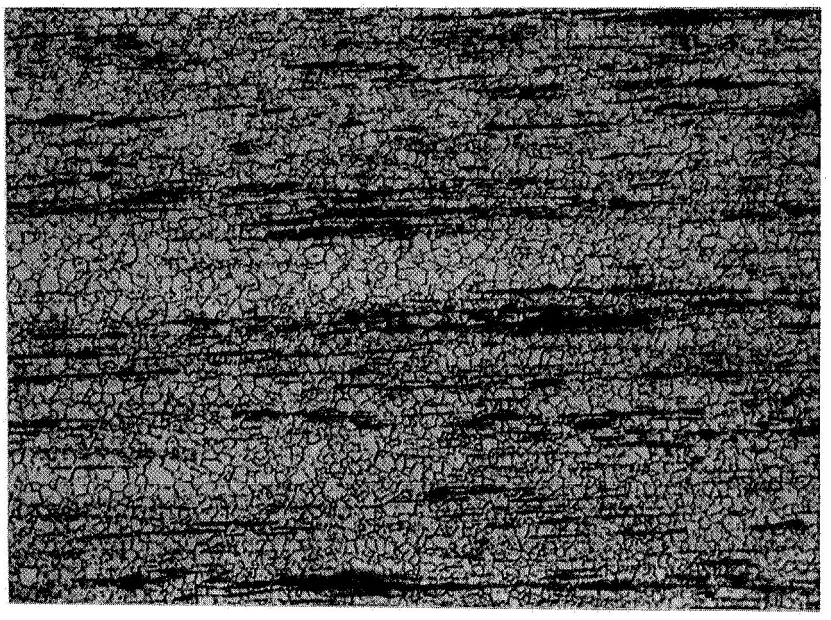

(a) 200X

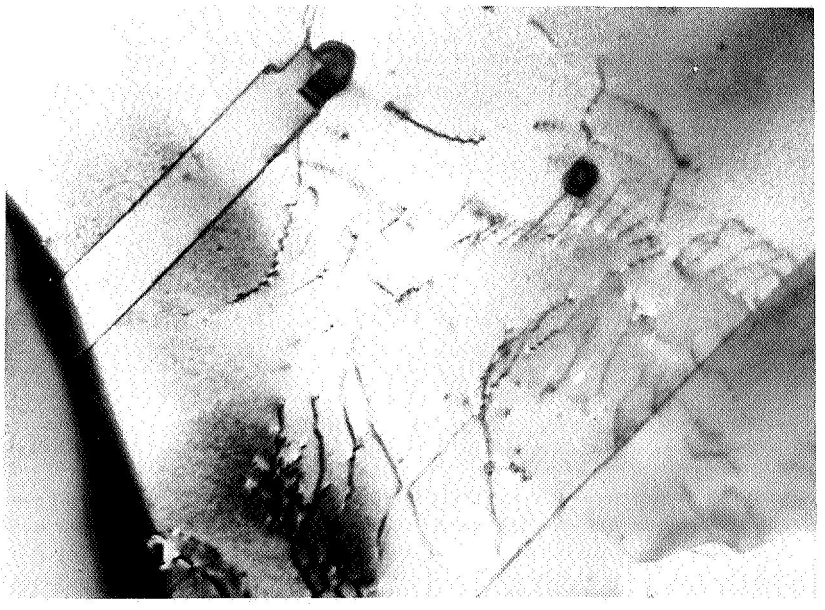

(b) 30,000X

FIGURE 36. Microstructure of extruded plus annealed Ni-20Cr-10W; (a) optical micrograph, (b) transmission electron micrograph. Note particle (presumably Cr_2O_3) blocking non-coherent twin boundary.

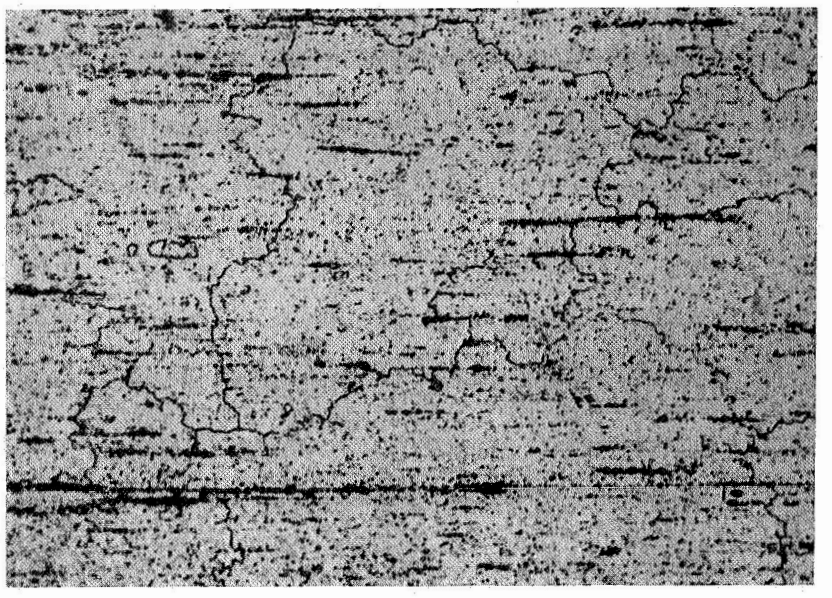

(a) 200X

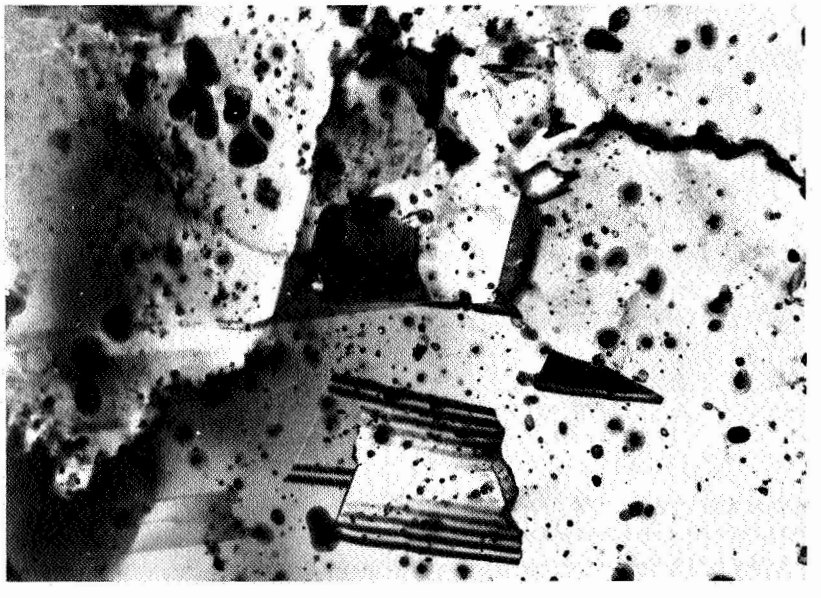

(b) 30,000X

FIGURE 37. Microstructure of extruded plus annealed Ni-20Cr-10W-2ThO_2; (a) optical micrograph, (b) transmission electron micrograph.

subboundaries present, in addition to the fine annealing twins. Swaging the two tungsten-containing alloys 53.9% by Procedure B (using 1200°C anneals), gave resulting microstructures (Figure 38) which were fine grained and nearly equiaxed. The extremely fine grain size in the Ni-20Cr-10W alloy (Figure 38a) caused this material to exhibit superplastic tendencies when tensile tested at 1093°C.*

It was observed that annealing the Ni-20Cr-2ThO_2 and Ni-20Cr-10W-2ThO_2 alloys for 1 hour at 1200°C after working by Procedure B, always produced fine nearly equiaxed grains, regardless of whether the working was by extrusion, drawing, or swaging. However, the annealing treatment (1 hour at 1316°C) used by Fansteel on the extruded Ni-20Cr-10W-2ThO_2 produced a coarse somewhat elongated recrystallized grain structure. An attempt was made to develop such a structure in Ni-20Cr-2ThO_2 by annealing for 1 hour in H_2 at 1316°C. The optical micrograph in Figure 39(a) shows that this attempt was successful.** The TEM in Figure 39(b) reveals fine annealing twins and very little dislocation substructure, which is typical of commercial TD Nickel chromium.[5,12,42,65] Thus it appears that there is a critical annealing temperature between 1200 and 1316°C required to produce the coarse elongated recrystallized structure in extruded Ni-20Cr-2ThO_2 and Ni-20Cr-10W-2ThO_2 alloys.

Tensile Deformation

The results of tensile deformation studies at 25 and 1093°C are listed in Tables 13 (Ni-20Cr), 14 (Ni-20Cr-2ThO_2), and 15 (the two W-containing alloys).

---

* See Table 15.

** This procedure for producing coarse elongated grains in Ni-20Cr-2ThO_2 was discovered near the end of the experimental program, and it was not possible to perform any tensile or creep tests on material with this structure.

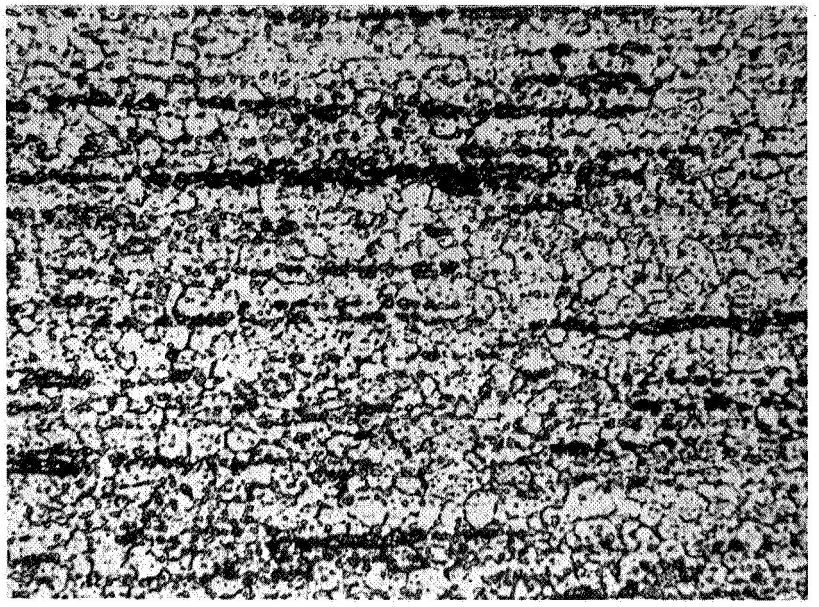

(a) 500X

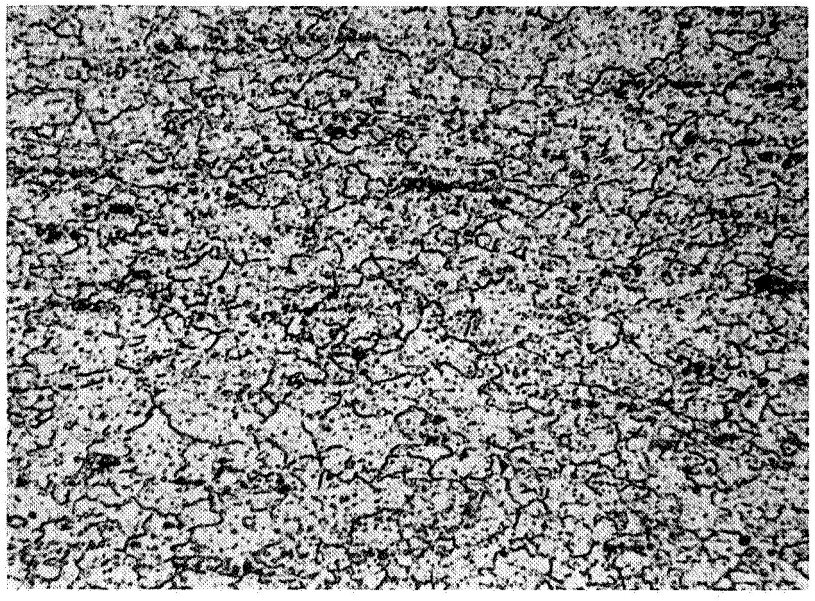

(b) 500X

FIGURE 38. Optical micrographs of (a) Ni-20Cr-10W swaged 53.9% by Procedure B, (b) Ni-20Cr-10W-2ThO_2 swaged 53.9% by Procedure B.

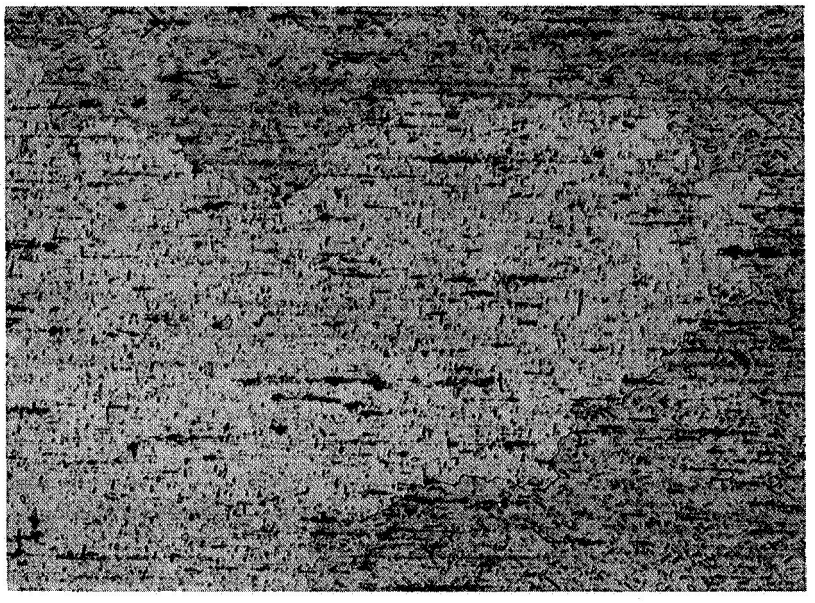

(a) 200X

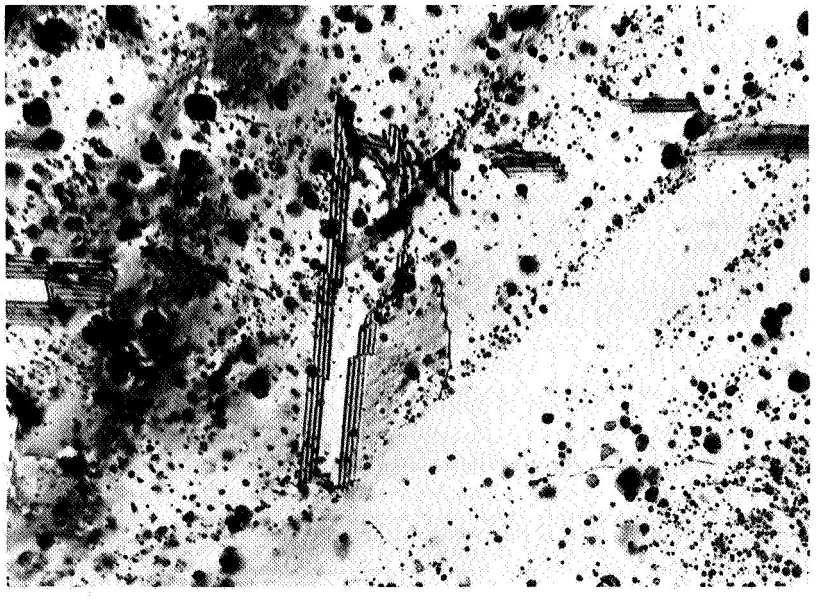

(b) 30,000X

FIGURE 39. Recrystallized microstructure of Ni-20Cr-2ThO_2 annealed 1 hour in H_2 at 1316°C; (a) optical micrograph, (b) transmission electron micrograph.

TABLE 13. TENSILE PROPERTIES OF Ni-20Cr AT 25 AND 1093°C AFTER DRAWING AND SWAGING BY PROCEDURES A AND B

Test T, °C	Rod or Wire Dia., in.	Method of Working	Total % Reduction by Drawing or Swaging	True Drawing or Swaging Strain	Prop. Lim., psi	0.2% Y.S., psi	U.T.S., psi	RA,%	Uniform Elongation,%	Total Elongation,%
				Procedure A (no intermediate anneals)						
25	0.375	As-extruded	0	0	41,000	45,600	101,500	39.3	23.7	25.0
25	0.326	Drawing	24.4	0.28	106,000	122,000	124,500	31.0	1.0	3.8
25	0.306	Drawing	33.4	0.41	101,500	123,000	126,000	25.0	1.1	3.1
1093	0.375	As-extruded	0	0	3,640	4,600	4,600	3.4	0.3	2.0
1093	0.326	Drawing	24.4	0.28	4,030	4,650	4,650	1.6	0.2	1.1
1093	0.306	Drawing	33.4	0.41	2,660	3,030	3,030	0.9	0.2	2.1
				Procedure B (intermediate anneals, 1200°C, 1 hour, H_2, after each 25% reduction)						
25	0.375	Extruded + annealed	0	0	31,500	40,600	95,700	41.3	24.9	26.8
25	0.326	Drawing	24.4	0.28	47,800	54,400	110,000	35.2	27.9	27.9
25	0.269	Swaging	49.1	0.68	40,300	45,000	98,700	44.9	33.2	35.8
25	0.243	Drawing	58.0	0.87	40,700	42,300	95,000	38.5	38.6	41.2
1093	0.375	Extruded + annealed	0	0	3,760	4,110	4,110	2.1	0.3	1.3
1093	0.326	Drawing	24.4	0.28	3,830	4,230	4,230	1.5	0.2	1.4
1093	0.269	Swaging	49.1	0.68	2,490	3,210	3,280	1.7 (a)	0.4 (a)	5.1 (a)
1093	0.243	Drawing	58.0	0.87	2,040	2,720	2,830	-	-	-

(a) Specimen broke outside gage length at flaw--no ductility measurements possible.

TABLE 13a. SAME AS TABLE 13, SI UNITS

Test, T, °C	Rod or Wire Dia., cm	Method of Working	Total % Reduction by Drawing or Swaging	True Drawing or Swaging Strain	Prop. Lim., MN/m^2	0.2% Y.S., MN/m^2	U.T.S., MN/m^2	RA, %	Uniform Elongation, %	Total Elongation, %
				Procedure A (no intermediate anneals)						
25	0.951	As-extruded	0	0	283	311	700	39.3	23.7	25.0
25	0.827	Drawing	24.4	0.28	771	841	860	31.0	1.0	3.8
25	0.776	Drawing	33.4	0.41	700	849	869	25.0	1.1	3.1
1093	0.951	As-extruded	0	0	25.1	31.7	31.7	3.4	0.3	2.0
1093	0.827	Drawing	24.4	0.28	27.8	31.1	31.1	1.6	0.2	1.1
1093	0.776	Drawing	33.4	0.41	18.4	20.9	20.9	0.9	0.2	2.1
				Procedure B (intermediate anneals, 1200°C, 1 hour, H_2, after each 25% reduction)						
25	0.951	Extruded + annealed	0	0	217	208	659	41.3	24.9	26.8
25	0.827	Drawing	24.4	0.28	330	368	759	35.2	27.9	27.9
25	0.682	Swaging	49.1	0.68	278	311	680	44.9	33.2	35.8
25	0.617	Drawing	58.0	0.87	282	292	655	38.5	38.6	41.2
1093	0.951	Extruded + annealed	0	0	25.9	28.3	28.3	2.1	0.3	1.3
1093	0.827	Drawing	24.4	0.28	26.4	29.2	29.2	1.5	0.2	1.4
1093	0.682	Swaging	49.1	0.68	17.3	22.1	22.6	1.7(a)	0.4(a)	5.1(a)
1093	0.617	Drawing	58.0	0.87	14.1	18.8	19.5	-(a)	-(a)	-(a)

(a) Specimen broke outside gage length at flaw--no ductility measurements possible.

TABLE 14. TENSILE PROPERTIES OF Ni-20Cr-2ThO_2 AT 25 AND 1093°C AFTER DRAWING AND SWAGING BY PROCEDURES A AND B

Test T, °C	Rod or Wire Dia., in.	Method of working	Total % Reduction by Drawing or Swaging	True Drawing or Swaging Strain	Prop. Lim., psi	0.2% Y.S., psi	U.T.S., psi	RA,%	Uniform Elongation,%	Total Elongation,%
			Procedure A (no intermediate anneals)							
25	0.350	As-extruded	0	0	123,880	142,620	152,000	29.4	8.8	11.2
25	0.306	Drawing	23.7	0.27	174,000	195,000	197,000	11.5	0.6	2.0
25	0.271	Swaging	40.1	0.51	142,000	165,000	168,000	27.1	1.3	4.0
25	0.256	Swaging	46.3	0.62	151,000	173,000	176,000	23.9	0.7	3.2
25	0.239	Swaging	53.4	0.76	160,000	181,000	185,000	22.4	0.8	3.4
1093	0.350	As-extruded	0	0	950	1,640	2,660	27.1	6.6	23.7
1093	0.306	Drawing	23.7	0.27	5,700	7,200	7,900	3.3	1.2	2.7
1093	0.256	Swaging	46.3	0.62	2,450	3,590	4,680	18.3	3.5	7.5
		Procedure B (intermediate anneals, 1200°C, 1 hour, H_2, after each 25% reduction)								
25	0.400	Extruded + annealed	0	0	121,650	137,060	144,360	36.3	10.7	13.6
25	0.345	Drawing	25.6	0.30	103,000	107,000	141,000	30.0	15.6	17.1
25	0.290	Swaging	47.7	0.65	118,000	127,000	143,000	39.2	11.1	16.9
25	0.272	Drawing	53.8	0.77	136,500	143,000	161,500	22.4	11.8	14.9
25	0.257	Drawing	58.8		114,500	123,000	153,000	19.5	13.8	15.3
1093	0.400	Extruded + annealed	0	0	1,310	2,030	2,720	34.5	8.1	25.1
1093	0.245	Drawing	25.6	0.30	4,930	6,100	6,320	3.3	1.0	4.7
1093	0.290	Swaging	47.7	0.65	3,260	3,670	4,230	13.9	4.7	13.0
1093	0.272	Drawing	53.8	0.77	5,410	7,680	9,250	6.0	3.2	5.0
1093	0.257	Drawing	58.8	0.89	6,680	8,330	9,300	4.7	1.0	3.6

TABLE 14a. SAME AS TABLE 14, SI UNITS

Test, T, °C	Rod or Wire Dia., cm	Method of Working	Total % Reduction by Drawing or Swaging	True Drawing or Swaging Strain	Prop. Lim., MN/m^2	0.2% Y.S., MN/m^2	U.T.S., MN/m^2	RA, T	Uniform Elongation, %	Total Elongation, %
			Procedure A (no intermediate anneals)							
25	0.889	As-extruded	0	0	815	983	1049	29.4	8.8	11.2
25	0.777	Drawing	23.7	0.27	1200	1345	1360	11.5	0.6	2.0
25	0.686	Swaging	40.1	0.51	980	1138	1160	27.1	1.3	4.0
25	0.675	Swaging	46.3	0.62	1040	1192	1215	23.9	0.7	3.2
25	0.607	Swaging	53.4	0.76	1105	1250	1276	22.4	0.8	3.4
1093	0.889	As-extruded	0	0	6.5	11.3	18.3	27.1	6.6	23.7
1093	0.777	Drawing	23.7	0.27	39.3	49.7	54.5	3.3	1.2	2.7
1093	0.675	Swaging	46.3	0.62	16.9	24.7	32.3	18.3	3.5	7.5
			Procedure B (intermediate anneals, 1200°C, 1 hour, H_2, after each 25% reduction)							
25	1.016	Extruded + annealed	0	0	840	945	997	36.3	10.7	13.6
25	0.875	Drawing	25.6	0.30	711	737	973	30.0	15.6	17.1
25	0.737	Swaging	47.7	0.65	813	876	987	39.2	11.1	16.9
25	0.691	Drawing	53.8	0.77	942	987	1115	22.4	11.8	14.9
25	0.650	Drawing	58.8		790	848	1055	19.5	13.8	15.3
1093	1.016	Extruded + annealed	0	0		14.0	18.8	34.5	8.1	25.1
1093	0.622	Drawing	25.6	0.30	34.0	42.1	43.5	3.3	1.0	4.7
1093	0.737	Swaging	47.7	0.65	22.5	25.3	29.3	13.9	4.7	13.0
1093	0.691	Drawing	53.8	0.77	37.3	53.0	63.7	6.0	3.2	5.0
1093	0.650	Drawing	58.8	0.89	46.2	57.5	64.2	4.7	1.0	3.6

TABLE 15. TENSILE PROPERTIES OF Ni-20Cr-10W AND Ni-20Cr-10W-2ThO_2 AT 25 AND 1093°C AFTER SWAGING BY PROCEDURE B (Intermediate anneals, 1200°C, 1 hour, H_2 after each 25% reduction.)

Test T, °C	Rod or Wire Dia. in.	Total % Reduction by Swaging	True Swaging Strain	Prop. Lim., psi	0.2% Y.S., psi	U.T.S., psi	RA,%	Uniform Elongation,%	Total Elongation,%
				Ni-20Cr-10W					
25	0.376[a]	0	0	65,600	70,000	125,800	26.1	28.3	28.3
25	0.256	53.9	0.78	78,000	79,300	121,300	24.5	22.6	22.6
1093	0.376[a]	0	0	1,230	2,210	2,290	4.3	0.4	5.1
1093	0.256	53.9	0.78	600	710	870	22.9	7.4	91.0[b]
				Ni-20Cr-10W-2ThO_2					
25	0.377[a]	0	0	94,000	103,500	156,000	11.6	10.9	10.9
25	0.256	53.9	0.78	99,000	109,000	139,000	16.9	8.6	8.6
1093	0.377[a]	0	0	7,220	7,800	7,800	2.0	0.2	0.2
1093	0.256	53.9	0.78	3,240	4,050	4,450	3.6	0.8	7.7

(a) Extruded plus annealed.

(b) This specimen exhibited superplastic tendencies.

TABLE 15a. SAME AS TABLE 15, SI UNITS

Test T, °C	Rod or Wire Dia. cm	Total % Reduction by Swaging	True Swaging Strain	Prop. Lim., MN/m^2	0.2% Y.S., MN/m^2	U.T.S., MN/m^2	RA, %	Uniform Elongation, %	Total Elongation, %
				Ni-20Cr-10W					
25	0.955[a]	0	0	453	483	862	26.1	28.3	28.3
25	0.650	53.9	0.78	538	547	837	24.5	22.6	22.6
1093	0.955[a]	0	0	8.5	15.3	15.8	4.3	0.4	5.1
1093	0.650	53.9	0.78	4.1	4.9	6.0	22.9	7.4	91.0[b]
				Ni-20Cr-10W-2ThO_2					
25	0.956[a]	0	0	648	713	1072	11.6	10.9	10.9
25	0.650	53.9	0.78	683	752	959	16.9	8.6	8.5
1093	0.956[a]	0	0	49.8	53.8	53.8	2.0	0.2	0.2
1093	0.650	53.9	0.78	22.4	22.9	30.7	3.6	0.8	7.7

(a) Extruded plus annealed.

(b) This specimen exhibited superplastic tendencies.

The data for Ni-20Cr and Ni-20Cr-2ThO_2 are plotted as a function of drawing or swaging reduction in Figures 40-43 for tests at room temperature and 1093°C. The strength of both alloys at room temperature (Figures 40-41) increased substantially as a result of drawing by Procedure A, and this was due to the substructure refinement (see Figure 33). However, drawing or swaging by Procedure B caused essentially no increase in room temperature strength (Figures 40 and 41), and this is attributed to the fact that the 1200°C anneals recrystallized both alloys to a more or less constant fine grain size.

At 1093°C, both alloys were relatively weak (Figures 42 and 43), compared with Ni-2ThO_2 (Figure 16) although drawing the Ni-20Cr-2ThO_2 alloy by Procedures A and B did increase the elevated temperature yield strength from $\sim$ 2000 psi (13.8 MN/m^2) to $\sim$ 8000 psi (55.2 MN/m^2). The lower strength at 1093°C, compared with Ni-2ThO_2, is associated with the lower grain aspect ratio in the Ni-20Cr-2ThO_2 specimens.

Only a limited number of tensile deformation studies were made on the two tungsten-containing alloys (Table 15). The yield strength of extruded plus annealed Ni-20Cr-10W at room temperature was about 30,000 psi (207 MN/m^2) higher than the Ni-20Cr alloy in the same condition. This was probably due to a finer grain size in the W-containing alloy as well as some additional solid solution strengthening. When both of the W-containing alloys were swaged by Procedure B, they recrystallized during annealing, and the resultant room temperature strengths were only marginally increased. However, the strength of both alloys at 1093°C was greatly <u>decreased</u> by the swaging operation.

As in the case of Ni and Ni-2ThO_2, the room temperature yield strength data of Ni-20Cr and Ni-20Cr-2ThO_2 were analyzed in terms of the Hall-Petch relation. Figure 44 is a plot of the 0.2% yield strength at 25°C as a function of $\ell^{-1/2}$, and data of Webster[13] are included for both Ni-20Cr and Ni-20Cr-2ThO_2.

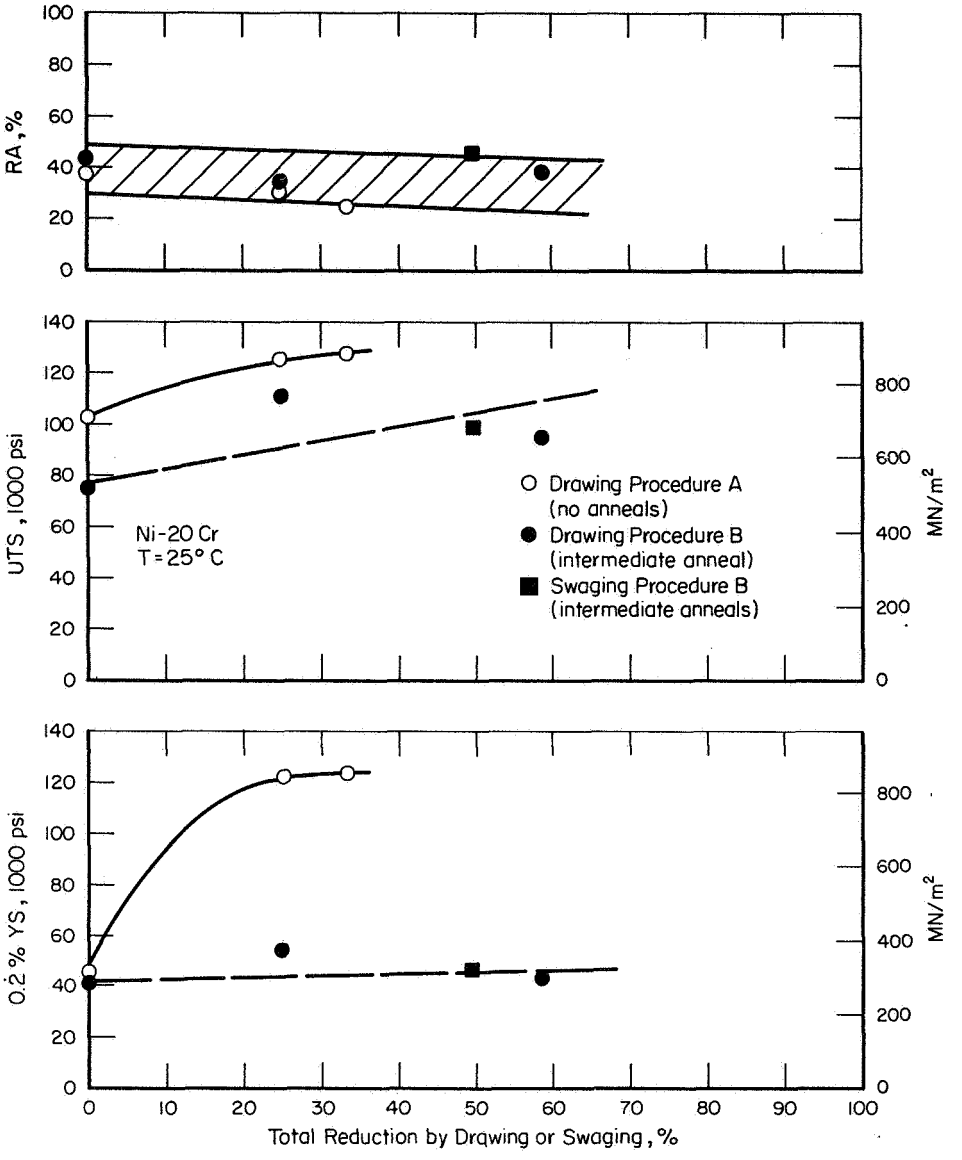

FIGURE 40. Effect of drawing and swaging by Procedures A and B on tensile properties of Ni-20Cr at 25°C.

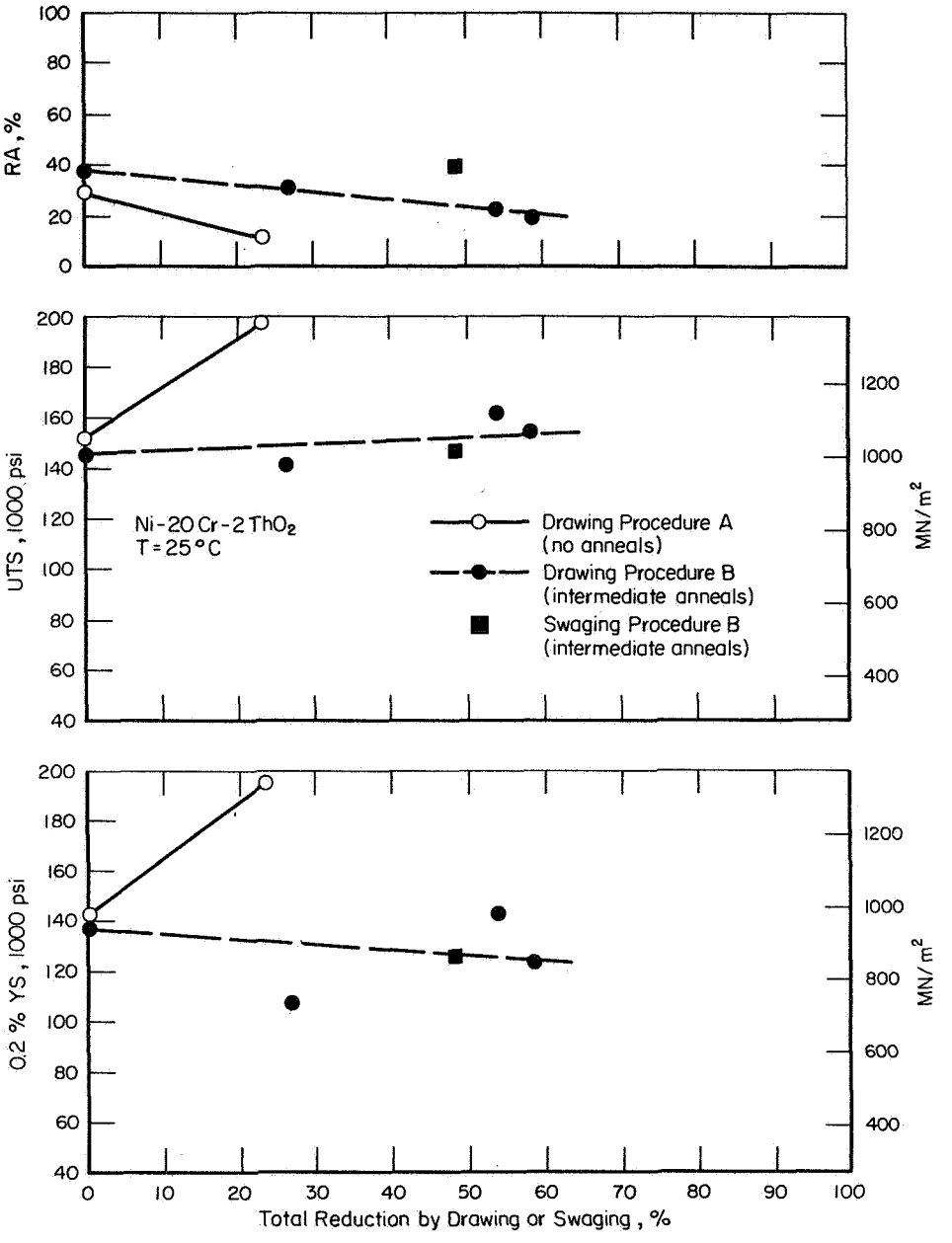

FIGURE 41. Effect of drawing and swaging by Procedures A and B on tensile properties of Ni-20Cr-2ThO_2 at 25°C.

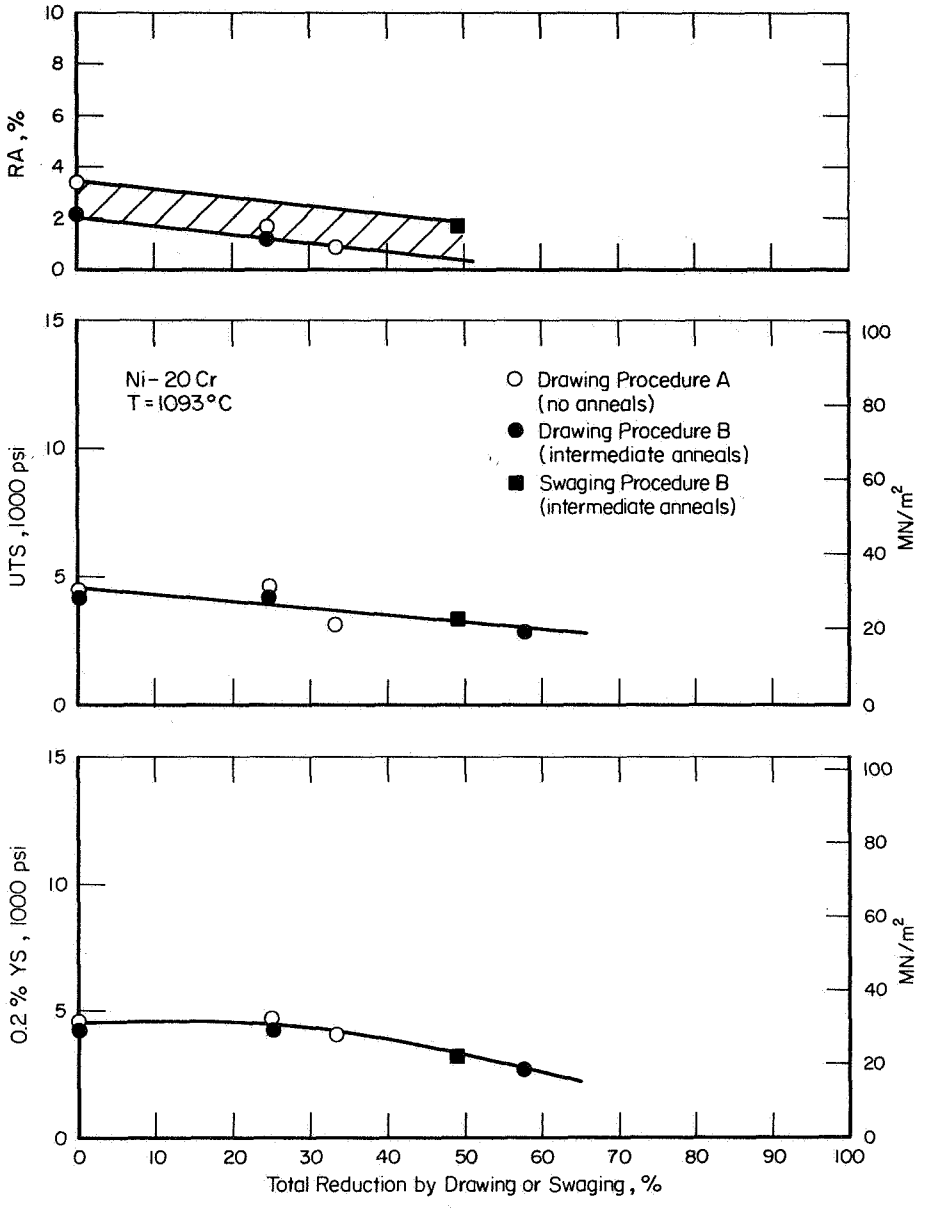

FIGURE 42. Effect of drawing and swaging by Procedures A and B on tensile properties of Ni-20Cr at 1093°C.

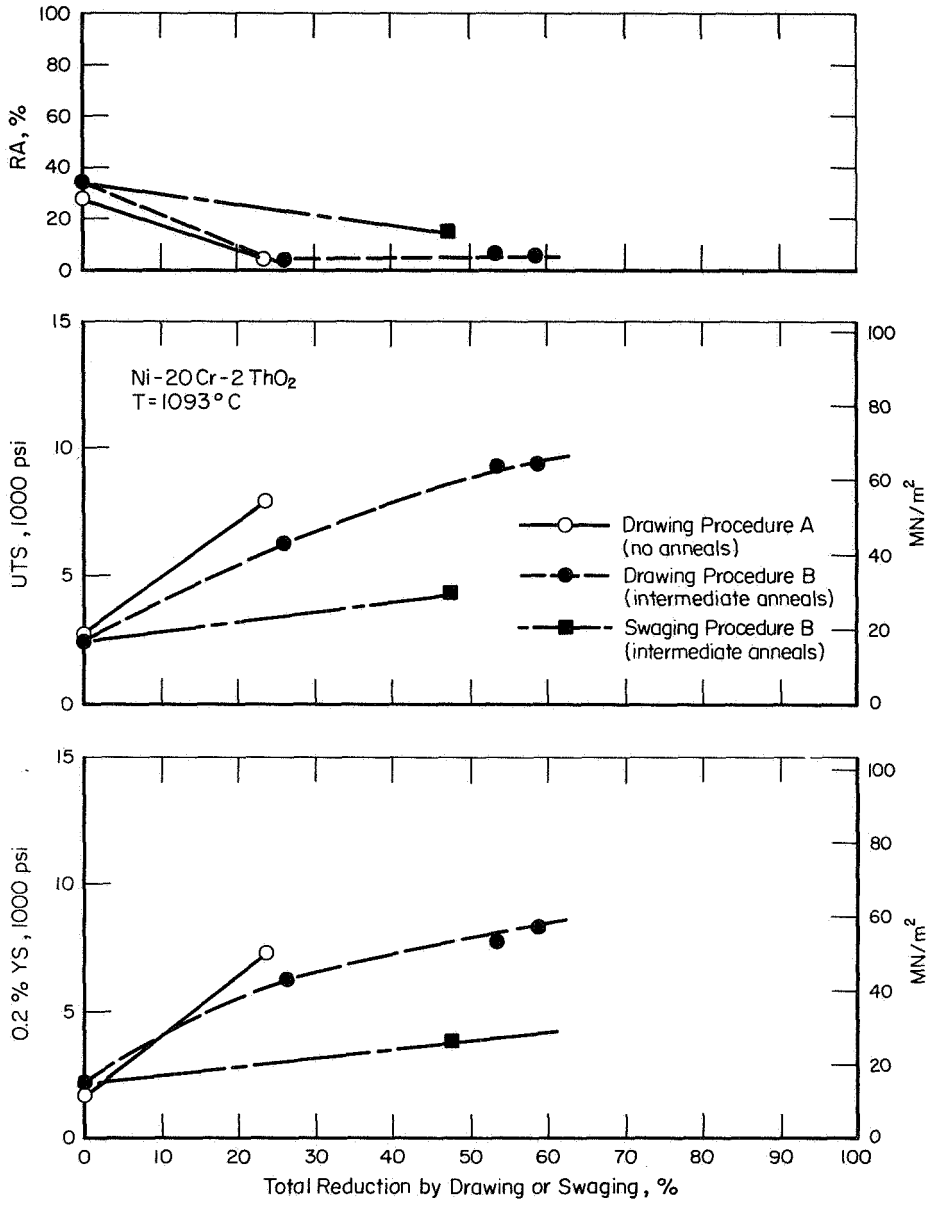

FIGURE 43. Effect of drawing and swaging by Procedures A and B on tensile properties of Ni-20Cr-2ThO_2 at 1093°C.

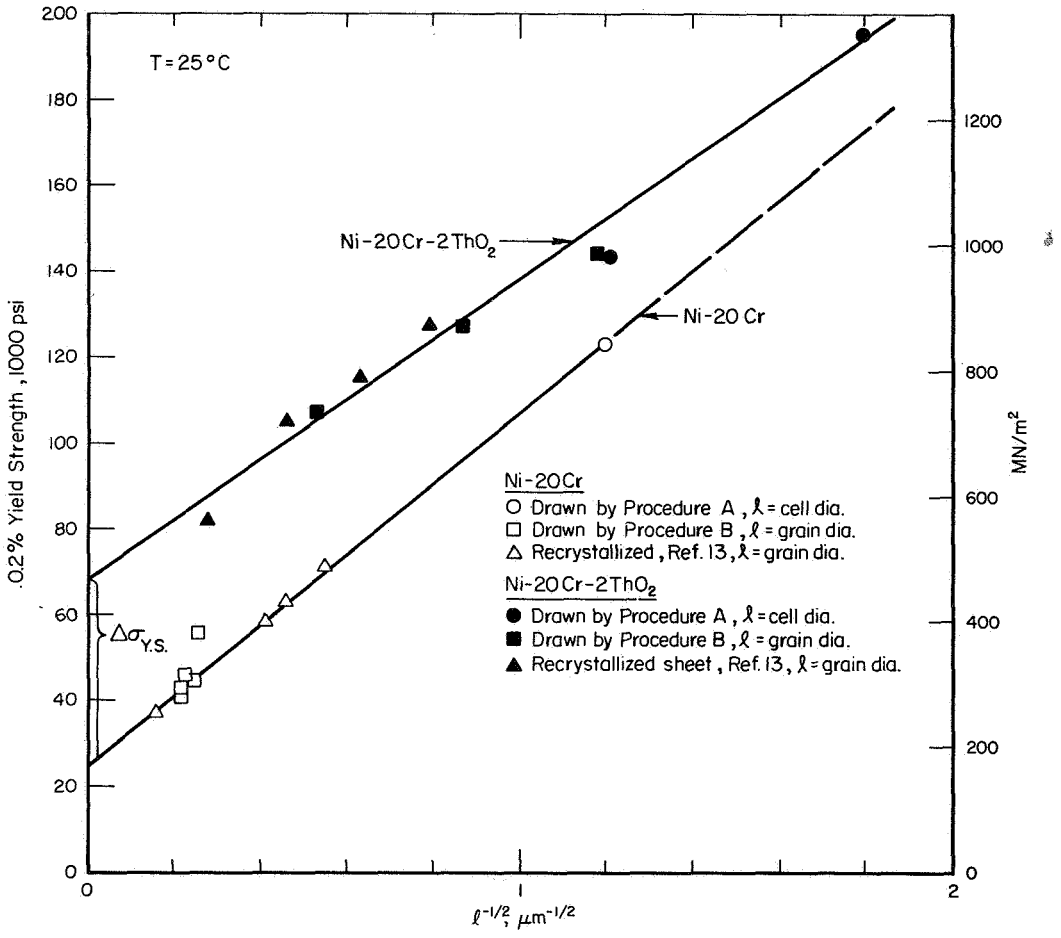

FIGURE 44. Dependence of room temperature yield strength (0.2% offset) of Ni-20Cr and Ni-20Cr-2ThO_2 on grain size and cell size. The value of $\Delta \sigma_{Y.S.}$ at $\ell^{-1/2} = 0$ is 42,000 psi (290 MN/m^2).

The general trend is the same here as in the case of Ni and Ni-2ThO_2 (Figure 18). The slope of the Ni-20Cr plot is greater than that for Ni-20Cr-2ThO_2, and there is a tendency for convergence of the two curves at smaller grain or cell sizes; i.e., larger $\ell^{-1/2}$ values. At $\ell^{-1/2} = 0$, the yield strength increase due to ThO_2 particles is $\Delta\sigma_{Y.S.}$ = 42,000 psi (290 MN/m^2), compared with $\Delta\sigma_{Y.S.}$ = 21,000 psi (145 MN/m^2) for Ni-2ThO_2 (Figure 18). This increase in yield strength due to ThO_2 particles in Ni-20Cr is higher than that calculated from Equation 6 for the Orowan mechanism, i.e., σ_p = 24,700 psi (171 MN/m^2). There is no obvious reason why agreement with the Orowan mechanism is realized for Ni-2ThO_2 but not for Ni-20Cr-2ThO_2. It has been reported that short range order (SRO) can occur in Ni-20Cr[66], and this may have a complicating effect on the room temperature yield strength. However, for SRO to account for part of the strength increase would mean that the Ni-20Cr-2ThO_2 alloy was more ordered than the Ni-20Cr alloy, and there is no a priori reason to believe that this is the case.

Creep and Creep Rupture

The creep results for Ni-20Cr-2ThO_2 are summarized in Table 16 and those for Ni-20Cr-10W-2ThO_2 are listed in Table 17. A plot of log $\dot{\epsilon}_{min}$ versus log σ for Ni-20Cr-2ThO_2 tested at 1093°C is shown in Figure 45, and a similar rupture life plot is illustrated in Figure 46. As in the case of Ni-2ThO_2, processing of Ni-20Cr-2ThO_2 by Procedure B increased the creep strength, and also slightly increased the stress exponents. Drawing 53.8% by Procedure B was more effective than swaging 47.7% in increasing the creep strength and rupture life. A discussion of this difference in terms of the resulting grain aspect ratio will be given in the General Discussion Section.

The creep results on the Ni-20Cr-10W-2ThO_2 alloy are plotted in Figure 47 (minimum creep rate) and Figure 48 (rupture life). The extruded plus

TABLE 16. CREEP PROPERTIES OF Ni-20Cr-2ThO_2 AT 1093°C AS A FUNCTION OF DRAWING AND SWAGING BY PROCEDURE B (intermediate anneals at 1200°C). Each specimen was tested in the annealed condition.

Rod or Wire Diameter in.	Rod or Wire Diameter cm	Total % Red. by Swaging or Drawing	Stress psi	Stress MN/m^2	Min. Creep Rate, hr^{-1}	Time to Rupture, hr	% Elongation	% RA
Extruded and Annealed								
0.400	1.016	0	1,000	6.9	1.53×10^{-4}	90.4	2.5	7.9
0.400	1.016	0	1,500	10.3	3.45×10^{-3}	38.3	5.2	2.9
0.400	1.016	0	1,800	12.4	1.17×10^{-2}	3.7	13.5	8.8
0.400	1.016	0	2,000	13.8	1.50×10^{-2}	2.0	7.6	3.0
Swaged to 0.290	0.736	47.7	1,800	12.4	3.00×10^{-5}	> 177 (a)	--	--
Swaged to 0.290	0.736	47.7	2,000	13.8	5.20×10^{-5}	100.1	5.0	4.1
Swaged to 0.290	0.736	47.7	3,000	20.7	1.11×10^{-3}	3.0	7.2	4.4
Drawn to 0.272	0.692	53.8	3,500	24.1	7.70×10^{-5}	160.0	2.9	1.3
Drawn to 0.272	0.692	53.8	4,000	27.6	4.67×10^{-4}	10.2 (b)	1.0	0.8
Drawn to 0.272	0.692	53.8	5,000	34.5	2.90×10^{-3}	5.9	3.0	1.4
Drawn to 0.272	0.692	53.8	6,000	41.3	6.28×10^{-3}	2.6	2.9	1.3

(a) Test stopped after 177 hours.

(b) Flaw in specimen, premature failure.

TABLE 17. CREEP PROPERTIES OF Ni-20Cr-10W-2ThO_2 AT 1093°C. All specimens tested in annealed condition (1 hr, 1200°C, H_2 atm.).

Rod or Wire Diameter in.	Rod or Wire Diameter cm	Total % Red. by Swaging	Stress psi	Stress MN/m^2	Min. Creep Rate, hr^{-1}	Time to Rupture, hr	% Elongation	% RA
Extruded and Annealed								
0.377	0.957	0	2,000	13.8	7.80×10^{-6}	80.2	0.5	0.2
0.377	0.957	0	5,000	34.5	3.50×10^{-3}	0.4	0.7	0.4
0.377	0.957	0	6,000	41.3	7.20×10^{-3}	0.2	0.9	0.1
Swaged and Annealed								
0.256	0.650	53.9	1,500	10.3	2.40×10^{-5}	> 143 (a)	--	--
0.256	0.650	53.9	2,000	13.8	2.02×10^{-4}	7.7	5.0	3.6
0.256	0.650	53.9	2,300	15.9	6.14×10^{-2}	0.65	5.7	5.2
0.256	0.650	53.9	3,000	20.7	1.42×10^{-1}	0.2	7.7	3.9

(a) Test stopped after 143 hours.

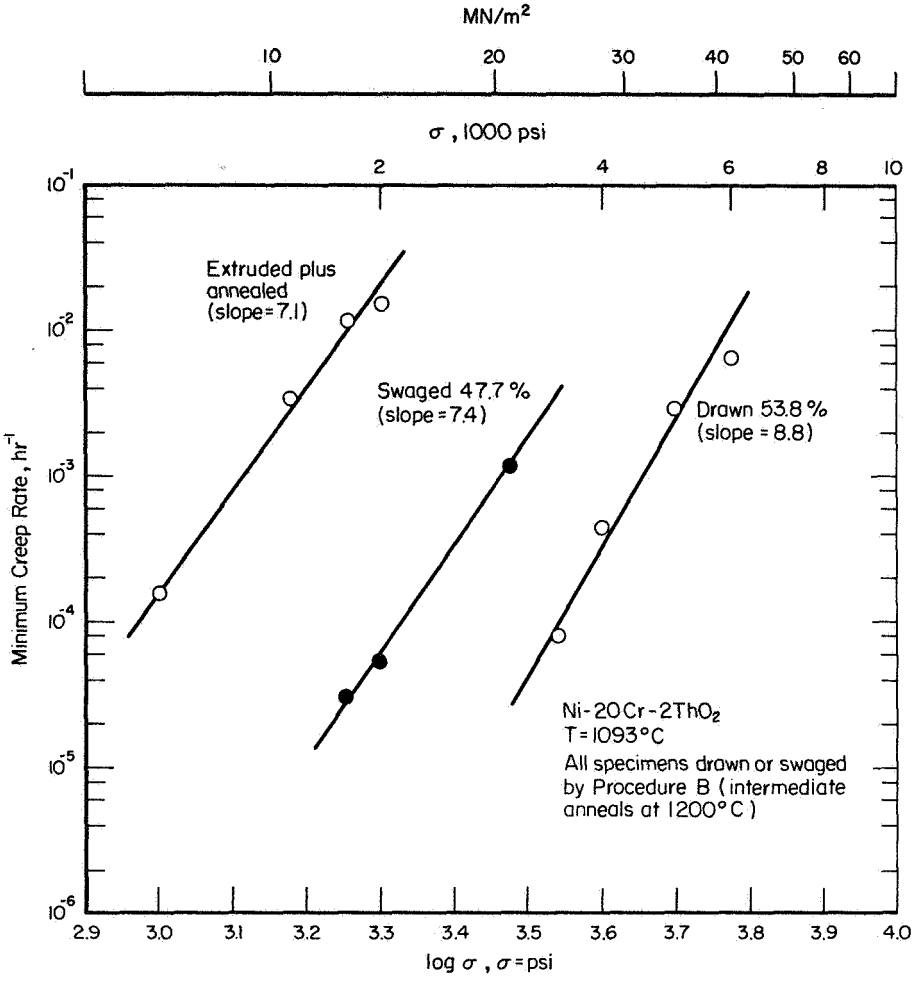

FIGURE 45. Effect of drawing or swaging by Procedure B on minimum creep rate of Ni-20Cr-2ThO_2 at 1093°C.

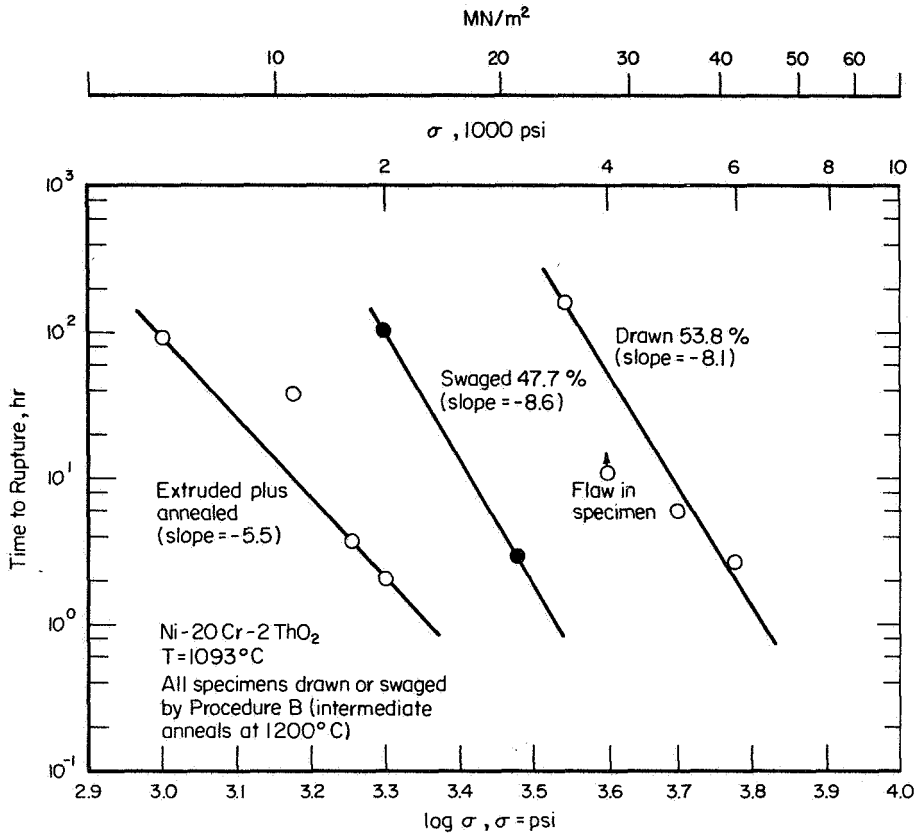

FIGURE 46. Effect of drawing or swaging by Procedure B on creep rupture life of Ni-20Cr-2ThO_2 at 1093°C.

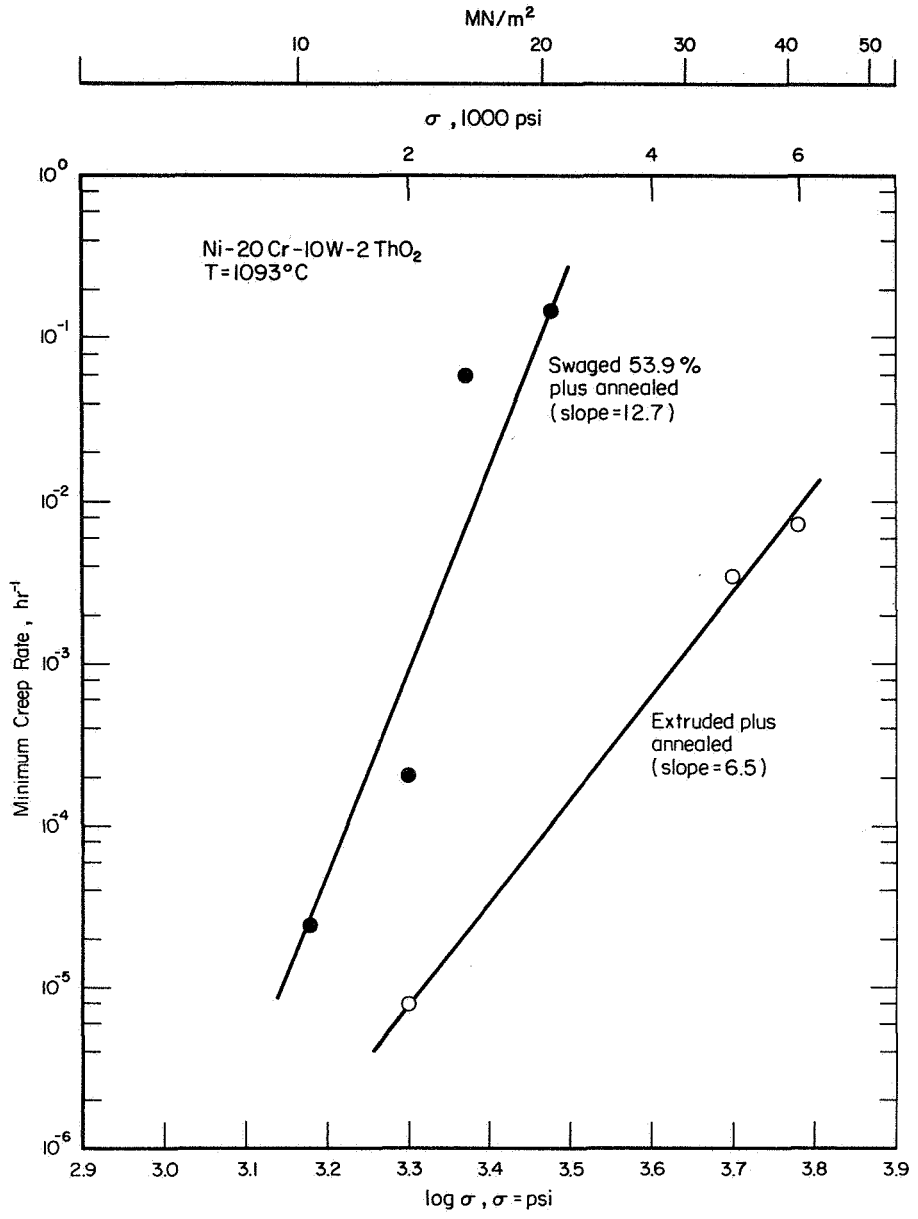

FIGURE 47. Effect of swaging by Procedure B on the minimum creep rate of Ni-20Cr-10W-2ThO_2 at 1093°C.

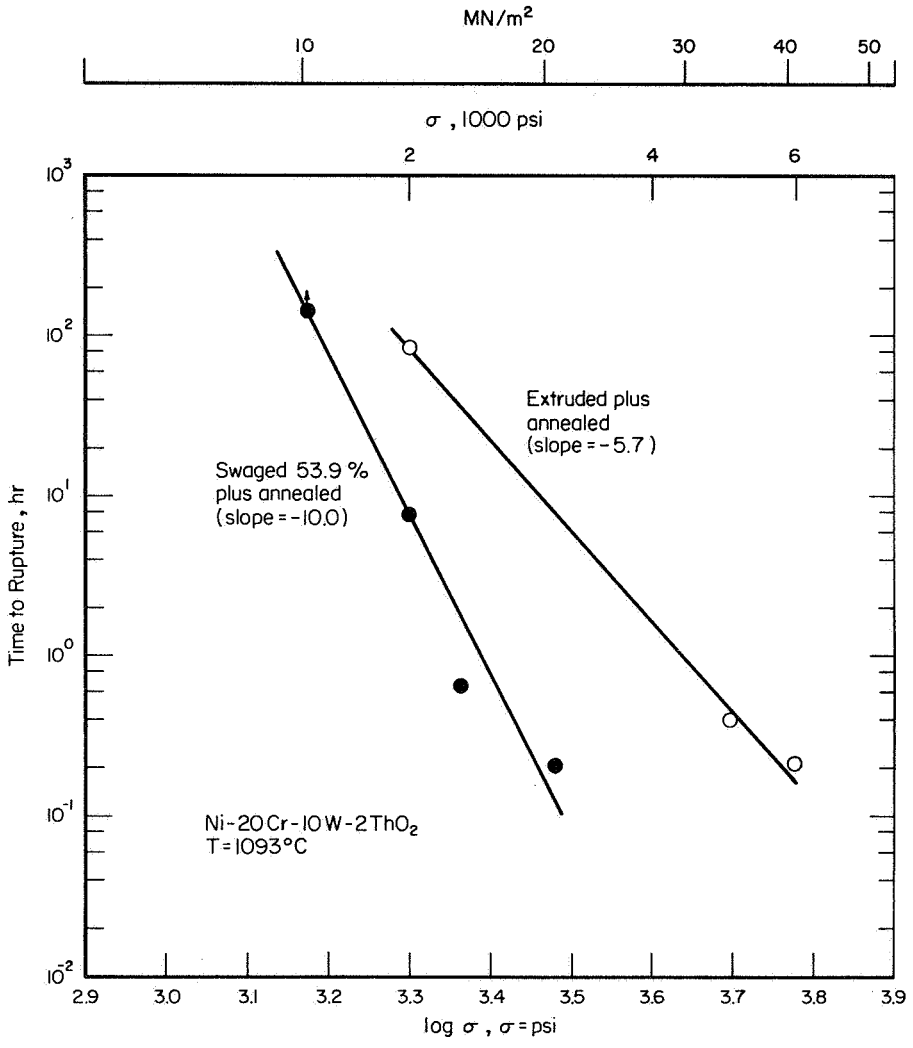

FIGURE 48. Effect of swaging by Procedure B on the rupture life of Ni-20Cr-10W-2ThO_2 at 1093°C.

annealed material is seen to be stronger than that which was swaged 53.9% by Procedure B. This is consistent with the yield strength results at 1093°C (Table 15), and is associated with the fact that the extruded plus annealed material had a coarse somewhat elongated grain structure (Figure 37a), whereas the swaged material had a fairly fine nearly equiaxed grain size (Figure 38b).

Texture

The results of texture determinations on the four Cr-containing alloys are presented in Table 18. Figures 21A-37A in the Appendix correspond to the specimen numbers (21-37) in Table 18. The results on these alloys are not as well defined as those for Ni and Ni-2ThO_2, and thus here it is only possible to indicate trends.

The non-thoriated alloys behaved rather like the pure nickel. The extrusion textures were mixed <100> and <112>, but the strengths of the components varied considerably. Possibly, the position in the extrusion was an important factor. Procedure B processing gave recrystallized structures and almost random textures. The extrusion texture in the Ni-20Cr-10W-2ThO_2 alloy was very weak, but after annealing (and recrystallization to a large grain size) it showed sharp <100> and <111> components. Swaging treatments by Procedure B rendered it very nearly random.

The results for Ni-20Cr-2ThO_2 are difficult to rationalize. The extruded bar had a moderate <100> texture which was apparently somewhat strengthened on light drawing by Procedure A. Drawing by Procedure B caused <100> to decrease and <111> to increase more rapidly than in the Ni-2ThO_2 alloy. However, specimen 34, which was swaged by Procedure B, had a quite different texture, with <100> much stronger than in any other specimen of this alloy. The explanation for this observation is not clear, since it seems unlikely that this is a result of swaging as opposed to drawing.

TABLE 18. QUANTITATIVE MEASURES OF TEXTURE INTENSITY IN Ni-20Cr, Ni-20Cr-2ThO_2, Ni-20Cr-10W AND Ni-20Cr-10W-2ThO_2 AFTER DRAWING OR SWAGING BY PROCEDURES A AND B

Alloy	Drawing or Swaging Procedure	Total Reduction by Drawing or Swaging, %	Specimen Number	$\frac{Pk_{200}}{(X \text{ random})}$	$\frac{Pk_{111}}{(X \text{ random})}$	$\frac{Pk_{200}}{Pk_{111}}$	Texture Concentration, %, Within 10° or 20° of Rod Axis			
							<100>, 10°	<100>, 20°	<111>, 10°	<111>, 20°
Ni-20Cr-2ThO_2	A[a]	As-extruded	21	8.6	1.6	5.4	19	40	7.7	21
"	Drawn-A	23.7	22	13	2.4	5.4	26	41	11	26
"	B[b]	Extruded + Annealed	23	11	1.6	6.9	23	42	6.8	19
"	Drawn-B	25.6	24	9.2	2.9	3.2	12	20	19	49
"	Swaged-B	47.7	34	32	6.9	4.6	39	46	19	38
"	Drawn-B	53.8	25	3.9	6.3	0.62	9.8	21	21	47
Ni-20Cr	A	As-extruded	26	37	0.31	119	30	33	7.2	48
"	Drawn-A	24.4	31	19	1.5	13	40	52	17	28
"	B	Extruded + Annealed	27	67	0.14	475	66	72	1.1	7.8
"	Drawn-B	24.4	32	0.5	0.8	0.6	1.3	8.9	7.7	43
"	Swaged-B	49.1	35	0.5	0.7	0.7	2.0	13	6.7	35
"	Drawn-B	58.0	37	1.0	0.55	1.8	6.7	24	3.8	16.6
Ni-20Cr-10W-2ThO_2	A	As-extruded[c]	28	2.4	1.4	1.7	8.5	25	8.0	25
"	B	Extruded + Annealed	29	8.3	20	0.41	6.6	11	45	61
"	Swaged-B	53.9	36	0.7	1.7	0.4	2.6	8.2	8.4	30
Ni-20Cr-10W	B	Extruded + Annealed	30	11	2.0	5.5	18	29	12	34
"	Swaged-B	53.9	33	1.7	1.3	1.3	5.6	16	8.4	29

(a) Procedure A: Draw or swage at 200°C; no intermediate anneals.

(b) Procedure B: Draw or swage at 200°C, with intermediate anneals (1200°C, 1 hour, H_2 atm.) after each 25% reduction. Texture measurements were on annealed specimens.

(c) A small piece of as-extruded Ni-20Cr-10W-2ThO_2 was sent from Fansteel. There was enough material for texture determinations, but not for mechanical property studies.

GENERAL DISCUSSION

Microstructure and Mechanical Properties

The results of this program show that thermomechanical processing can significantly alter the microstructure, texture, and mechanical properties of dispersion strengthened and dispersion-free Ni alloys. The microstructural changes cause changes in both room temperature and high temperature strength but different aspects of the microstructure are important in each temperature range.

Fine grain sizes or cell sizes promote strengthening at room temperature for all the alloys via the Hall-Petch relation. A summary plot in Figure 49 shows the room temperature yield strength versus $\ell^{-1/2}$ for Ni, Ni-2ThO_2, Ni-20Cr, and Ni-20Cr-2ThO_2. Several features are apparent in Figure 49.

For a given alloy base (Ni or Ni-20Cr) there is a convergence of the dispersion strengthened and dispersion-free curves. This is associated with the fact that grain size and particle strengthening are not directly additive. As the grain or cell size approaches the interparticle spacing of the thoriated alloys, the average spacing between barriers to dislocation motion, whether they are particles or boundaries, becomes about the same. Thus the particle strengthening and the grain size strengthening merge at very fine cell spacings. The convergence of Ni and Ni-2ThO_2 plots is more pronounced for the proportional limit (Figure 17) than for the 0.2% offset yield strength (Figure 18).

At $\ell^{-1/2} = 0$, the yield strength increment due to particles is 21,000 psi (145 MN/m^2) for Ni-2ThO_2 and 42,000 psi (290 MN/m^2) for Ni-20Cr-2ThO_2. For Ni-2ThO_2 this strengthening corresponds to that expected if the Orowan mechanism controlled yielding (Equation 6). However, for Ni-20Cr-2ThO_2, the increment in strength is about 1.7 times that expected from the Orowan mechanism. The reason for this difference in the two alloy bases is not clear.

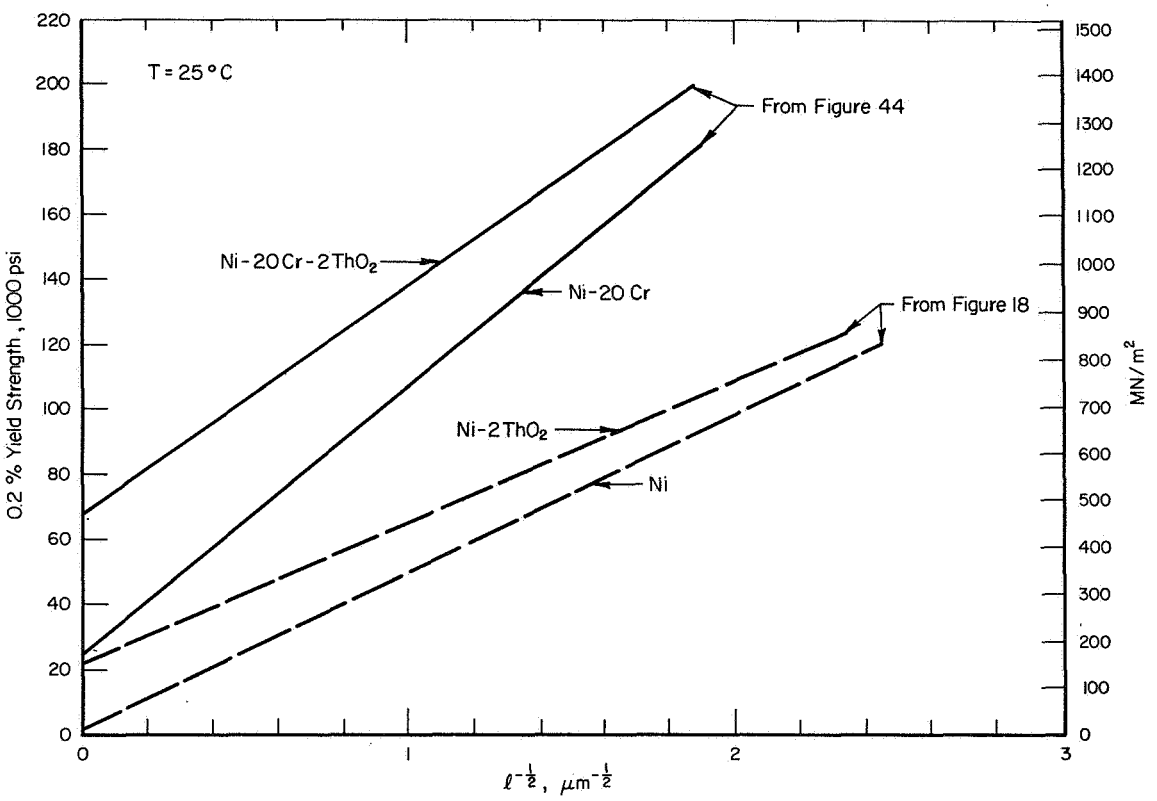

FIGURE 49. Hall-Petch plots for Ni, Ni-2ThO_2, Ni-20Cr, and Ni-20Cr-2ThO_2 at room temperature.

If the grain or cell size of Ni or Ni-20Cr were refined to the same size as the corresponding mean planar edge-to-edge ThO_2 particle spacings in Ni-2ThO_2 and Ni-20Cr-2ThO_2 (0.134 and 0.145 μm, respectively), the yield strength increments, σ_y - (σ_y at $\ell^{-1/2} = 0$), would be as follows:

	ℓ, μm	$\ell^{-1/2}$, $\mu m^{-1/2}$	σ_y psi	σ_y MN/m^2	$\sigma_y - (\sigma_y$ at $\ell^{-1/2} = 0)$ psi	$\sigma_y - (\sigma_y$ at $\ell^{-1/2} = 0)$ MN/m^2
Ni	0.134	2.73	135,500	935	133,500	921
Ni-20Cr	0.145	2.63	243,000	1675	218,000	1505

These values for substructure strengthening are considerably greather than the particle strengthening contributions at $\ell^{-1/2} = 0$, (21,000 psi [145 MN/m^2] Ni-2ThO_2 and 42,000 psi [290 MN/m^2] for Ni-20Cr-2ThO_2). Thus it appears that grain size or substructure strengthening at room temperature is about 5 to 6 times more potent than dispersion strengthening in these alloys, based on a comparison at the same spacing between particles and grain or cell boundaries.

Strengthening due to refinement of grain size or substructure is not directly additive to solid solution strengthening, since the Ni and Ni-20Cr plots are not parallel to Figure 49. In the two Cr-containing alloys strength increases more rapidly with increasing $\ell^{-1/2}$ than for the two corresponding Cr-free alloys. This effect has also been observed[71] when comparing Hall-Petch plots of Cu with Cu-30% Zn. Here it was found that the slope (k in Equation 8) was greater for the alloy. Thus it is concluded that the additivity relation in Equation 7 is not valid for the present alloys. No single values σ_p or σ_{sol} can be directly added to σ_{gb}, because the absolute values of σ_p and σ_{sol} depend upon grain or cell size.

The influence of microstructure on high temperature strength is both similar to and different from that at room temperature. Dispersion strengthening

(and possibly substructure strengthening) can be obtained at high temperatures as well as at room temperature. However, before this can be achieved, it is necessary to prevent or minimize flow by the weakest link; i.e., grain boundary sliding. This can be done by elongating the grains, and testing such that the tensile stress axis is parallel to the long axis of the grains. As the grain aspect ratio (L/ℓ), increases, the average shear stress on boundaries decreases and this decreases the overall sliding rate. Alternatively, a higher applied stress is required to produce sliding. The importance of grain aspect ratio on yielding, creep, and creep-rupture life of Ni-2ThO_2 at 1093°C was demonstrated in Figure 20. Other data from the literature have been analyzed and the results are listed in Table 19 and various strength parameters are plotted versus L/ℓ in Figure 50. The important features of Figure 40 are discussed below.

The yield strength, 100 hour rupture strength and stress required to produce a minimum creep rate of 10^{-4} hr^{-1} at 1093°C all increase linearly with increasing L/ℓ. This holds true, not only for Ni-2ThO_2, but for Ni-20Cr-2ThO_2, Ni-Cr-W-ThO_2 alloys, and dispersion strengthened Ni-base superalloys as well. It is recalled from Figure 20(a) and (c) that yield and creep results for coarse-grained recrystallized Ni-2ThO_2 fit the aspect ratio plots together with results from non-recrystallized specimens with fine elongated grains. Thus, in this case, it appears that grain size effects are not significant, and the dominant microstructural feature is grain aspect ratio. The same appears to hold true for alloys other than Ni-2ThO_2. The results on dispersion strengthened superalloys[33,34] (some of the open squares in Figure 50) appear to fall within the range of other data points. Although these materials were extruded they had a very coarse elongated grain structure. Cook, et al.[35] plotted the ultimate strength of Ni-Cr-Al-Ti-ThO_2 alloys at 1093°C versus grain size, and

TABLE 19. SUMMARY OF GRAIN ASPECT RATIO EFFECTS ON YIELD STRENGTH, CREEP RATE, AND RUPTURE LIFE OF DISPERSION STRENGTHENED Ni ALLOYS AT 1093°C[d]. All alloys had 2 to 3 vol.% ThO_2 (or Y_2O_3)

Alloy	Condition	L/ℓ	0.2% Y.S., psi	Stress to give $\dot{\epsilon}_{min} = 10^{-4}hr^{-1}$, psi	100-hour rupture stress, psi	Reference
Ni-20Cr-2ThO_2	As-extruded	1.4	1,640	-	-	This work
"	Drawn 23.7%, Procedure A	3.2	7,200	-	-	"
"	Extruded + Annealed	1.2	2,030	930	1,000	"
"	Drawn 25.6%, Procedure B	2.2	6,100	-	-	"
"	Swaged 47.7%, Procedure B	1.8	3,670	2,140	2,000	"
"	Drawn 53.8%, Procedure B	3.3	7,680	3,510	3,670	"
"	TD Ni Cr Sheet	~ 7.6[a]	18,200[b]	-	7,500-9,500	68
"	TD Ni Cr Foil	~ 1.9[a]	5,300	-	-	69
"	"	~ 2.1[a]	8,700[b]	-	-	"
"	"	~ 2.3[a]	8,400[b]	-	-	"
"	"	~ 4.8[a]	12,000[b]	-	-	"
"	"	~ 6.2[a]	14,500[b]	-	-	"
Ni-20Cr-10W-2ThO_2	Extruded + annealed	2.0	7,800	2,990	1,930	This work
"	Swaged 53.9%, Procedure B	1.9	4,050	1,680	1,580	"
Ni-Cr-W-ThO_2 Alloys	Fine grain recrystallized sheet	~ 2.4[a]	11,100[b]	-	-	67
"	"	~ 3.7[a]	13,400[b]	-	-	"
"	"	~ 4.4[a]	16,300[b]	-	-	"
"	"	~ 5.0[a]	18,300[b]	-	-	"
Ni-Cr-Al-Ti-ThO_2	Recrystallized, fine grain	~ 1.8[a]	8,200[b]	-	-	35
"	Recrystallized, very fine grain	~ 1[a]	4,200[b]	-	-	"
Ni-Cr-Al-Ti-Y_2O_3-Al_2O_3	Coarse grain, elongated	> 14[a]	~ 18,200[b,c]	~ 14,000[c]	~ 13,500[c]	34
Ni-Cr-Al-Ti-Y_2O_3	Coarse grain, elongated	> 11[a]	19,200[b,c]	-	~ 15,000[c]	33

(a) Values are approximate, since measurements of L/ℓ were made from only 1 micrograph in paper or report.
(b) Only ultimate strength reported; estimated 0.2% Y.S. by UTS - 800 psi (UTS - 0.2% Y.S. at 1093°C ≈ 800 psi on average).
(c) Interpolated from authors' results.
(d) When L/ℓ was determined for sheet, the value of ℓ was that measured from micrographs of the longitudinal sheet thickness.

TABLE 19a. SAME AS TABLE 19, SI UNITS

Alloy	Condition	L/ℓ	0.2% Y.S., MN/m^2	Stress to give $\dot{\epsilon}_{min} = 10^{-4}hr^{-1}$, MN/m^2	100-hour rupture stress, MN/m^2	Reference
Ni-20Cr-2ThO_2	As-extruded	1.4	11.3	-	-	This work
"	Drawn 23.7%, Procedure A	3.2	49.7	-	-	"
"	Extruded + Annealed	1.2	14.0	6.4	6.9	"
"	Drawn 25.6%, Procedure B	2.2	42.1	-	-	"
"	Swaged 47.7%, Procedure B	1.8q	25.3	14.8	13.8	"
"	Drawn 53.8%, Procedure B	3.3	53.0	24.2	25.3	"
"	TD Ni Cr Sheet	~ 7.6[a]	125[b]	-	51.7-65.5	68
"	TD Ni Cr Foil	~ 1.9[a]	36.6	-	-	69
"	"	~ 2.1[a]	60.0[b]	-	-	"
"	"	~ 2.3[a]	57.9[b]	-	-	"
"	"	~ 4.8[a]	82.8[b]	-	-	"
"	"	~ 6.2[a]	100[b]	-	-	"
Ni-20Cr-10W-2ThO_2	Extruded + Annealed	2.0	53.8	20.6	13.3	This work
"	Swaged 53.9%, Procedure B	1.9	28.0	11.6	10.9	"
Ni-Cr-W-ThO_2 Alloys	Fine grain recrystallized sheet	~ 2.4[a]	76.5[b]	-	-	67
"	"	~ 3.7[a]	92.5[b]	-	-	"
"	"	~ 4.4[a]	113[b]	-	-	"
"	"	~ 5.0[a]	126[b]	-	-	"
Ni-Cr-Al-Ti-ThO_2	Recrystallized, fine grain	~ 1.8[a]	56.5[b]	-	-	35
"	Recrystallized, very fine grain	~ 1[a]	29.0[b]	-	-	"
Ni-Cr-Al-Ti-Y_2O_3-Al_2O_3	Coarse grain, elongated	> 14[a]	~ 125[b,c]	~ 96.5[c]	~ 93.2[c]	34
Ni-Cr-Al-Ti-Y_2O_3	Coarse grain, elongated	> 11[a]	133[b,c]	-	~ 103[c]	33

(a) Values are approximate, since measurements of L/ℓ were made from only 1 micrograph in paper or report.
(b) Only ultimate strength reported; estimated 0.2% Y.S. by UTS - 5.5 MN/m^2 (UTS - 0.2% Y.S. at 1093°C ≈ 5.5 MN/m^2 on average).
(c) Interpolated from authors' results.
(d) When L/ℓ was determined for sheet, the value of ℓ was that measured from micrographs of the longitudinal sheet thickness.

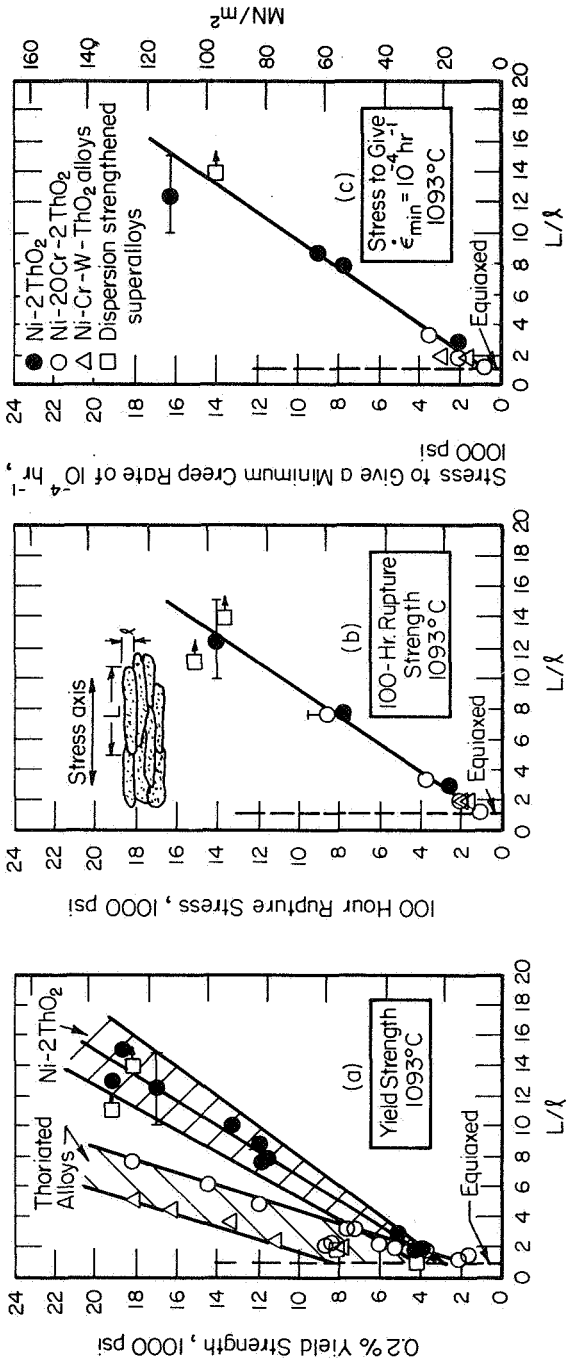

FIGURE 50. The effect of grain or cell aspect ratio, L/ℓ, in dispersion strengthened Ni alloys on strength properties at 1093°C: (a) 0.2% offset yield strength, (b) 100-hour rupture strength, and (c) stress to give a minimum creep rate of $10^{-4}hr^{-1}$. See Tables 19 and 9 for a description of specimen compositions and conditions.

found that strength increased with increasing grain size. However, examination of several of their micrographs revealed that their "coarse-grained" specimens had a higher grain aspect ratio than their fine grained specimens. The same general observation was made for Ni-20Cr-2ThO_2 specimens in the present program. Based on the preceding discussion, it appears that the grain size effect of Cook, et al.[35], may have been fortuitous, since the results appear to be equally explicable by the grain aspect ratio effect.

Even though the present results at 1093°C suggest that grain aspect ratio effects seem to overshadow the influence of grain size per se in high temperature strengthening, grain size certainly must have an influence. For example, a coarse grained material with $L/\ell = 1$ would have fewer grain boundaries and thus less overall sliding than a fine grained material with the same aspect ratio. In the limit, very fine grained material would deform superplastically at relatively low flow stresses. Furthermore, the relative importance of grain aspect ratio and grain size in high temperature strengthening will depend upon test temperature, strain rate (in tension tests), and stress (in creep tests). The anticipated effects of these variables are depicted in Figure 21.

Figures 50(b) and (c) show that creep rates and rupture lives of thoriated alloys at 1093°C fall on the same aspect ratio plots as the data for Ni-2ThO_2. Thus, here, there appears to be no influence of solid solution or γ' strengthening, and the grain aspect ratio effect appears to be dominant. However, the yield strength versus L/ℓ values for Ni-Cr-ThO_2 and Ni-Cr-W-ThO_2 alloys in Figure 50(a) lie consistently above those for Ni-2ThO_2. It may be that the higher strain rates in tensile deformation (compared with creep deformation) necessitate more accommodation of grain boundary sliding by deformation within grains than in the case of creep. Then any solid solution strengthening effects within grains would come

into play, and higher stresses would be required to cause macroscopic yielding--even though the major mode of flow was grain boundary sliding.

The Possible Role of Texture

In order to optimize both room temperature and high temperature strength in dispersion strengthened Ni alloys it is desirable to have a fine very elongated grain structure. It is possible to obtain this in Ni-2ThO_2 bar or rod, where processing can be done such that recrystallization does not take place. Yet it does not appear possible to develop a similar structure in dispersion strengthened Ni alloys which contain Cr, where high temperature annealing causes recrystallization--sometimes with resulting fine nearly equiaxed grains and sometimes with coarse elongated grains. Under certain processing conditions, Ni-2ThO_2 can be made to recrystallize, and here the grain structure is usually coarse and elongated.

The questions arise: (1) Does texture have anything to do with the relative difficulty of recrystallization of Ni-2ThO_2 bar? (2) Is texture related to the fact that Cr-containing alloys are more susceptible to recrystallization than Ni-2ThO_2?; and (3) If the thoriated alloys are processed such that recrystallization does occur, does the deformation texture influence the recrystallized microstructure; i.e., coarse elongated grains versus fine equiaxed grains?

Complete answers to these questions require more information than is presently available. The present results suggest that the ease of recrystallization increases from Ni-2ThO_2 to the Cr-containing thoriated alloys. It is observed that the sharpness of the <100> fiber texture decreases in the same order. This could indicate a stabilizing influence of the <100> texture. Also, the Ni-2ThO_2 material drawn by Procedure B did not begin to recrystallize at 1200°C until 92.5% total drawing strain, where the <100> component of the

texture (within 20^{o} of the rod axis) dropped to ~ 50%. Other evidence for the stabilizing influence of <100> is that when recrystallization occurred, it usually commenced at the specimen sides where the texture was most diffuse. There are several reasons why the <100> texture might be stable to formation of recrystallization nuclei. The equivalent states of stress in all grains would eliminate differences in stored energy which could lead to nucleation by grain boundary migration. The substructure formed on deformation might be so uniform that no single cell or subgrain was favored for growth to form a recrystallized grain. The shape, as well as the size distribution of cells, may be important here in conferring stability.

However, a problem with equating textures and structural stability is that none of the textures appear to be strong enough to consist only of the necessary orientations, particularly as nucleation appears to be the controlling process, and this can occur in very small volumes of material. The easier recrystallization of the chromium containing alloys is possibly a result of the lower stacking fault energy of these alloys. This, and the presence of any short range order, would lead to locally concentrated planar dislocation glide which would be expected to create large gradients of stored energy. Nucleation, for example by grain boundary bowing at the end of a slip band, would then be more favored than in the Ni-2ThO_2, where the high local stress might be alleviated by cross-slip.

The deformation texture may have an effect on the recrystallized microstructure when conditions are such that recrystallization does occur. The production of elongated recrystallized grains suggests that grain growth parallel to the rod axis is much faster than it is transverse to the axis. This directional growth may be related to Gleiter's[63,64] ideas regarding the dependence of boundary migration rate on the boundary orientation and the growth direction.

CONCLUSIONS

(1) Thermomechanical processing (TMP) of dispersion strengthened nickel alloys produces various microstructures which influence subsequent room temperature and high temperature mechanical properties.

(2) One important microstructural feature observed was the elongated grain structure. Under the conditions employed here this was always present in Ni-2ThO_2. However, in dispersion alloys containing Cr, the materials often recrystallized to a fine equiaxed grain structure.

(3) At room temperature, substructure refinement of thoriated and ThO_2-free alloys results in strengthening by the usual Hall-Petch relation, $\sigma_y = \sigma_o + k\ell^{-1/2}$, where σ_y is the yield strength (or proportional limit), ℓ is the grain or cell size, and σ_o and k are constants.

(4) When plots of σ_y vs. $\ell^{-1/2}$ are extrapolated to $\ell^{-1/2} = 0$ there is a strength increment, $\Delta\sigma_o = \sigma_o$ (dispersion alloy) - σ_o (dispersion free alloy) which corresponds to the Orowan stress for Ni-2ThO_2, but is about 1.7 times the Orowan stress for Ni-20Cr-2ThO_2.

(5) Refining the substructure of Ni or Ni-20Cr by TMP to a cell spacing equivalent to the interparticle spacing in Ni-2ThO_2 and Ni-20Cr-2ThO_2 increases the room temperature yield strength five to six times more than dispersion strengthening alone.

(6) At fine cell sizes (large values of $\ell^{-1/2}$), Hall-Petch plots of thoriated and thoria-free base materials converge. This means that dispersion strengthening and substructure strengthening are not additive, since the magnitude of dispersion strengthening is a function of the cell size.

(7) Similarly, Hall-Petch plots of Cr-containing and Cr-free base alloys are not parallel, which means that solid solution strengthening is not directly additive to grain size or substructure strengthening.

(8) At 1093°C it was shown that the yield strength, 100 hour creep rupture life, and stress to produce a creep rate of 10^{-4} hr^{-1} all increased linearly with increasing grain aspect ratio, L/ℓ, where L = grain length and ℓ = grain width. This correlation holds for Ni-2ThO_2, Ni-20Cr-2ThO_2, Ni-Cr-W-ThO_2 alloys, and dispersion strengthened Ni-base superalloys, and emphasizes the importance of having a large grain aspect ratio for improved high temperature strength.

(9) The grain aspect ratio correlation at 1093°C appears to be essentially independent of grain size, since results from coarse-elongated (recrystallized) grain materials behave similarly to non-recrystallized materials containing a fine stable elongated fiberous structure.

(10) The grain aspect ratio effect is attributed to the fact that grain boundary sliding is the major mode of deformation in dispersion strengthened Ni alloys at high temperatures. When testing is performed such that the tension axis is parallel to the fiber axis, then increasing the L/ℓ lowers, on average, the shear stress on boundaries, and this in turn reduces the amount of grain boundary sliding.

(11) From general experience regarding grain boundary sliding, it was concluded that the influence of L/ℓ on mechanical properties at high temperatures would depend on test temperature and strain rate, the effect being more pronounced with increasing temperature and decreasing strain rate. Thus at $\sim 0.5\ T_m$ ($\sim 600°C$) under creep conditions ($\dot{\epsilon} \sim 10^{-5}$ to 10^{-3} hr^{-1}) the L/ℓ effect should be important, whereas at 1200°C ($\sim 0.85\ T_m$) the grain aspect ratio may not affect mechanical properties under high rate deformation conditions ($\dot{\epsilon} \sim 10^{4}$ hr^{-1}).

(12) The role of deformation texture in the "indirect" aspects of dispersion strengthening is not completely clear. Extruded Ni-2ThO_2 has a very strong <100> component of the dual <100>-<111> fiber texture, and this material does not recrystallize.

(13) Working of Ni-2ThO_2 by drawing (with and without intermediate anneals) reduces the <100> component and increases the <111> components of the texture. At very high drawing strains, Ni-2ThO_2 will recrystallize (to coarse elongated grains). Thus, the presence of a strong <100> fiber texture may promote recrystallization resistance.

ACKNOWLEDGEMENTS

The authors are indebted to M. R. Cantin, G. F. Mead, R. E. Higgins, and the late R. D. Tenaglia for their skillful assistance with various experiments. The X-ray texture studies were conducted in the Department of Physical Metallurgy and Science of Materials, The University of Birmingham, Birmingham, England. We are grateful to Professor R. E. Smallman for the provision of laboratory facilities at Birmingham for this portion of the study. We are grateful to T. K. Glasgow of NASA-Lewis Research Center for calling tc our attention Reference 72.

REFERENCES

(1) G. S. Ansell, "The Mechanism of Dispersion-Strengthening: A Review", Oxide Dispersion Strengthening, G. S. Ansell, T. D. Cooper, and F. V. Lenel, Eds. Gordon and Breach, New York (1968), p. 61.

(2) B. A. Wilcox and R. I. Jaffee, "Direct and Indirect Strengthening Effects of ThO_2 Particles in Dispersion-Hardened Nickel", Proc. of International Conference on the Strength of Metals and Alloys, Tokyo, Supplement to Trans. Japan Inst. Met., 9, 575 (1968).

(3) B. A. Wilcox and A. H. Clauer, "Creep of Thoriated Nickel Above and Below 0.5 T_m", Trans. AIME, 236, 570 (1966).

(4) M. F. Ashby, "The Hardening of Metals by Non-Deforming Particles", Z. für Metallk., 55, 5 (1964).

(5) B. A. Wilcox, A. H. Clauer, and W. S. McCain, "Creep and Creep Fracture of a Ni-20Cr-2ThO_2 Alloy", Trans. AIME, 239, 1791 (1967).

(6) A. H. Clauer and B. A. Wilcox, "Steady-State Creep of Dispersion-Strengthened Nickel", Met. Sci. J., 1, 86 (1967).

(7) B. A. Wilcox and A. H. Clauer, "Creep of Dispersion-Strengthened Nickel-Chromium Alloys", Met. Sci. J., 3, 26 (1969).

(8) I. G. Palmer and G. C. Smith, "Fracture of Internally Oxidized Copper Alloys", Oxide Dispersion Strengthening, G. S. Ansell, T. D. Cooper, and F. V. Lenel, Eds., Gordon and Breach, New York (1968), p. 253.

(9) M. F. Ashby, "The Theory of the Critical Shear Stress and Work Hardening of Dispersion-Hardened Crystals", ibid, p. 143.

(10) R. J. Olsen and G. S. Ansell, "The Strength Differential in Two-Phase Alloys", Trans. ASM, 62, 711 (1969).

(11) D. Webster, "Grain Growth and Recrystallization in Thoria-Dispersed Nickel and Nichrome", Trans AIME, 242, 640 (1968).

(12) D. H. Killpatrick, A. Phillips and V. Kerlins, "Fracture in Dispersion-Strengthened Nickel-Chromium Alloys", Trans. AIME, 242, 1657 (1968).

(13) D. Webster, "Strengthening Mechanisms in Dispersion-Hardened Nichrome", Trans. ASM, 62, 937 (1969).

(14) J. D. Embury and R. M. Fisher, "The Structure and Properties of Drawn Pearlite", Acta. Met., 14, 147 (1966).

(15) J. D. Embury, A. S. Keh, and R. M. Fisher, "Substructural Strengthening in Materials Subject to Large Plastic Strains", Trans. AIME, 236, 1252 (1966).

(16) V. K. Chandhok, A. Kasak, and J. P. Hirth, "Structures and Strengthening Mechanisms in Carbon Steel Wire", Trans. ASM, 59, 288 (1966).

(17) G. Langford and M. Cohen, "Strain Hardening of Iron by Severe Plastic Deformation", Trans. ASM, 62, 623 (1969).

(18) B. A. Wilcox and A. Gilbert, "Substructural Strengthening of a Precipitation Hardened Molybdenum Alloy", Acta Met., 15, 601 (1967).

(19) E. S. Meieran and D. A. Thomas, "Structure of Drawn and Annealed Tungsten Wire", Trans. AIME, 233, 937 (1965).

(20) V. A. Tracey and D. K. Worn, "Some Observations on the Cold Drawing and Annealing Behavior of Nickel Containing a Dispersed Phase of Thoria", Powder Met., No. 10, 34 (1962).

(21) D. K. Worn and S. F. Marton, "Some Properties of Nickel Containing a Dispersed Phase of Thoria", Powder Metallurgy, Interscience Pub., New York (1961), p. 309.

(22) M. von Heimendahl and G. Thomas, "Substructure and Mechanical Properties of TD Nickel", Trans. AIME, 230, 1520 (1964).

(23) E. Macherauch and O. Vöhringer, "The Deformation Behavior of Polycrystalline Nickel", Phys. Stat. Sol., 6, 491 (1964).

(24) P. Haasen, "Plastic Deformation of Nickel Single Crystals at Low Temperatures", Phil. Mag., 3, 384 (1958).

(25) C. Susse, "Measurement of the Shear Modulus of Nickel up to 1000°C", J. Phys. Radium, 17, 910 (1956).

(26) A. Kelly and R. B. Nicholson, Precipitation Hardening, Progress in Mat. Sci., 10 (3), Pergamon Press, New York (1963), p. 338.

(27) N. Hansen and H. Lilholt, "Matrix Hardening in Dispersion Strengthened Powder Products", paper presented at the International Powder Met. Conf., July 12-16, 1970, New York.

(28) B. A. Wilcox and A. H. Clauer, "High Temperature Deformation of Dispersion Strengthened Nickel Alloys", NASA CR-72367, Feb. 29, 1968.

(29) R. W. Fraser and D. J. I. Evans, "The Strengthening Mechanism in Dispersion Strengthened Nickel", Oxide Dispersion Strengthening, G. S. Ansell, T. D. Cooper, and F. V. Lenel, Eds., Gordon and Breach, New York (1968), p.375.

(30) G. S. Doble, L. Leonard, and L. J. Ebert, "The Effect of Deformation on Dispersion Hardened Alloys", Final Report on NASA Grant NGR 36-033-094, November, 1967.

(31) D. Tromans and J. A. Lund, "Grain Boundary Effects in Oxide Dispersion Strengthened Zinc", Trans. ASM, 59, 672 (1966).

(32) F. L. Ver Snyder and R. W. Guard, "Directional Grain Structure for High Temperature Strength", Trans. ASM, 52, 485 (1960).

(33) J. S. Benjamin, "Dispersion Strengthened Superalloys by Mechanical Alloying", Met. Trans., 1, 2943 (1970).

(34) J. S. Benjamin and R. L. Cairns, "Elevated Temperature Mechanical Properties of a Dispersion Strengthened Superalloy", paper presented at the International Powder Met. Conf. July 12-16, 1970, New York.

(35) R. C. Cook, R. H. MacDonald, and L. F. Norris, "Development of Precipitation Hardened Dispersion Strengthened Nickel-Chromium Alloys", AFML-TR-69-166, June, 1969.

(36) G. S. Doble and R. J. Quigg, "Effect of Deformation on the Strength and Stability of TD Nickel", Trans. AIME, 233, 410 (1965).

(37) "TD Nickel, A Dispersion Strengthened Metal", Fansteel Inc., Metals Division, Bulletin TD-007-1.

(38) F. Garofolo, Fundamentals of Creep and Creep-Rupture in Metals, Macmillan Co., New York (1965).

(39) M. F. Ashby and R. Raj, "On Continuum Aspects of Grain Boundary Sliding and Diffusional Creep", Contract NOOO14-67-A-0298-0020, June, 1970.

(40) M. C. Inman, K. M. Zwilsky, and D. H. Boone, "Recrystallization Behavior of Cold Rolled TD-Nickel", Trans ASM, 57, 701 (1964).

(41) P. B. Mee and R. A. Sinclair, "Cold-Rolling and Annealing Behavior in Nickel-Thoria Sheet, With Particular Reference to Preferred-Orientation Development", J. Inst. of Met., 94, 319 (1966).

(42) D. H. Killpatrick and J. D. Young, "Texture and Room Temperature Mechanical Properties of Dispersion Strengthened Ni-Cr Alloys", Met. Trans. 1, 955 (1970).

(43) E. R. Kimmel and M. C. Inman, "Recrystallization in Thoria-Dispersed Nickel Sheet", Trans. ASM, 62, 390 (1969).

(44) W. Scheithauer and R. F. Chaney, "Development of Dispersion-Strengthened Nickel-Base Alloys", AFML-TR-69-285, January, 1970.

(45) I. L. Dillamore and W. T. Roberts, "Preferred Orientation in Wrought and Annealed Metals", Met. Rev., 10, 271 (1965).

(46) A. T. English and G. Y. Chin, "On the Variation of Wire Texture With Stacking Fault Energy in FCC Metals and Alloys", Acta Met, 14, 1013 (1965).

(47) G. Y. Chin, Textures in Research and Practice, J. Grewen and G. Wasserman Eds., Springer-Verlag (1969).

(48) C. J. McHargue, L. K. Jetter, and J. C. Ogle, "Preferred Orientation in Extruded Aluminum Rod", Trans. AIME, 215, 831 (1959).

(49) K. V. Gow and R. W. Cahn, "Textures in Extruded Aluminum", Acta Met., 1, 238 (1953).

(50) H. Stadelmaier and F. Brown, "Influence of Elastic Stressing on Recrystallization Textures", Z. für Metallk., 47, 1 (1956).

(51) I. L. Dillamore, private communication.

(52) H. Hu, Recovery and Recrystallization of Metals, L. Himmel Ed., Interscience Publishers, New York (1963), p 311.

(53) C. A. Clark and P. B. Mee, "Deformation and Recrystallization Textures in Nickel and Nickel-Base Alloys", Z. für Metallk., 53, 756 (1962).

(54) C. Liesner and G. Wassermann, Textures in Research and Practice, J. Grewen and G. Wasserman Eds., Springer-Verlag (1969).

(55) N. Hansen, "Effect of Grain Size on the Mechanical Properties of Dispersion-Strengthened Aluminum/Aluminum Oxide Products", Trans. AIME, 245, 1305 (1969).

(56) F. V. Lenel, A. B. Backensto, and M. V. Rose, "Properties of Aluminum Powders and of Extrusions Produced from Them", Trans. AIME, 209, 124 (1957).

(57) D. Merz and G. Wassermann, "Formation of Deformation Textures in Heterogeneous Alloys", Z. für Metallkunde, 56, 516 (1965).

(58) G. Bonissoni and M. Paganelli, "Textures of Crystallite Size in Rolled Sheets and Extruded Bars of SAP", Appl. Mater. Res., 4, 84 (1965).

(59) J. J. Petrovic, L. Leonard, and L. J. Ebert, "Recrystallization Characteristics of TD Nickel", Contract NGR 36-003-094, February, 1969, see also second report, February, 1970.

(60) R. D. Doherty and J. W. Martin, "The Effect of a Dispersed Second Phase on the Recrystallization of Aluminum-Copper Alloys", J. Inst. Met., 91, 332 (1962-63).

(61) F. J. Humphreys and J. W. Martin, "The Effect of Dispersed Phases Upon the Annealing Behavior of Plastically Deformed Copper Crystals", Phil. Mag., 17, 365 (1968).

(62) D. T. Gawne and G. T. Higgins, Textures in Research and Practice, J. Grewen and G. Wassermann Eds., Springer-Verlag (1969).

(63) H. Gleiter, "The Mechanism of Grain Boundary Migration", Acta Met., 17, 565 (1969).

(64) H. Gleiter, "Theory of Grain Boundary Migration Rate", Acta Met., 17, 853 (1969).

(65) R. Johnson and D. H. Killpatrick, "Dispersion-Strengthened Metal Structural Development", AFFDL-TR-68-130, Part I, July 1968.

(66) E. E. Stansbury, C. R. Brooks, and T. L. Arledge, "Specific-Heat Anomalies in Solid Solutions of Chromium and Molybdenum in Nickel: Evidence for Short-Range Order", J. Inst. Met., 94, 136 (1966).

(67) L. F. Norris, B. W. Kushnir, and R. W. Fraser, "Improvement of the Properties of Dispersion Strengthened Nickel-Chromium Alloys", AFML-TR-68-67, March, 1968.

(68) D. B. Arnold and L. J. Klingler, "Dispersion-Strengthened Nickel-Base Alloys", Oxide Dispersion Strengthening, G. S. Ansell, T. D. Cooper, and F. V. Lenel, Eds., Gordon and Breach, New York (1968), p. 611.

(69) P. G. Baily, "A Manufacturing Process for Thin Sheet and Foil of TD Nickel-Chromium Alloy", AFML-TR-68-87, April, 1968.

(70) B. A. Wilcox and A. H. Clauer, unpublished results.

(71) R. Armstrong, I. Codd, R. M. Douthwaite, and N. J. Petch, "The Plastic Deformation of Polycrystalline Aggregates", Phil. Mag., 7, 45 (1962).

(72) A. A. Bourne, J. C. Chaston, A. S. Darling, and G. C. Bond, "Methods of Improving the Mechanical Properties of Metals and Their Alloys", British Patent No. 1,134,492, November 27, 1968.

APPENDIX A

PLOTS OF NORMALIZED INTENSITY VERSUS ANGLE OF INCLINATION FOR THE {111} AND {200} REFLECTIONS

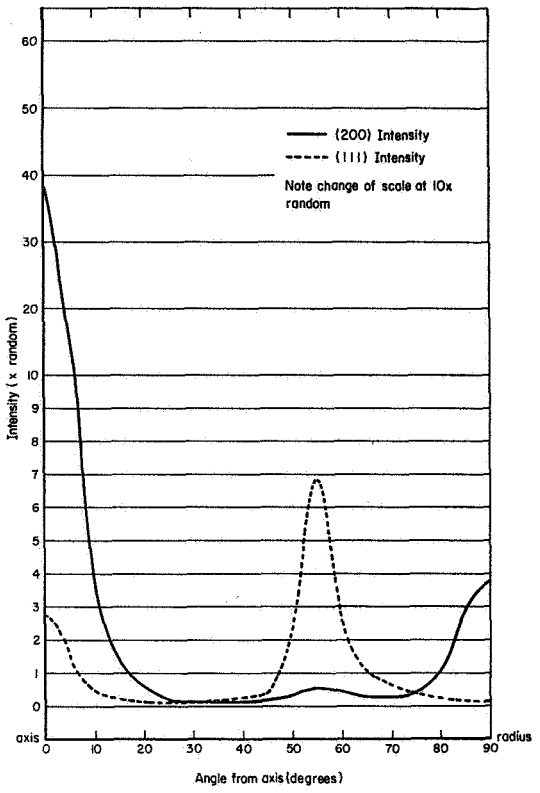

FIGURE 1-A. NORMALISED INTENSITY GRAPH FOR SPECIMEN 1 ($Ni\text{-}2ThO_2$, AS-EXTRUDED)

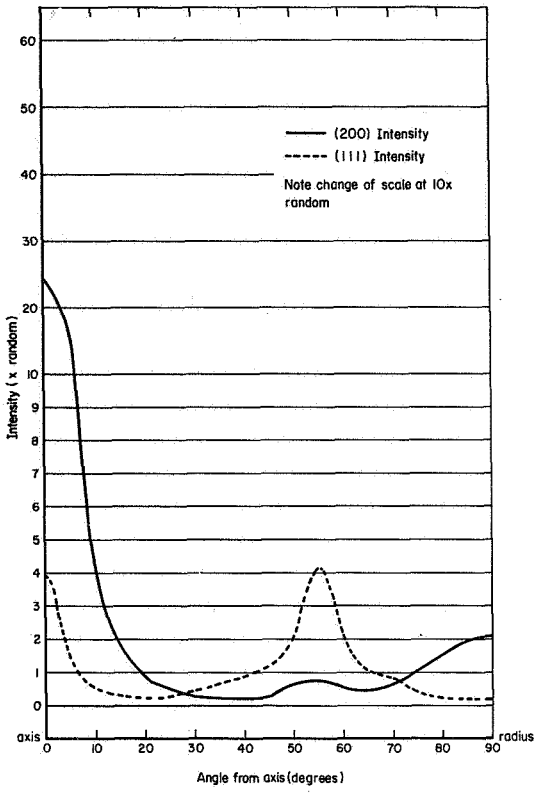

FIGURE 2-A. NORMALISED INTENSITY GRAPH FOR SPECIMEN 2 ($Ni\text{-}2ThO_2$, DRAWN 49.4% BY PROCEDURE A)

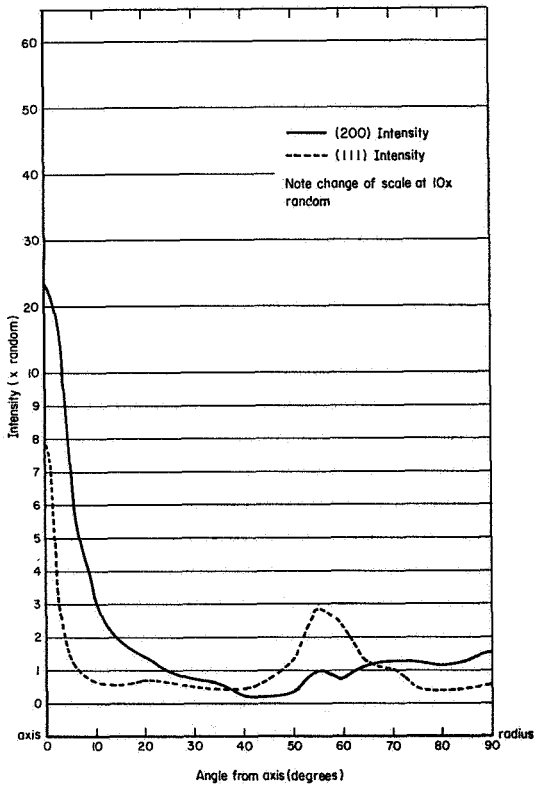

FIGURE 3-A. NORMALISED INTENSITY GRAPH FOR SPECIMEN 3 ($Ni\text{-}2ThO_2$, DRAWN 73.3% BY PROCEDURE A)

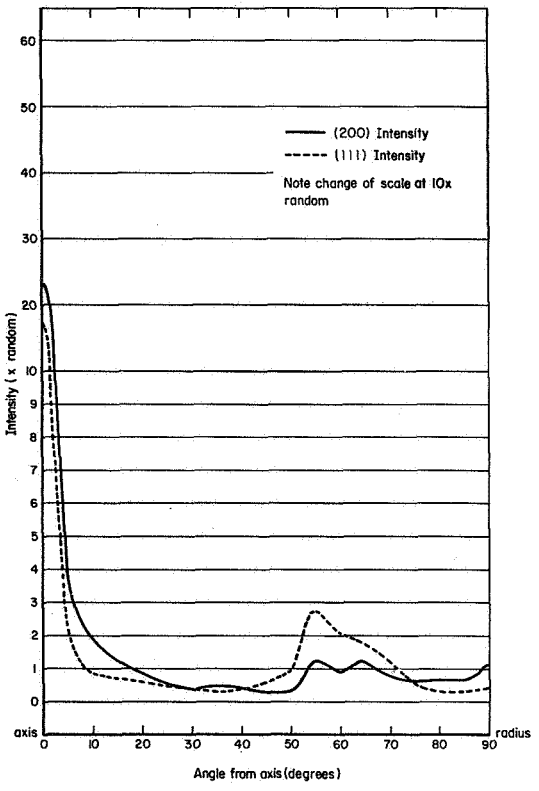

FIGURE 4-A. NORMALISED INTENSITY GRAPH FOR SPECIMEN 4 ($Ni\text{-}2ThO_2$, DRAWN 86.8% BY PROCEDURE A)

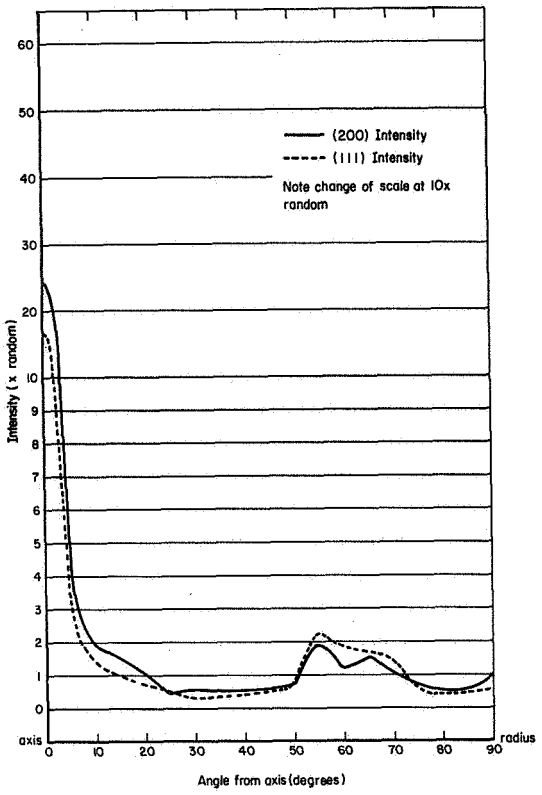

FIGURE 5-A. NORMALISED INTENSITY GRAPH FOR SPECIMEN 5 ($Ni\text{-}2ThO_2$, DRAWN 92.5% BY PROCEDURE A)

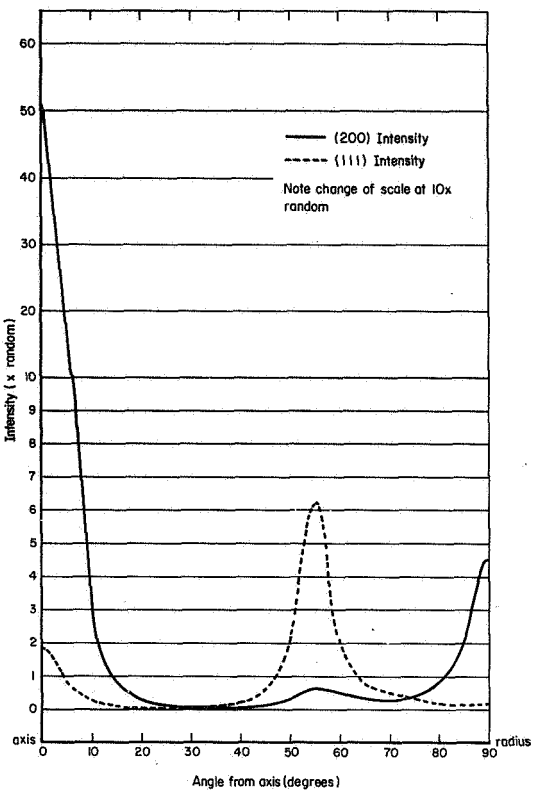

FIGURE 6-A. NORMALISED INTENSITY GRAPH FOR SPECIMEN 6 ($Ni\text{-}2ThO_2$, EXTRUDED PLUS ANNEALED)

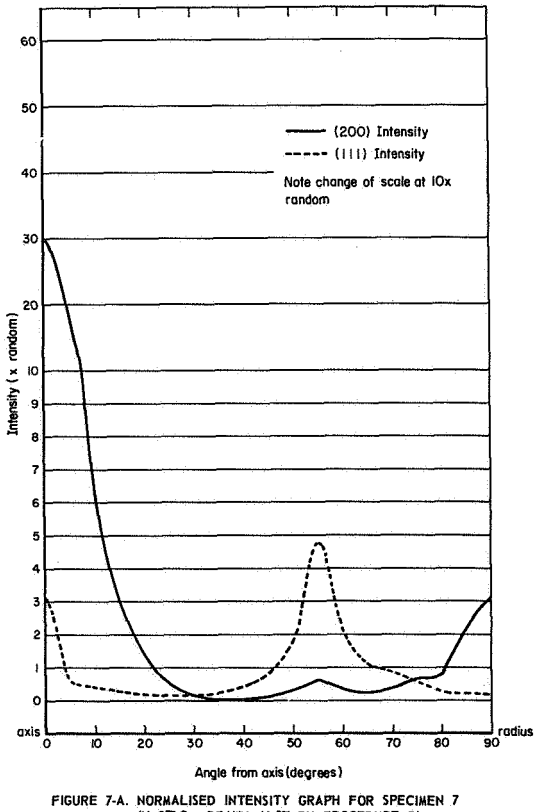

FIGURE 7-A. NORMALISED INTENSITY GRAPH FOR SPECIMEN 7 ($Ni\text{-}2ThO_2$, DRAWN 46.5% BY PROCEDURE B)

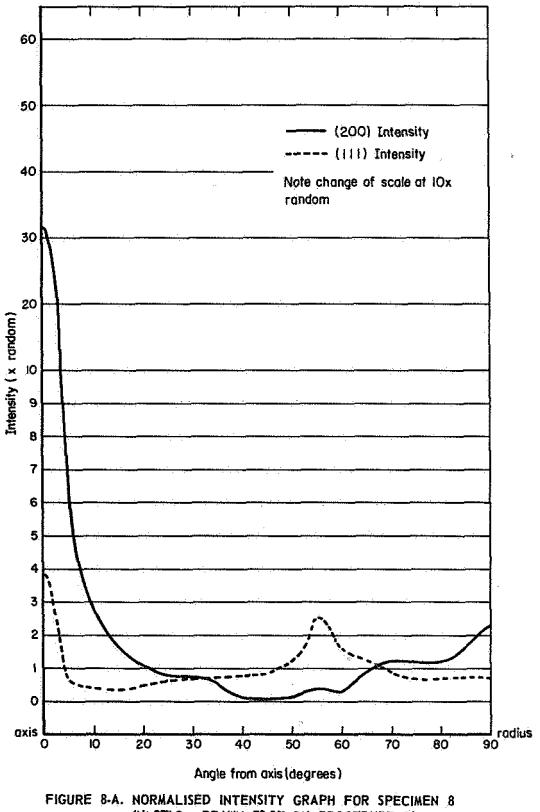

FIGURE 8-A. NORMALISED INTENSITY GRAPH FOR SPECIMEN 8 ($Ni\text{-}2ThO_2$, DRAWN 73.3% BY PROCEDURE B)

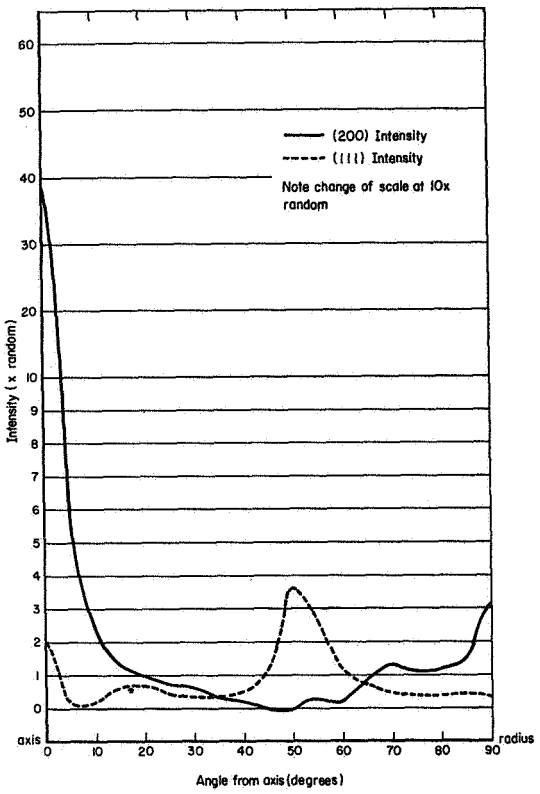

FIGURE 9-A. NORMALISED INTENSITY GRAPH FOR SPECIMEN 9 ($Ni\text{-}2ThO_2$, DRAWN 86.8% BY PROCEDURE B)

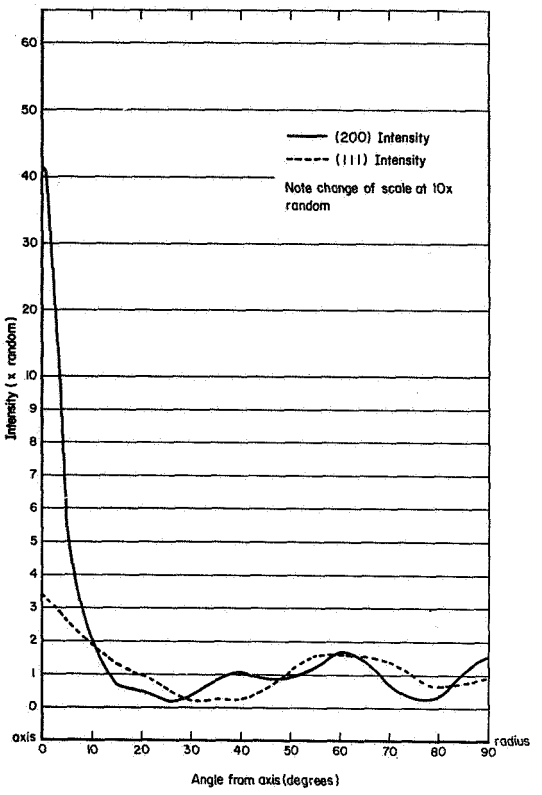

FIGURE 10-A. NORMALISED INTENSITY GRAPH FOR SPECIMEN 10 ($Ni\text{-}2ThO_2$, DRAWN 92.5% BY PROCEDURE B)

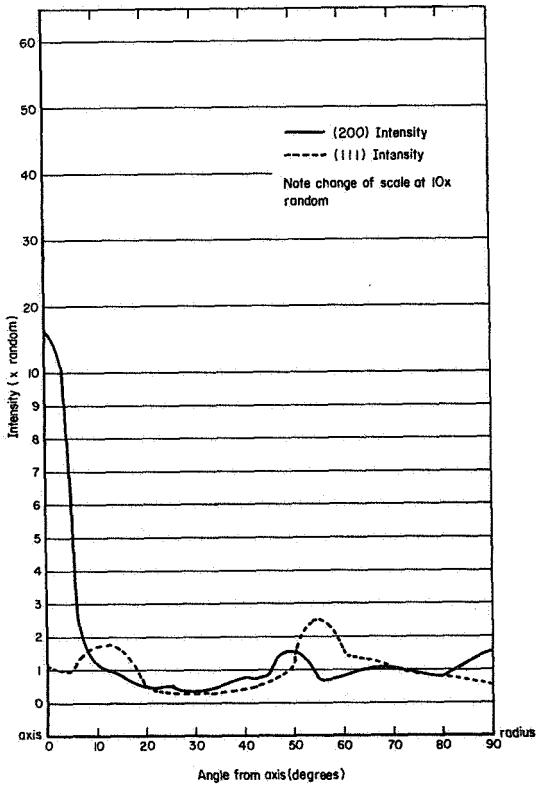

FIGURE 11-A. NORMALISED INTENSITY GRAPH FOR SPECIMEN 11 (Ni, AS-EXTRUDED)

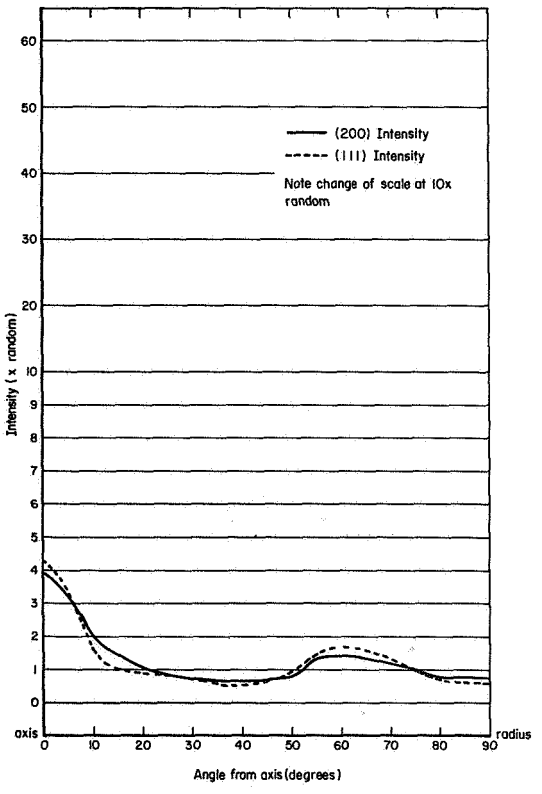

FIGURE 12-A. NORMALISED INTENSITY GRAPH FOR SPECIMEN 12 (Ni, DRAWN 53.4% BY PROCEDURE A)

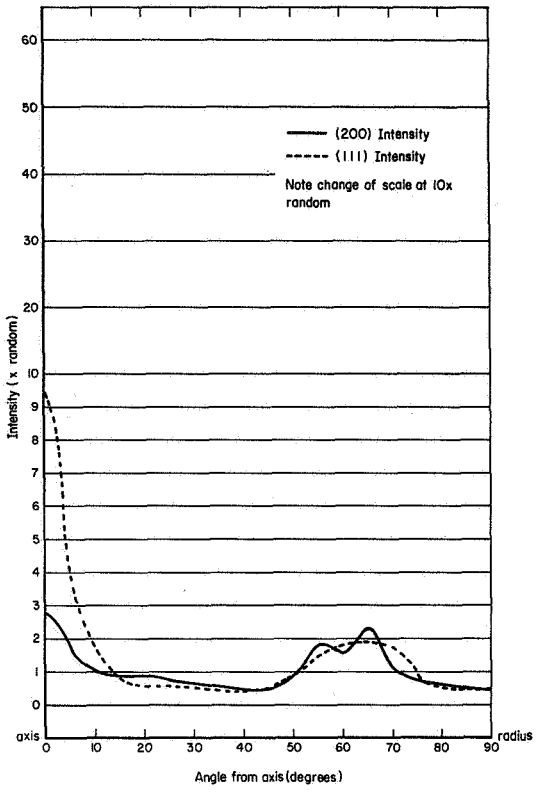

FIGURE 13-A. NORMALISED INTENSITY GRAPH FOR SPECIMEN 13 (Ni, DRAWN 76.7% BY PROCEDURE A)

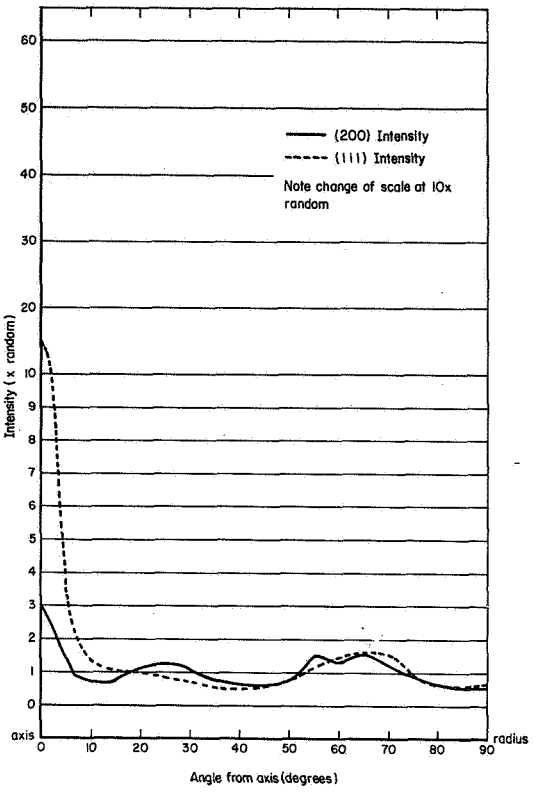

FIGURE 14-A. NORMALISED INTENSITY GRAPH FOR SPECIMEN 14 (Ni, DRAWN 88.5% BY PROCEDURE A)

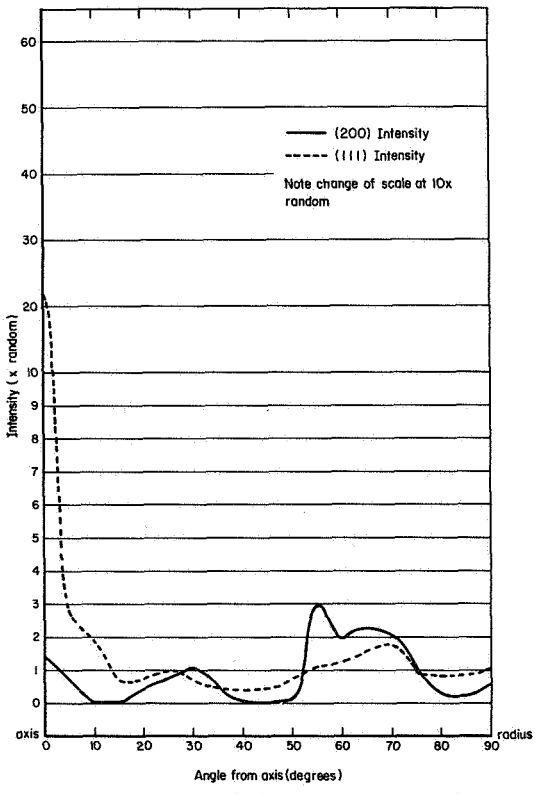

FIGURE 15-A. NORMALISED INTENSITY GRAPH FOR SPECIMEN 15 (Ni, DRAWN 93.4% BY PROCEDURE A)

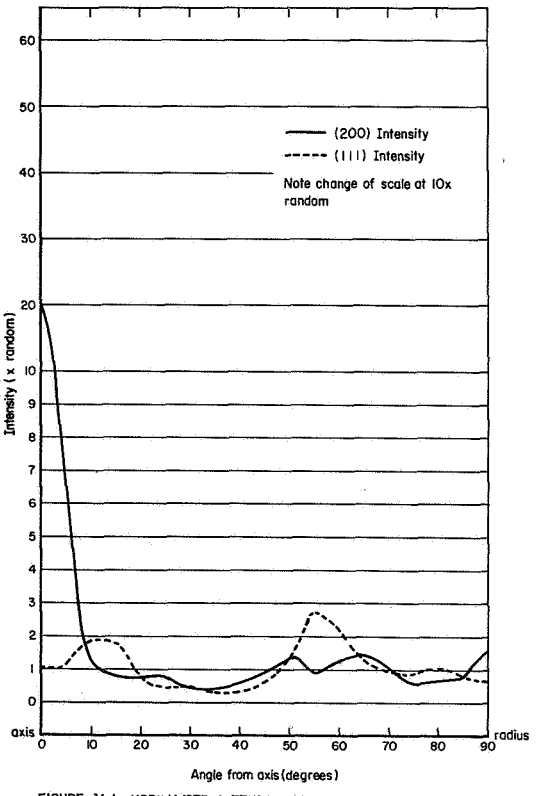

FIGURE 16-A. NORMALISED INTENSITY GRAPH FOR SPECIMEN 16 (Ni, EXTRUDED PLUS ANNEALED)

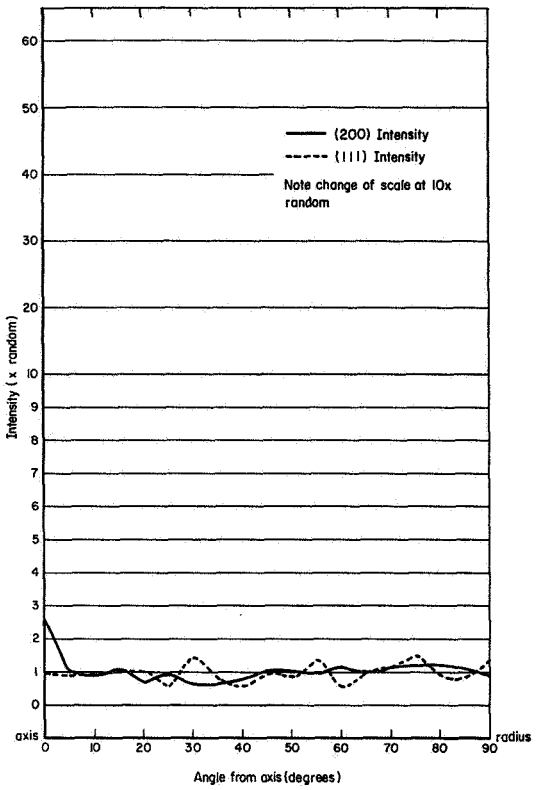

FIGURE 17-A. NORMALISED INTENSITY GRAPH FOR SPECIMEN 17 (Ni, DRAWN 53.4% BY PROCEDURE B)

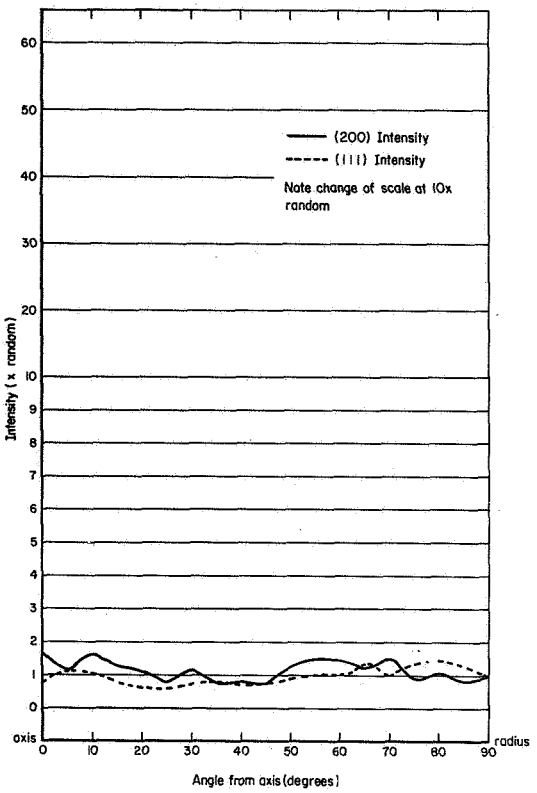

FIGURE 18-A. NORMALISED INTENSITY GRAPH FOR SPECIMEN 18 (Ni, DRAWN 76.7% BY PROCEDURE B)

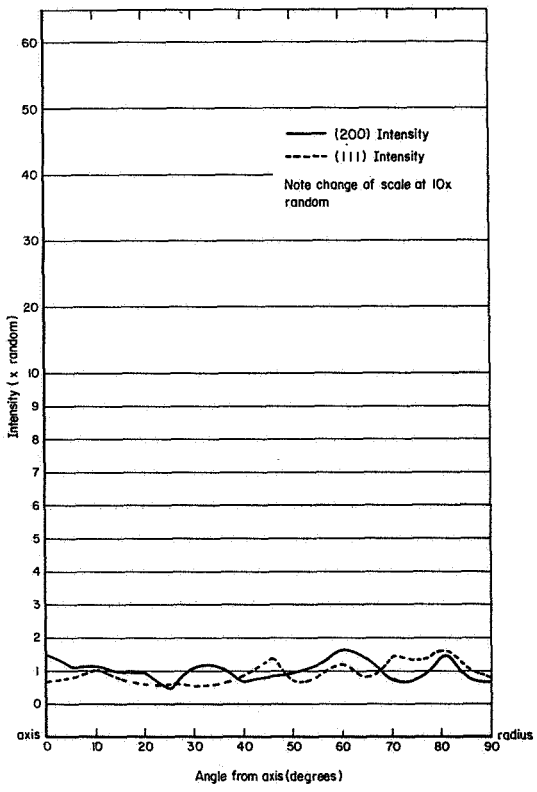

FIGURE 19-A. NORMALISED INTENSITY GRAPH FOR SPECIMEN 19 (Ni, DRAWN 88.5% BY PROCEDURE B)

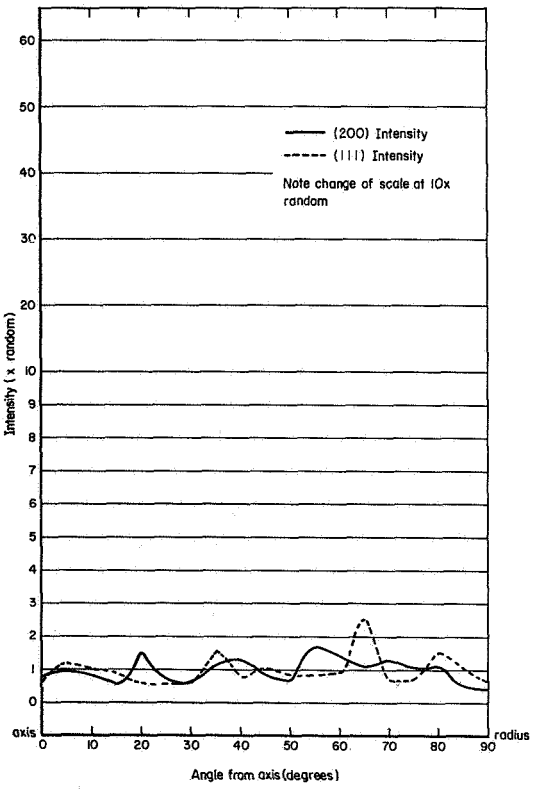

FIGURE 20-A. NORMALISED INTENSITY GRAPH FOR SPECIMEN 20 (Ni, DRAWN 93.4% BY PROCEDURE B)

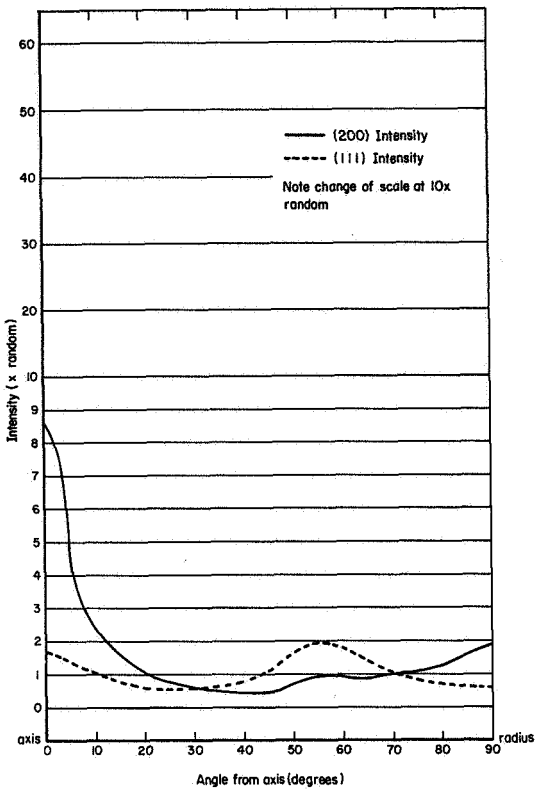

FIGURE 21-A. NORMALISED INTENSITY GRAPH FOR SPECIMEN 21 (Ni-20Cr-2ThO_2, AS EXTRUDED)

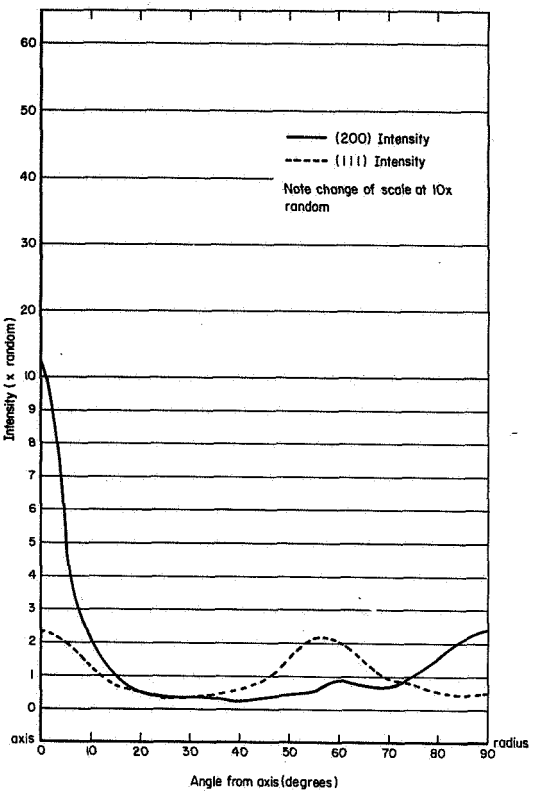

FIGURE 22-A. NORMALISED INTENSITY GRAPH FOR SPECIMEN 22 (Ni-20Cr-2ThO_2, DRAWN 23.7% BY PROCEDURE A)

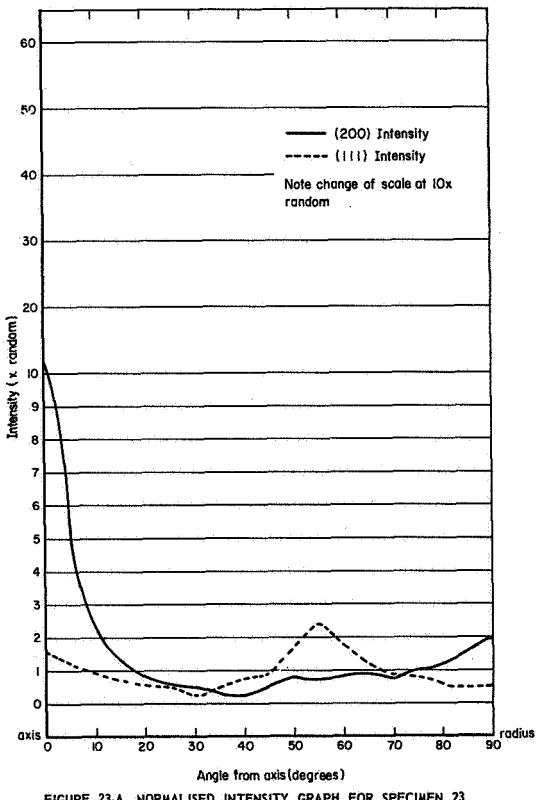

FIGURE 23-A. NORMALISED INTENSITY GRAPH FOR SPECIMEN 23 (Ni-20Cr-2ThO_2, EXTRUDED PLUS ANNEALED)

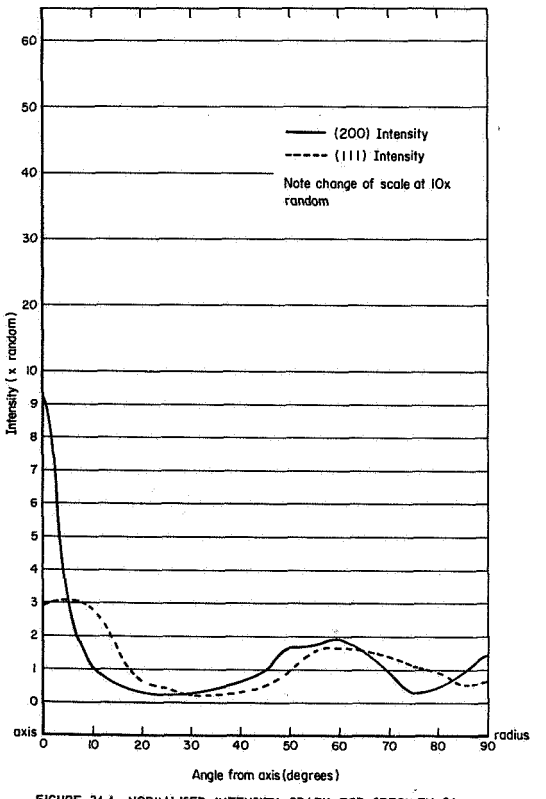

FIGURE 24-A. NORMALISED INTENSITY GRAPH FOR SPECIMEN 24 (Ni-20Cr-2ThO_2, DRAWN 25.6% BY PROCEDURE B)

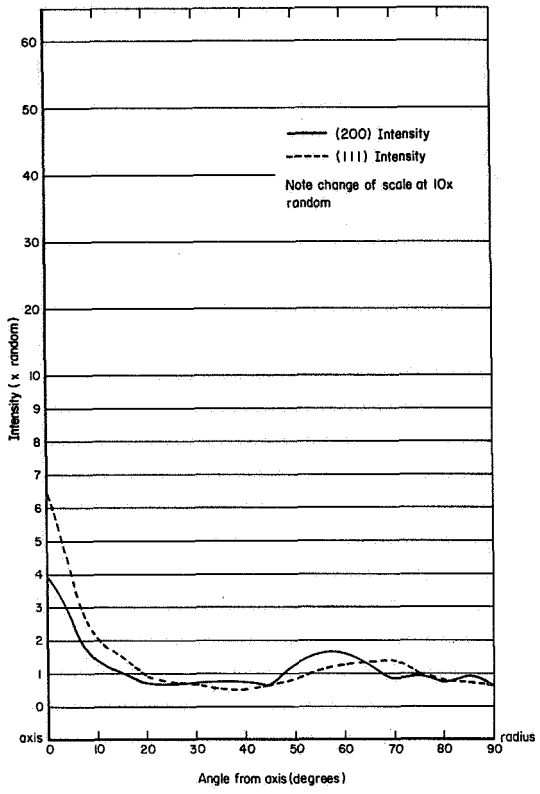

FIGURE 25-A. NORMALISED INTENSITY GRAPH FOR SPECIMEN 25 (Ni-20Cr-2ThO_2, DRAWN 53.8% BY PROCEDURE B)

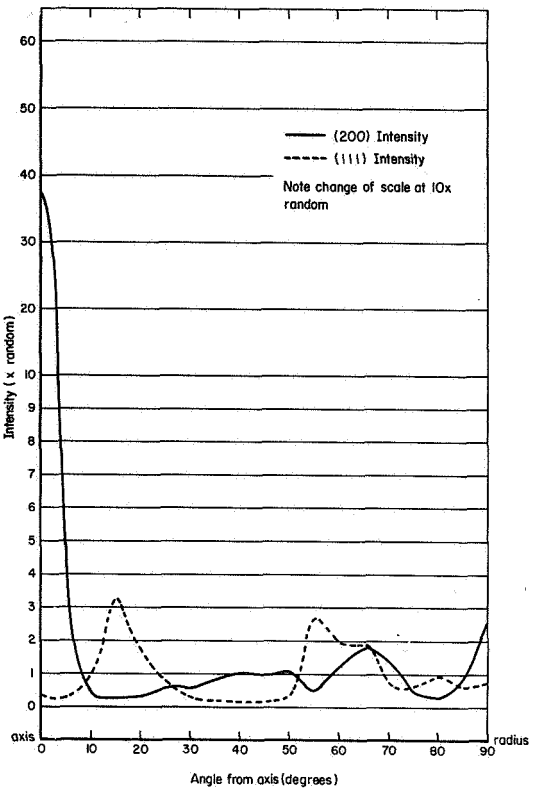

FIGURE 26-A. NORMALISED INTENSITY GRAPH FOR SPECIMEN 26 (Ni-20Cr, AS-EXTRUDED)

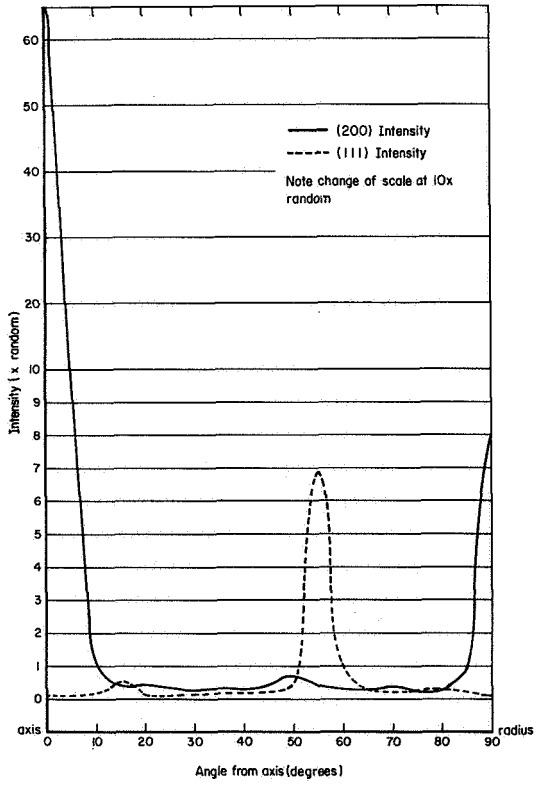

FIGURE 27-A. NORMALISED INTENSITY GRAPH FOR SPECIMEN 27 (Ni-20Cr, EXTRUDED PLUS ANNEALED)

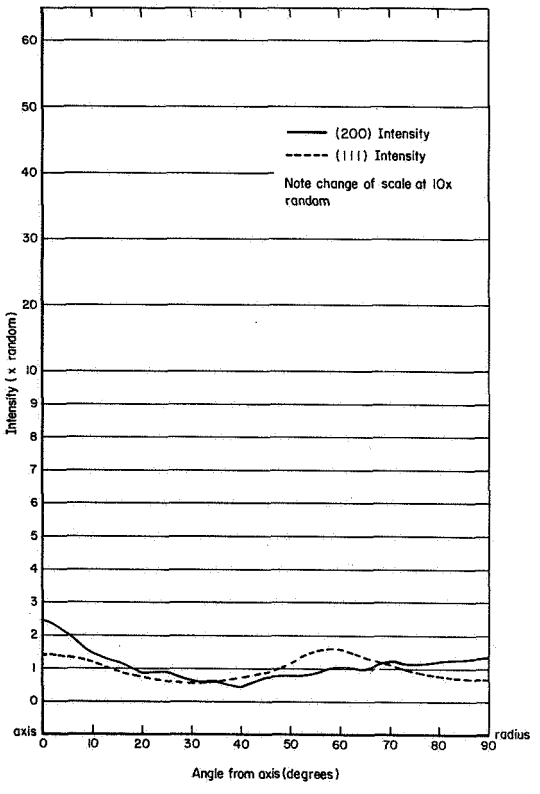

FIGURE 28-A. NORMALISED INTENSITY GRAPH FOR SPECIMEN 28 (Ni-20Cr-10W-2ThO_2, AS-EXTRUDED)

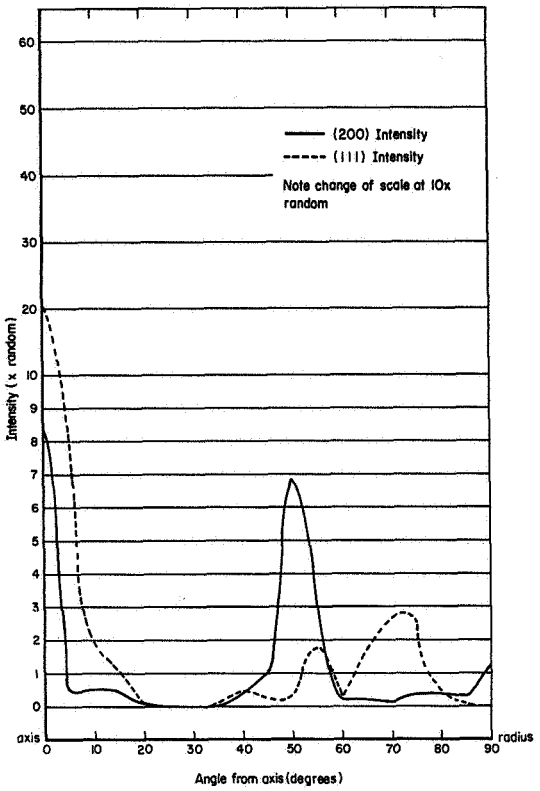

FIGURE 29-A. NORMALISED INTENSITY GRAPH FOR SPECIMEN 29 (Ni-20Cr-10W-2ThO_2, EXTRUDED PLUS ANNEALED)

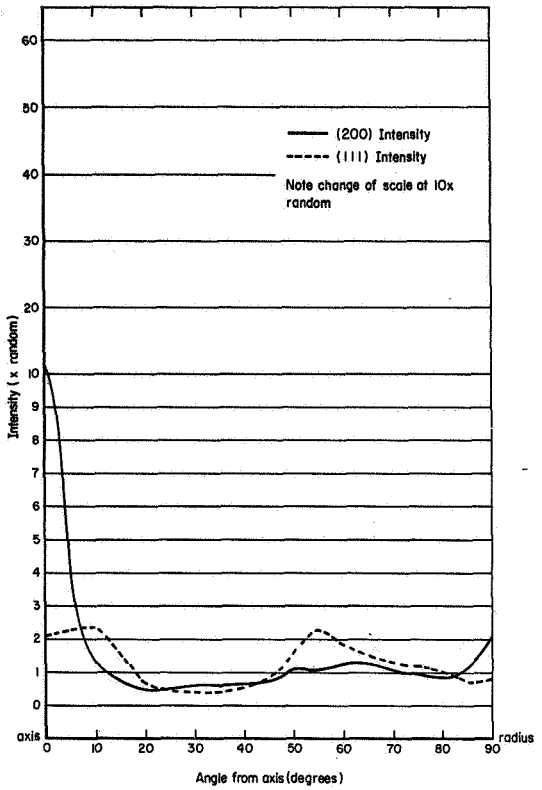

FIGURE 30-A. NORMALISED INTENSITY GRAPH FOR SPECIMEN 30 (Ni-20Cr-10W, EXTRUDED PLUS ANNEALED)

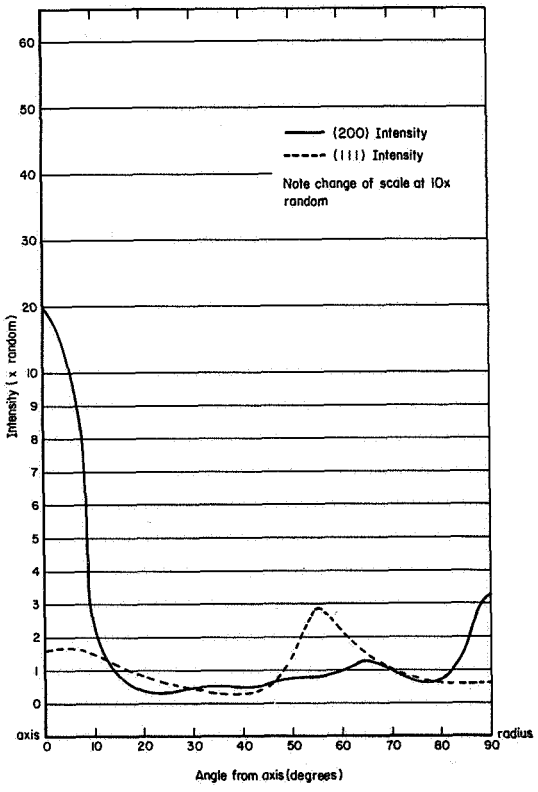

FIGURE 31-A. NORMALISED INTENSITY GRAPH FOR SPECIMEN 31 (Ni-20Cr, DRAWN 24.4% BY PROCEDURE A)

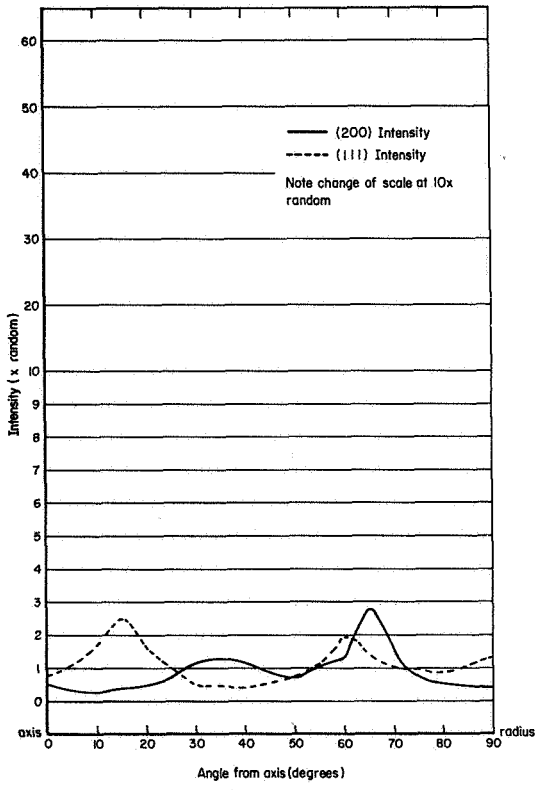

FIGURE 32-A. NORMALISED INTENSITY GRAPH FOR SPECIMEN 32 (Ni-20Cr, DRAWN 24.4% BY PROCEDURE B)

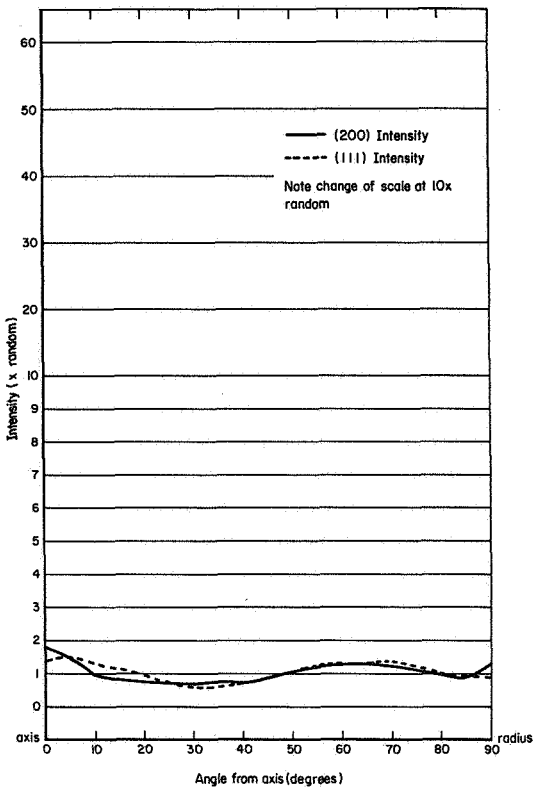

FIGURE 33-A. NORMALISED INTENSITY GRAPH FOR SPECIMEN 33 (Ni-20Cr-10W, SWAGED 53.9% BY PROCEDURE B)

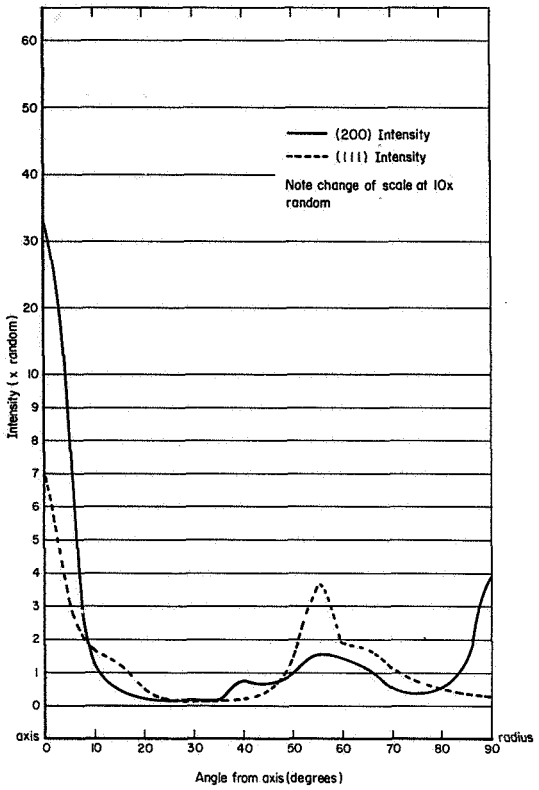

FIGURE 34-A. NORMALISED INTENSITY GRAPH FOR SPECIMEN 34 (Ni-20Cr-2ThO_2, SWAGED 47.7% BY PROCEDURE B)

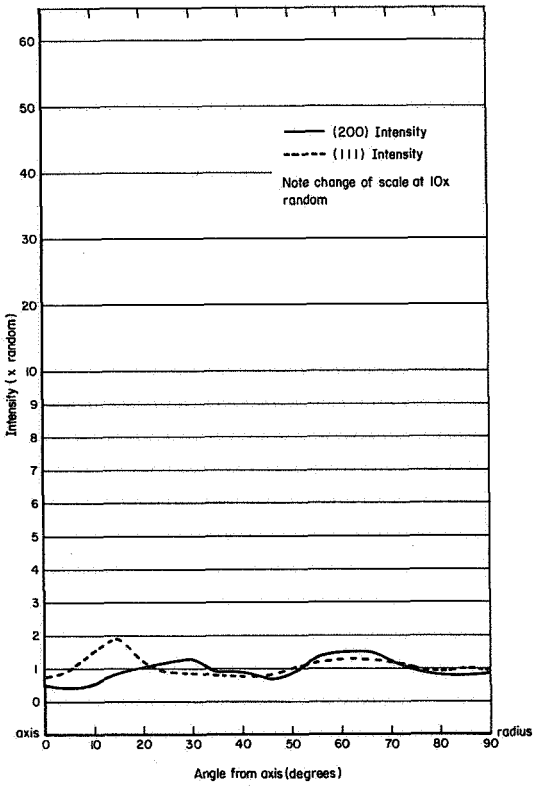

FIGURE 35-A. NORMALISED INTENSITY GRAPH FOR SPECIMEN 35 (Ni-20Cr, SWAGED 49.1% BY PROCEDURE B)

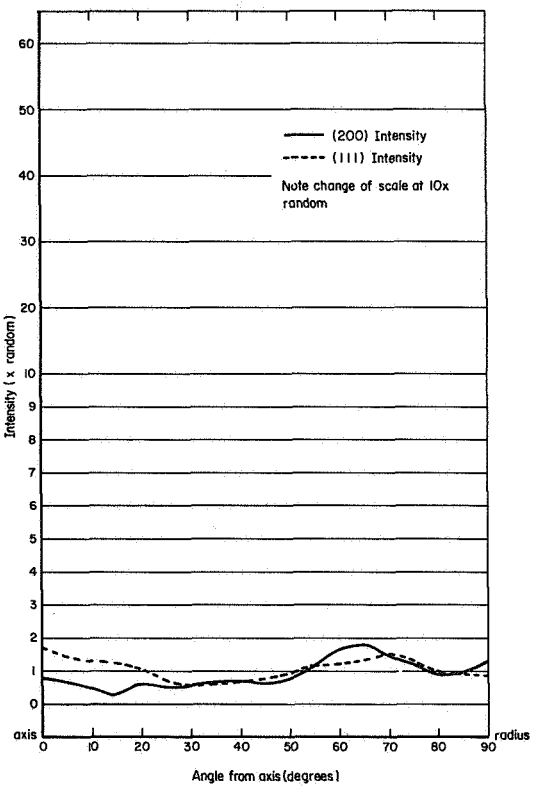

FIGURE 36-A. NORMALISED INTENSITY GRAPH FOR SPECIMEN 36 (Ni-20Cr-10W-2ThO_2, SWAGED 53.9% BY PROCEDURE B)

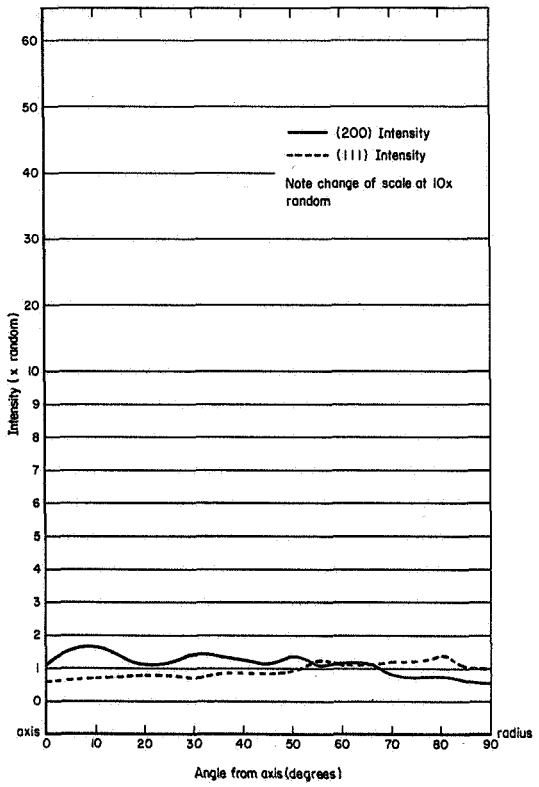

FIGURE 37-A. NORMALISED INTENSITY GRAPH FOR SPECIMEN 37
(Ni-20Cr, DRAWN 58.0% BY PROCEDURE B)

APPENDIX B

NEW TECHNOLOGY

THE ROLE OF GRAIN SIZE AND SHAPE ON THE MECHANICAL BEHAVIOR OF DISPERSION STRENGTHENED NICKEL ALLOYS

The research in this report has provided New Technology, which is briefly described below, including pertinent pages in this report describing the New Technology.

Item 1.

Substantial improvement in room temperature strength can be achieved by substructure strengthening. This strengthening is 5 to 6 times more potent than is dispersion strengthening. (Discussion is on pp 42-46, 103-109, 118-120.)

Item 2.

At 1093^{o}C, the yield strength and creep strength of dispersion strengthened Ni alloys increase linearly with the grain aspect ratio, L/ℓ, where L = grain length and ℓ = grain width. (Discussion is on pp 49-59, 67, 120-126.)

APPENDIX C

DISTRIBUTION LIST FOR SUMMARY REPORT

DISTRIBUTION LIST FOR SUMMARY REPORT
CONTRACT NAS3-11167

ADDRESSEE	NUMBER OF COPIES
NASA Headquarters Washington, D.C. 20546	
Attention: N. F. Rekos (RAP)	(1)
R. H. Raring (RRM)	(1)
G. Deutsch (RRM)	(1)
M. Comberiate (RAP)	(1)
J. Gangler (RRM)	(1)
NASA-Lewis Research Center 21000 Brookpark Road Cleveland, Ohio 44135	
Attention:	
Tech. Utilization Off. M.S. 3-19	(1)
Report Control Office M.S. 5-5	(1)
Fluid System Components Division	
I. I. Pinkel M.S. 5-3	(1)
P. T. Hacker M.S. 5-3	(1)
Air-Breathing Engine Division	
J. Howard Childs M.S. 60-4	(1)
Aeronautics Procurement Section	
L. W. Schopen M.S. 77-3	(1)
Patent Counsel M.S. 501-3	(1)
Materials & Stresses Division	
S. S. Manson M.S. 49-1	(1)
G. M. Ault M.S. 3-13	(1)
R. W. Hall M.S. 49-1	(1)
J. W. Weeton M.S. 49-1	(1)
J. Freche M.S. 49-1	(1)
M. Quatinetz M.S. 49-1	(1)
F. H. Harf M.S. 49-1	(1)
A. Anglin M.S. 106-1	(1)
N. T. Saunders M.S. 105-1	(1)
W. F. Brown,Jr. M.S. 105-1	(1)
R. H. Kemp M.S. 49-1	(1)
Dr. C.W. Andrews M.S. 49-1	(1)
R. A. Signorelli M.S. 106-1	(1)
T. K. Glasgow M.S. 49-1	(5)
Dr. T. Herbell M.S. 49-1	(1)
C. Blankenship M.S. 49-1	(1)
J. D. Wittenberger M.S. 105-1	(1)
FAA Headquarters 800 Independence Avenue S.W. Washington, D.C. 20553	
Attention: F. B. Howard/SS-210	(1)
Brig. Gen.J.C. Maxwell	(1)
Supersonic Transport Office Wright-Patterson AFB Ohio 45433	
Attention: J. L. Wilkins, SESHS	(2)
NASA Scientific & Technical Information Facility P.O. Box 3300 College Park, Maryland 20740	
Attention: NASA Representative RQT-2448	(6)
Aerospace Corporation P. O. Box 95085 Los Angeles, California 90245	
Attention: Dr. K. Kamber	(1)
Dr. L. Raymond	(1)
Dr. G. Kendall	(1)
Air Force Flight Dynamics Laboratory (FDTS) Wright-Patterson AFB Dayton, Ohio 45433	
Attention: C. L. Ramsey	(1)
AiResearch Manufacturing Co. 9851-9951 Sepulveda Blvd. Los Angeles, California 90009	
Attention: H. H. Block	(1)
American Society for Metals Metals Park Novelty, Ohio 44073	
Attention: Dr. Taylor Lyman	(1)
U. S. Army Materials and Mechanics Research Center Watertown, Massachusetts 02172	
Attention: S. V. Arnold	(1)
Dr. E. S. Wright	(1)
Dr. A. Gorum	(1)
Boeing Company Commercial Airplane Division Materials Research Unit P. O. Box 707 Renton, Washington 98055	
Attention: Dr. D. Webster	(1)

DISTRIBUTION LIST
(Continued)

ADDRESSEE	NUMBER OF COPIES
Boeing Company P. O. Box 733 Renton, Washington 98055	
Attention: Walter E. Binz,Jr. SST Unit Chief	(1)
Curtiss-Wright Corporation Metals Processing Division 760 Northland Avenue Buffalo, New York 14215	
Attention: Dr. B. Triffleman	(1)
McDonnell Douglas Corporation Materials Research Division 3000 Ocean Park Blvd. Santa Monica, California 90406	
Attention: Dr. D. Killpatrick	(1)
Defense Documentation Center (DDC) Cameron Station 5010 Duke Street Alexandria, Virginia 22314	(1)
Air Force Materials Laboratory Wright-Patterson AFB, Ohio 45433	
Attention: N. Geyer (MAMP)	(1)
Dr. A. M. Lovelace, Director (MAG)	(1)
E. Beardslee (MAAE)	(1)
R. O. Hughes (MAAM)	(1)
C. Lombard (MAMP)	(1)
Dr. H. M. Burte (MAM)	(1)
T. D. Cooper (MAMP)	(1)
I. Perlmutter (MAMP)	(1)
Dr. H. Gegel (MAMP)	(1)
Department of the Navy Office of Naval Research Code 429 Washington, D.C. 20350	
Attention: Dr. G. Rausch	(1)
Chief, Bureau of Naval Weapons Department of the Navy Washington, D.C. 20350	
Attention: RRMA-2/T.F. Kearns	(1)
RRMA/I. Machlin	(1)

ADDRESSEE	NUMBER OF COPIES
NASA-Langley Research Center Langley Station Hampton, Virginia 23365	
Attention: Technical Library	(1)
E. E. Mathauser	(1)
Irvin Miller MS214	(1)
R. Pride	(1)
NASA-Manned Spacecraft Center Structures & Mechanics Div. 2101 Webster-Seabrook Road Houston, Texas 77058	
Attention: Branch Chief (ES441)	(1)
Library	(1)
Dr. J. Youngblood	(1)
U. S. Army Aviation Materials Lab. Fort Eustis, Virginia 23604	
Attention: John White, Chief, SMOFE-APG	(1)
Jet Propulsion Laboratory 4800 Oak Grove Drive Pasadena, California 91103	
Attention: Library	(1)
NASA-Ames Research Center Moffet Field, California 94035	
Attention: Library	(1)
NASA-Goddard Space Flight Center Greenbelt, Maryland 20771	
Attention: Library	(1)
NASA-Flight Research Center P. O. Box 273 Edwards,California 93523	
Attention: Library	(1)
Department of the Navy U. S. Navy Marine Engineering Lab. Annapolis, Maryland 21402	
Attention: Dr. Klaus M. Zwilsky	(1)

DISTRIBUTION LIST
(Continued)

ADDRESSEE	NUMBER OF COPIES
Air Reduction Company Central Research Lab. Murray Hill, New Jersey 07971 Attention: Dr. E. Gregory	(1)
Lockheed Missile and Space Company 3251 Hanover Street Palo Alto, California 94304 Attention: Dr. E. C. Burke, Materials Science Lab	(1)
Dr. T. E. Tietz, Materials Science Lab	(1)
Lockheed Palo Alto Research Labs. Materials & Science Lab 52-30 3251 Hanover Street Palo Alto, California 94304 Attention: Dr. Clause G. Goetzel	(1)
Lockheed-Georgia Company Research Laboratory Marietta, Georgia 30060 Attention: Dr. W. S. Cremens	(1)
Department of Metallurgy University of British Columbia Vancouver, B.C., Canada Attention: Prof. D. Tromans	(1)
Prof. J. Lund	(1)
Titanium Metals Corp. of America 233 Broadway New York, New York 10007 Attention: Ward Minkler, Mgr. of Technical Service	(1)
General Electric Company Materials & Process Labs. Schenectady, New York 12301 Attention: C. T. Sims	(1)
General Electric Company Advanced Technology Lab Schenectady, New York 12305	(1)

ADDRESSEE	NUMBER OF COPIES
General Electric Company Materials Devel. Lab. Oper. Advanced Engine & Technology Dept. Cincinnati, Ohio 45215 Attention: L. P. Jahnke	(1)
Dr. W. Chang	(1)
Dr. R. E. Allen	(1)
International Nickel Company Paul D. Merica Research Lab Sterling Forest Suffern, New York 10901 Attention: Dr. R. F. Decker	(1)
Dr. J.S. Benjamin	(1)
Dr. R. L. Cairns	(1)
International Nickel Company 67 Wall Street New York, New York 10005 Attention: R. R. Dewitt	(1)
International Nickel Company Huntington, W. Virginia 25701 Attention: Library	(1)
Massachusetts Institute of Technology Department of Metallurgy Rm. 8-305 77 Massachusetts Avenue Cambridge, Massachusetts 02138 Attention: Prof. N. J. Grant	(1)
Narmco Research & Development Division Whittaker Corporation 3540 Aero Court San Diego, California 92123 Attention: Dr. F. J. Riel, Technical Director	(1)
Pratt & Whitney Aircraft Div. United Aircraft Corporation 400 Main Street East Hartford, Connecticut 06108 Attention: E. F. Bradley	(1)
G. Andreini	(1)
F. Talboom	(1)
Research Div. Library	(1)

DISTRIBUTION LIST
(Continued)

ADDRESSEE	NUMBER OF COPIES
Solar, A. Division of International Harvester 2200 Pacific Highway San Diego, California 92112	
Attention: J. V. Long	(1)
M. J. Klein	(1)
Sylvania Electric Products, Inc. Chemical & Metallurgical Div. Towanda, Pennsylvania 18848	
Attention: Dr. J. S. Smith	(1)
R. F. Cheney	(1)
TRW Inc. TRW Electromechanical Div. 23, 555 Euclid Avenue Cleveland, Ohio 44117	
Attention: Dr. G. Doble	(1)
Dr. R. Quigg	
Universal-Cyclops Steel Corp. Bridgeville, Pennsylvania 15017	
Attention: C. P. Mueller	(1)
University of California at Los Angeles Los Angeles, California 90024	
Attention: Dr. G. Hoffman	(1)
Vitro Laboratories 200 Pleasant Valley Way West Orange, New Jersey 07052	
Attention: Dr. S. Grand	(1)
U. S. Atomic Energy Comm. Washington, D.C. 20545	
Attention: Jules Simmons, DRDT	(1)
Technical Reports Library	(1)
Air Force Office of Scientific Research 1400 Wilson Blvd. Arlington, Virginia 22209	
Attention: Capt. R. Austin	(1)

ADDRESSEE	NUMBER OF COPIES
Gordon McKay Laboratory Harvard University Cambridge, Mass. 02138	
Attention: Prof. M.F. Ashby	(1)
Advanced Materials Res. & Development Lab. Pratt & Whitney Aircraft Middletown, Conn. 06473	
Attention: Dr. D. H. Boone	(1)
Dr. B. Kear	(1)
Dr. F.L. Ver Snyder	(1)
Solid State Sciences Div. The Franklin Institute Philadelphia, Pa. 19103	
Attention: Dr. R. Jones	(1)
University of California Hearst Mining Bldg.-Room 268 Berkeley, California 94720	
Attention: Prof. J. E. Dorn	(1)
Prof. G. Thomas	
Materials Division Central Electricity Research Lab. Kingston Road Leatherhead, Surrey England	
Attention: Dr. I. Palmer	(1)
Dept. of Materials Science Pennsylvania State Univ. University Park, Pennsylvania 16802	
Attention: Prof. M. C. Inman	(1)
Department of Materials Science Stanford University Stanford, California 94305	
Attention: Prof. O. D. Sherby	(1)
Prof. C. Barrett	(1)
Prof. W. Nix	(1)
Department of Metallurgy Pembroke Street Cambridge University Cambridge, England	
Attention: G. C. Smith	(1)

DISTRIBUTION LIST
(Continued)

ADDRESSEE	NUMBER OF COPIES
Defense Metals Information Center (DMIC) Battelle Memorial Institute 505 King Avenue Columbus, Ohio 43201	(1)
General Motors Corporation Allison Division Indianapolis, Indiana 46206 Attention: D. K. Hanink, Materials Lab.	(1)
Ilikon Corporation Natick Industrial Center Natick, Massachusetts 01762 Attention: Dr. L. J. Bonis	(1)
Arthur D. Little, Inc. 20 Acorn Park Cambridge, Massachusetts 02140 Attention: Dr. B. Bovarnick	(1)
National Research Corporation 70 Memorial Drive Cambridge, Mass. 02142 Attention: Technical Information Center	(1)
Teledyne Materials Res. Co. 303 Bear Hill Road Waltham, Massachusetts 02154 Attention: Dr. R. Widmer	(1)
Rensselaer Polytechnic Inst. Department of Materials Science Troy, New York 12180 Attention: Prof. F. V. Lenel Prof. G. S. Ansell	(1) (1)
Sherritt Gordon Mines, Ltd. Research & Development Div. Fort Saskatchewan Alberta, Canada Attention: Dr. R. W. Fraser Dr. D.J.I. Evans Dr. F. L. Norris Dr. M. A. Clegg	(1) (1) (1) (1)

ADDRESSEE	NUMBER OF COPIES
Case Western Reserve Univ. Dept. of Metallurgy & Materials Science University Circle Cleveland, Ohio 44106 Attention: Prof. L. Ebert J. J. Petrovick	(1) (1)
Dept. of Physical Metallurgy & Science of Materials University of Birmingham Edgebaston Birmingham, England Attention: Prof. R.E. Smallman	(1)
Dept. of Metallurgy University of Kentucky Lexington, Kentucky 40506 Attention: Prof. Hans Conrad	(1)
Battelle-Institut e.V. Wiesbadenstrasse, Postfach 1337 Frankfurt/Main, W. 13 Germany Attention: Dr. R. Scharwaechter	(1)
Atomic Energy of Canada Ltd. CRNL Applied Materials Research Branch Chalk River, Ontario, Canada Attention: Dr. C. D. Williams	(1)
Westinghouse Research Lab. Metallurgy Department Pittsburgh, Pennsylvania Attention: R. T. Begley	(1)
McMaster University Dept. of Metallurgy & Materials Science Hamilton, Ontario, Canada Attention: Prof. J. D. Embary	(1)

DISTRIBUTION LIST
(Continued)

ADDRESSEE	NUMBER OF COPIES
Aerospace Research Lab. Wright-Patterson AFB, Ohio Attention: Dr. H. A. Lipsitt, ARZ	(1)
General Electric Research & Development Lab. Schenectady, New York Attention: Dr. E. W. Hart	(1)
Atomic Energy Commission Research Establishment RISO DK-4000 Roskilde Denmark Attention: Dr. N. Hansen	(1)
Dept. of Metallurgy Oxford University Oxford, England Attention: Dr. F. J. Humphreys Dr. J. W. Martin	(1) (1)
Fansteel Metallurgical Corp. 5101 Tantalum Place Baltimore, Maryland 21226 Attention: Dr. L. Klingler P. G. Bailey	(1) (1)
U. S. Army Research Office- Durham Box CM-Duke Station Durham, North Carolina 27706 Attention: Dr. H. M. Davis Dr. G. Mayer	(1) (1)
Institute de Recherches de la Siderurgie Francaise (IRSID) 185, Rue President-Roosevelt St. Germain-en Laye (S & O) FRANCE Attention: Dr. L. Roesch	(1)
Dr. Robert I. Jaffee Battelle Memorial Institute 505 King Avenue Columbus, Ohio 43201	(1)
Mr. William H. Freeman, Jr. Metallurgist Lycoming Division AVCO Manufacturing Company 505 South Main Street Stratford, Connecticut 06497	(1)
Mr. A. K. Forney Aerospace Engineer Federal Aviation Administration Department of Transportation Washington, D.C. 20553	(1)
Mr. Philip Goodwin Naval Air Systems Command AIR-5203, Room 2W98 Navy Department Washington, D.C. 20360	(1)
Professor Ray W. Guard Head, Department of Metallurgical Engineering Michigan Technical University Houghton, Michigan 49931	(1)
Dr. Harold D. Kessler Chief Metallurgist Reactive Metals, Inc. 100 Warren Avenue Niles, Ohio 44446	(1)
Mr. Ira Petker Technical Specialist Composite Structures Dept. Aerojet-General Corporation Azusa, California 91702	(1)

DISTRIBUTION LIST
(Continued)

ADDRESSEE	NUMBER OF COPIES
Professor Robert A. Rapp Department of Metallurgy The Ohio State University 116 West 19th Avenue Columbus, Ohio 43210	(1)
Mr. Hyman Rosenthal Research Advisor Metallurgy Research Lab. Frankford Arsenal Philadelphia, Pennsylvania 19137	(1)